The Dynamic Interplay Between Lentiviral Vif and Human APOBEC3 Proteins

A DISSERTATION
SUBMITTED TO THE FACULTY OF
THE UNIVERSITY OF MINNESOTA
BY

Jiayi Wang

IN PARTIAL FULFILLMENT OF THE REQUIREMENTS
FOR THE DEGREE OF
DOCTOR OF PHILOSOPHY

Advisor: Reuben S. Harris

July 2019

ACKNOWLEDGEMENT

My whole-hearted gratitude to the following:

My advisor, Dr. Reuben Harris, who poured in his time and patience to guide me and support me during this journey, for all the “how’s it going” greetings, the “thx r” emails, and the paper drafts in red…

Current and past Harris lab members, for making the lab such a supportive and collaborative environment,

My thesis committee members, Alex Sobeck, Ryan Langlois, Jeongsik Yong, and Anja Bielinsky, for the guidance and advices,

My friends, for being my family when my family is on the other side of the earth, for being there for me during hard times,

My parents and brother, for everything,

And my lover, Hao Wen, for making me the happiest person in the world, even when I am mad at you.

DEDICATION

This work is dedicated to my mother, Hong Zeng, for her unwavering support.

ABSTRACT

Four members of the APOBEC3 (A3) family of DNA cytosine deaminases are capable of inhibiting HIV-1 replication by deaminating viral cDNA cytosines and interfering with reverse transcription. HIV-1 counteracts restriction with its Vif protein, which nucleates a ubiquitin ligase complex that directly binds A3 enzymes and targets them for proteasomal degradation. My thesis research aims at understanding the dynamic interplay between lentiviral Vif and human A3 enzymes, from the molecular determinants of this interaction to its implications in HIV-1 transmission within a large patient cohort. This has been addressed through three separate studies.

The primate A3 repertoires show considerable variations likely due to positive selection during evolution. Lentiviral Vif proteins have rapidly evolved to counteract this immune pressure, resulting in present-day host-pathogen interactions that are largely species specific. However, a simian immunodeficiency virus (SIV) Vif exhibits cross-species degradation capability against multiple human A3 enzymes. We used mutagenesis coupled with functional assays to determine the residues involved in the interaction between the SIV Vif and A3B, and demonstrated that it resembles the HIV-1 Vif-human A3G interaction. This may be a molecular remnant of an ancestral Vif activity or result of molecular mimicry between human A3B and A3G.

A3H is unique among family members by dimerizing through cellular and viral duplex RNA species. RNA binding is required for proper localization of A3H to the cytoplasmic compartment, for efficient packaging into nascent HIV-1 particles, and ultimately for effective virus restriction activity. To investigate the role of RNA in HIV-1

Vif-mediated degradation of A3H, we used structural and cell biology approaches to study RNA binding mutants and their sensitivity to Vif-mediated degradation. We found that RNA is not strictly required for Vif-mediated degradation of A3H and that RNA and Vif bind the enzyme on largely distinct surfaces, but the degradation process may be affected by changes in subcellular localization/mobility and/or differences in the constellation of A3H interaction partners.

In humans, A3H is the most polymorphic member of the family and includes seven haplotypes with three encoding for stable proteins and the rest unstable. Stable A3H proteins contribute to HIV-1 restriction and can only be counteracted by fully functional Vif variants (dictated by amino acids at key positions). We tested the hypothesis that stable A3H enzymes provide a transmission barrier to HIV-1 isolates harboring less-than-fully functional Vif alleles. We have determined the A3H and viral Vif genotypes of a large cohort of African HIV-1 serodiscordant couples and have shown stable A3H is unlikely to be a general protective factor in HIV-1 acquisition. However, stable A3H enzymes may still serve positive roles in slowing virus spread and disease progression.

Overall, my thesis research contributes to the growing knowledge of the A3-Vif interaction, particularly interactions between the Vif protein of pandemic HIV-1 and the contemporary restriction factor A3H. These studies will help guide future efforts to disrupt this interaction as an antiviral therapy.

TABLE OF CONTENTS

List of Tables

CHAPTER 3

CHAPTER 4

List of Figures

CHAPTER 1

CHAPTER 2

CHAPTER 3

CHAPTER 4

CHAPTER 1

Introduction - Human APOBEC3 Enzymes and Lentiviral Vif

FORWORD

HIV/AIDS is a global epidemic. Since the discovery of HIV as the causing agent of AIDS in the 1980s, the development of various antiviral drugs has enabled long-term inhibition of viral replication in HIV-positive individuals. This makes HIV/AIDS a manageable chronic disease to those who have access and adhere to lifelong treatment regimens. Despite this success in antiviral therapies, research and clinical trials have yet to yield a cure or vaccine. An under-explored area of HIV research is innate immune defense mechanisms that help control viral infections. This thesis focuses on one arm of the innate defense, the APOBEC3 proteins. The following introduction will provide an overview of HIV infection, pathogenesis, and relevant host restriction factors, before reviewing in detail the roles of restrictive APOBEC3 in the context of HIV infection, the viral counteraction mechanism utilizing Vif, the molecular interface between the two, and the natural variations of the A3 family with implications in viral adaptation.

HIV VIROLOGY AND PATHOGENESIS

HIV-1, the most pandemic type of HIV, is a single-stranded, positive-sense RNA virus that belongs to the *Lentivirus* genus in the *Retroviridae* family. The highly compact viral genome of HIV-1 has a length of only 9.7 kilobases (kb) and consists of multiple open-reading frames (**Figure 1-1**). Genes such as *gag*, *pol*, and *env* encode structural proteins and essential machineries. HIV-1 Gag is encoded by *gag* as a polyprotein precursor and later cleaved into p17 matrix (MA), p24 capsid (CA), and p7 nucleocapsid (NC) during a process called maturation (reviewed in [1-3]). The polyprotein Gag plays a central role in the process of virion formation called viral assembly, and its cleavage products are major structural proteins [4]. The *pol* gene encodes for enzymes necessary for viral replication, including reverse transcriptase (RT) that ultimately synthesizes double-stranded DNA (dsDNA) from HIV-1 RNA genome, integrase (IN) that facilitate insertion of viral dsDNA into the host genome, and protease (PR) that cleaves larger viral proteins into smaller units [3, 5]. The *env* gene encodes for glycoproteins gp120 and gp41, which form heterodimeric spike called envelope on the surface of the virion, with gp120 proteins forming the head and gp41 forming the transmembrane stalk [6-8].

Genes *tat* and *rev* encode regulatory proteins that are critical for viral protein synthesis and particle production. The Tat protein expressed from *tat* is a transactivator of viral gene expression, and it functions by recruiting multiple histone modifying enzymes to relieve the repression of viral promoter within the long-terminal repeat (LTR) region [9-11]. The main function of Rev protein (encoded by rev) is facilitating nuclear export of intron-containing viral RNA, so that full-length viral RNA molecules can enter the

cytoplasm and assemble into nascent virions [12, 13]. HIV-1 also utilizes a variety of genes (*i.e. vif*, *vpr*, *vpu*, and *nef*) to encode accessory proteins [5, 14]. Most of these proteins counteract certain host defense mechanisms to ensure the infectivity of HIV-1 and will be discussed in detail later in this chapter.

HIV-1 virion is spherical with approximately 100 nm in diameter [15, 16]. It consists of an outmost bilayer of lipid membrane on top of a layer of MA proteins. Envelope proteins are anchored in the membrane using its transmembrane stalk while protruding its trimeric head outside of the virion. Within the virion, a conical-shaped capsid is formed with CA proteins and encloses two molecules of viral genomic RNA (gRNA) bound by RNA-binding proteins such as NC and RT.

Transmission of HIV-1 begins with one virus infecting one cell, often time at mucosa tissues [3, 17]. HIV-1 typically infect CD4+ T lymphocytes and macrophages through the binding of its trimeric envelope complex to a CD4 receptor and a chemokine coreceptor (most commonly CCR5 or CXCR4) on the surface of the cells [2, 3, 18]. Upon fusion of the virion to cell membrane, the contents of the virion including the capsid core are deposited into the cytoplasm [18]. Reverse transcription occurs within the capsid core, which is coupled with or precedes the dissolving of capsid shell, a process known as uncoating [19, 20]. RT synthesizes the viral complementary DNA (cDNA) from gRNA as well as the second strand of DNA, allowing the generation of the viral dsDNA [21, 22]. This viral dsDNA is imported into the nucleus and integrated into the host genome, mediated by a complex of proteins including IN [23]. Tat and Rev regulate the viral gene transcription and nuclear export, enabling viral gene expression and new virion production

[9-13]. The assembly of a virion is largely mediated by Gag polyproteins, which are cleaved by PR in an immature virion to yield an infectious mature virion [1, 4].

The acute primary phase of HIV-1 infection is signified by the onset of plasma viremia (presence of viral RNA in blood), as a result of viruses spreading from local mucosa and lymph nodes to bloodstream (reviewed in [3, 17]). Drastic increase of plasma viremia coupled with massive CD4+ T lymphocyte depletion occurs during this phase. The antiviral immune responses, particularly the cytotoxic CD8+ T cell response, controls the initial infection, leading to decreased viremia (viral load) and partial reversal to the number of CD4+ lymphocytes (clinically known as CD4 counts). Following the initial containment of viral replication is the long period of asymptomatic chronic infection. During this period of time, the virus continues to replicate and evolve, and CD4+ lymphocytes slowly deplete overtime. Without treatment, a fraction of HIV-1-positive individuals eventually enters the AIDS stage with destructed lymphoid system, and opportunistic infections by bacteria and other pathogens, as well as tumors, become lethal.

RETROVIRUS RESTRICTION FACTORS

One arm of the host innate immunity against HIV-1, and to a greater extent, retroviruses, is a group of proteins called restriction factors. They are dominantly acting proteins that can cause significant decrease in viral infectivity. They generally inhibit a certain step of the viral life cycle and are often time counteracted and/or evaded by contemporary viruses [24, 25]. Multiple members of the TRIM family, such as TRIM5α, are potent restriction factors in Old World and New World monkeys [25-28]. They inhibit the cross-species

transmission of HIV-1 by forming a mesh-like structure covering capsid and preventing its uncoating [26, 29]. Various strains of simian immunodeficiency virus (SIV) have evolved resistance to TRIM5α through mutations in capsid proteins that abolish the interaction [30]. Multiple human and simian APOBEC3 (A3) enzymes act as post-entry inhibitors by mutating the genomes of HIV and SIV [31-33]. The main function of the viral protein Vif of HIV and SIV is to counteract the host A3 repertoire, which will be discussed in depth later in this chapter. SAMHD1, a restriction factor in myeloid cells such as dendritic cells and macrophages, hinders viral reverse transcription by depleting the pool of deoxynucleoside triphosphates (dNTPs) [24, 25]. Most SIV strains and HIV-2 (a rarer type of HIV), but not HIV-1, encode protein Vpx to counteract SAMHD1 and target it for polyubiquitination and proteasomal degradation, allowing viruses to effectively infect myeloid cells. Other host restriction factors such as Tetherin/BST-2 and SERINC3/5 are located on the cellular membrane. They inhibit the release of budding virions and are counteracted by Vpu and Nef of HIV-1, respectively [34-36].

Although viruses have adapted to almost fully counteract these host innate immune defenses, the necessity of the counteraction to establish infection demonstrates the powerfulness of the host restriction factors. Therefore, better understanding these host-virus interactions can potentially allow us to disrupt them and therefore restore the restrictive capabilities of these restriction factors.

APOBEC3 FAMILY OF CYTOSINE DEAMINASES

The human A3 family consists of seven members (A, B, C, D, G, F, and H) that are encoded in tandem on chromosome 22 [37]. These seven A3 proteins are capable of catalyzing deamination of cytosine to uracil (C-to-U) on single-stranded DNA (ssDNA) substrates [32, 38]. The cytosine deamination mechanism involves a conserved His-X-Glu-X_{25-31}-Pro-Cys-X_{2-4}-Cys zinc-coordinating motif, which promotes deprotonation of a water molecule to hydroxide. The hydroxide subsequently attacks the carbon at 4-position of a cytosine nucleobase, resulting in replacement of the adjacent amine group with a carbonyl group. Deamination by A3 proteins occur in a preferred dinucleotide context. All of the A3 enzymes prefer targeted cytosine preceded by a thymine (5' TC), with the exception of A3G that prefers targeted cytosine preceded by another cytosine (5'- CC). Additionally, the minus-two and plus-one positions relative to targeted cytosine are also important, and base preferences can vary among family members [39, 40].

These seven *A3* genes differ in the number and type of zinc (Z)-coordinating domain(s) they encode. There is a total of three Z domain types, namely Z1, Z2, and Z3. Z1 domain differs from the others by a unique isoleucine residue after an arginine conserved among all DNA deaminases, whereas Z2 has a unique tryptophan-phenylalanine motif, and Z3 is signified by a conserved threonine [41]. Human *A3B*, *A3D*, *A3F*, and *A3G* encode double-Z-domain proteins that are either Z2-Z1 (A3B and A3G) or Z2-Z2 (A3D and A3F). Human *A3A*, *A3C*, and *A3H* encode single Z1-, Z2-, and Z3-domain proteins, respectively.

Extensive structural studies of A3 proteins of all three Z domain types have revealed a similar cytosine deaminase fold with five β strands forming a hydrophobic core in the middle surrounded by six α helices [40, 42-54]. A single zinc ion is anchored in the active site of the enzyme. The loops of different A3 proteins can be highly variable, and they play critical roles in substrate recognition and specificity [55, 56]. The loop adjacent to the active site (loop 7) is particularly important for governing nucleobase preference at minus-one position relative to targeted cytosine [40]. For example, swapping loop 7 of A3A to A3G converts A3G to prefer 5'-TC dinucleotide context instead of 5'-CC [56]. Moreover, the loop regions of certain A3 proteins can also mediate RNA binding [42, 49, 50, 57]. Recently published x-ray crystal structures of primate A3H proteins demonstrate a distinct function of loop 1 and loop 7 in mediating duplex RNA dependent dimerization [42, 49, 50]. This RNA-mediated dimerization mechanism enabled by the loops is unique and distinguishes A3H from other family members. Mutating certain conserved residues on loop 1 and loop 7 abolishes RNA binding, resulting in a monomeric protein (see **Chapter 3**).

Evolutionary studies of the A3 family have revealed that the *A3* locus is unique to mammals, however it has expanded dramatically in different mammalian lineages from only one *A3* gene in mouse to three in cow and sheep, four in cat, and seven in primates [58-61]. The mouse *A3* gene, which likely resembles the ancestral gene, encodes a Z2-Z3 protein [58]. Sequence analysis suggested that Z1 and Z2 domains diversified and duplicated from a common ancestral Z domain, whereas Z3 had always been kept singular [58]. The ancestral *A3* locus can be further traced back to a likely duplication of the similar

and more conserved *AID* (activation induced deaminase) locus [58-61]. The rapid expansion of the *A3* locus in primates suggests an urging need for its role in viral restriction in an everlasting arms race between host and virus.

THE COUNTERACTION OF APOBEC3-MEDIATED RESTRICTION BY VIF

Several members of the APOBEC3 family (A3C, A3D, A3G, A3F, and A3H) have been identified as restriction factors for HIV-1 (reviewed in [31-33]). In the absence of Vif, the restrictive A3 proteins from the infected cells assembly into budding virions (**Figure 1-2**). This packaging process is mediated by interaction with HIV-1 Gag and certain cellular or viral RNA molecules [50, 62-72]. A large fraction of A3 proteins enters the viral capsid core upon virion maturation, therefore retaining access to the viral genome [73, 74]. Upon fusion of the virion into a target cell and initial reverse transcription, A3 enzymes catalyze C-to-U deamination on the single-stranded viral cDNA. The resulting uracils template adenines instead of guanines in the subsequent second-strand synthesis. This leads to G-to-A hypermutation in the viral genome, rendering it non-functional. Multiple studies have supported an additional deaminase-independent mechanism of A3 restriction [50, 75-82]. This likely involve the RNA binding activity of A3 proteins, as them binding to the viral gRNA hinders the reverse transcription process. HIV-1 counteracts this restriction mechanism with accessory protein Vif. Vif hijacks host cellular protein CBF-β (core binding factor-beta) to adapt the restrictive A3 proteins to an E3 ubiquitin ligase complex and target them for polyubiquitination and proteasomal degradation [31-33]. The

neutralization of A3 proteins by Vif can successfully rescue the infectivity of HIV-1 viruses in their target CD4+ T lymphocytes.

Structural and mutagenesis studies of Vif have highlighted key residues and surfaces involved in the interaction with CBF-β and subunits within the E3 ligase complex. Vif interact with CBF-β using an extensive hydrophobic surface [83]. N-terminal residues such as W5, V7, and I9 form direct contacts with multiple β-strand residues of CBF-β [83]. The Vif-CBF-β interaction is essential in stabilizing Vif and enabling its interaction with A3 proteins and members of the E3 ligase [84, 85]. An evolutionarily conserved region of Vif, called BC-box (residues 144-155 including the SLQ motif) is required for interaction with adaptor proteins ELOB-ELOC (Elongin B-Elongin C), by mimicking a cellular SOCS-box motif [86, 87]. Mutating the three-amino-acid SLQ motif to triple alanine completely abrogate Vif's ability to mediate the degradation of any A3 proteins [88-90]. A zinc-coordinating HCCH motif (His 108, Cys 114, Cys 133, and His 139) is required for Vif interaction with CUL5 (Cullin 5) [88]. The presence of Vif-CBF-β also stabilizes the interaction between CUL5 and ELOB-ELOC [88]. When in complex with CBF-β and the E3 ligase, Vif adopts a conical shape with hydrophobic surface buried and extensive positively charged surface exposed [83].

At least a fraction of the solvent exposed positively charged Vif residues are reserved for A3 interaction. Despite the conserved motifs for interacting with subunits of the E3 ligase, HIV-1 Vif utilizes separable residues and surfaces to target restrictive human A3 proteins. The N-terminal DRMR motif is specifically required for interaction with and degradation of A3F, whereas the YRHHY motif is only required for A3G interaction and

degradation [91, 92]. Degradation of A3H requires Vif residues F39 and H48 [93-96]. Mutating any of these motifs or residues results in separation-of-function Vif mutants that no longer degrade the corresponding A3 protein but remain functional against others.

On the A3 side of the interaction, however, largely similar regions on A3 proteins appear to be targeted by HIV-1 Vif. The α3 and α4 helices of A3F, particularly E289 residue on α3 and E324 on α4, are required for Vif-mediated degradation [97-101]. The well-studied D128 and D130 residues of A3G at the junction of loop 7 and α4 are required for Vif interaction, and mutating any of them to an oppositely charged lysine confers resistance to Vif [65, 102-105]. As for A3H, multiple residues on the α3 and α4 (with the most well-studied being D121 on α4) are required for Vif [106-108]. Despite the lack of co-structure of Vif in complex with any of the A3 proteins, mutagenesis together with modeling has provided invaluable information about these A3-Vif interfaces.

PRIMATE APOBEC3 AS INTERSPECIES BARRIERS AND RECIPROCAL ADAPTATION OF LENTIVIRAL VIF

Rare cross-species transmission events often time lead to new linages of lentiviruses, including all types of HIV. According to previous phylogenetic analyses, the origins of HIV-1 are transmissions of SIV infecting chimpanzee (*Pan troglodytes*) (SIVcpz) and SIV infecting gorilla (*Gorilla gorilla*) (SIVgor) [109, 110]. HIV-2 originates from SIV infecting sooty mangabey (*Cercocebus atys*) (SIVsm) [111].

Many host restriction factors like A3 enzymes are under positive selection, a selective regime that results in more non-synonymous mutations than synonymous ones

[112]. This leads to variations in host restriction factors, particularly on virally targeted surfaces, to evade interaction. These host escape mutations in turn drive reciprocal viral evolution and adaptation, resulting in present-day host-pathogen interactions that are largely species-specific. The variations at the human and primate A3-Vif interfaces exemplify this point. The D128 residue of human A3G is required for HIV-1 Vif counteraction [89, 104, 113]. The A3G protein from African green monkey (agm) has an oppositely charged amino acid lysine at 128 position, which is required for interaction with SIVagm Vif [89, 104, 113]. Human A3G is degraded by HIV-1 but not SIVagm Vif, however a D128K substitution reverses the phenotype [89, 104]. On the side of Vif, the DRMR motif of HIV-1 Vif is mapped to a SEMQ motif on SIVagm Vif. Although it is not strictly required for HIV-1 Vif interaction with human A3G, the DRMR motif governs species specificity [89, 113]. Replacing the DRMR with SEMQ allows HIV-1 Vif to promote the degradation of A3G D128K [89, 113]. A similar phenomenon was reported for A3F. Residues E289 and E324 of human A3F dictate HIV-1 Vif interaction, and oppositely charged K289 and K324 of rhesus macaque A3F dictate SIVmac (SIV infecting rhesus macaque) Vif interaction [89, 97, 98, 101].

The species-specific host-pathogen interactions impose obstacles to cross-species transmissions. Previous studies have implicated multiple members of the primate A3 subfamily in roles as species barriers in lentiviral transmission, and that adaptation of viral Vif to counteract these restrictive A3 enzymes was essential to overcome the barrier [114-116]. For instance, chimpanzees in Africa are exposed to a high prevalence of SIVs in their monkey prey, but they are only infected by one strain of SIV, *i.e.* SIVcpz [115]. Analysis

of the Vif proteins from other monkey SIV strains show poor antagonization of chimpanzee A3 proteins, suggesting that these chimpanzee A3 proteins protect the hosts from infection by other SIV strains [115].

The largely species-specific A3-Vif interactions potentially enable A3 proteins as interspecies transmission barriers. However, there are exceptions in which the interaction can be promiscuous and cross-species. An example is the functional interaction between an SIV Vif and human A3B, with the latter not even exhibiting antiviral activity against HIV-1 (see **Chapter 2**).

NATURAL VARIATIONS IN THE HUMAN APOBEC3 FAMILY

Natural polymorphisms and variations have been identified in the human *A3* genes that in multiple cases lead to functional consequences, such as changes in enzymatic activity and protein stability. For instance, *A3B*, which encodes a nuclear localized A3 protein that restricts herpesviruses but also causes mutations in the host genome when mis-regulated [39, 117-119], is deleted in a large fraction of the Southeast Asian population [120]. This deletion is associated with increased risk of breast cancer in this population [121]. A3C, which has otherwise unknown functions despite having high expression levels in multiple human cell types, has a rare variant (S188I) that demonstrates anti-HIV activity [122-124]. An H186R variant of A3G that is common in African Americans but rare in European Americans is associated with accelerated progression to AIDS-defining conditions [125].

A3H is the most polymorphic member of the family with 13 known haplotypes differed by amino acids at five positions (15, 18, 105, 121, and 178) [126-129]. Haplotypes

that encode N15 and R105 (such as II) yield stably expressed proteins with restriction activity against HIV-1 [94, 96, 129]. Whereas haplotypes encoding deletion of N15 (such as III and IV) result in unstably expressed protein with no activity [94, 128, 129]. The most common haplotype outside of Africa, haplotype I, encodes a hypomorphic protein that is less stable and cannot restrict HIV-1 in primary CD4+ T lymphocytes [94, 96, 129, 130] (**Figure 1-3**). In contrast, the African population is enriched with the stably expressed A3H haplotype II with greater than 50% allele frequency [96, 129, 130].

In addition to the polymorphism, *A3H* can also be alternatively spliced into four common splice variants (SV154, SV182, SV183, and SV200) [127, 129]. SV154 is a truncated protein that is likely non-functional. SV182 and SV183 are structurally and functionally similar differing by only one residue at the C-terminal end. The SV200 variant is more active than the most common variant SV183, but is cleaved by HIV-1 proteases as a potential counteraction mechanism [127, 129]. The expression of SV200 variant is associated with A3H haplotype II as a result of a 3-bp deletion at a predicted polypyrimidine tract [129]. Therefore, it is anticipated that the African population that is enriched with A3H haplotype II also has higher expression levels of this more potent splice variant.

Differential distribution of the natural variations in the *A3* genes in human populations likely result in host A3 repertoires with strengths and weaknesses that are geographic region-specific. It is possible that the circulating viruses within a region can overtime adapt and become optimized to the locally predominant host A3 proteins. This is supported by the observation that African HIV-1 isolates more frequently encode Vif

proteins that are capable of counteracting stable A3H, the dominant form in African population. In contrast, Vif isolated from other populations with much lower frequencies of stable A3H tend to be incapable of counteracting stable A3H [96, 129, 130]. Chapter 4 contemplate the idea of whether these variations of A3H (and Vif) within the human populations forming an intraspecies transmission barrier. On a larger scale, whether there is a fitness trade-off for the virus to adapt to certain A3 variants, and whether this would impair their ability to infect the hosts of a different geographic region remain intriguing questions to be answered.

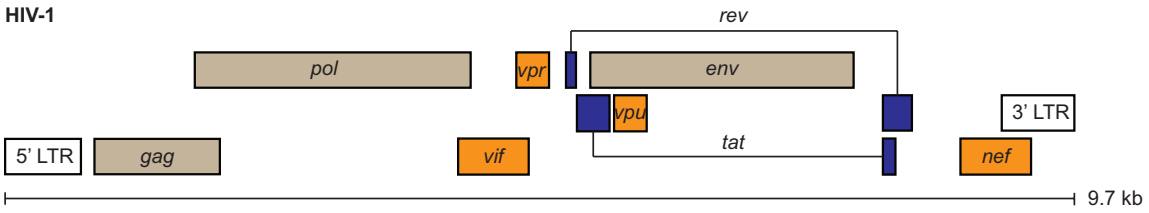

Figure 1-1. Schematic of the HIV-1 genome.

The 9.7-kb HIV-1 genome consists of multiple open reading frames. Structural proteins and machineries are encoded by *gag*, *pol*, and *env* (brown). Essential regulatory elements are encoded by *tat* and *rev* (blue). Accessory proteins are encoded by *vif*, *vpr*, *vpu*, and *nef* (orange).

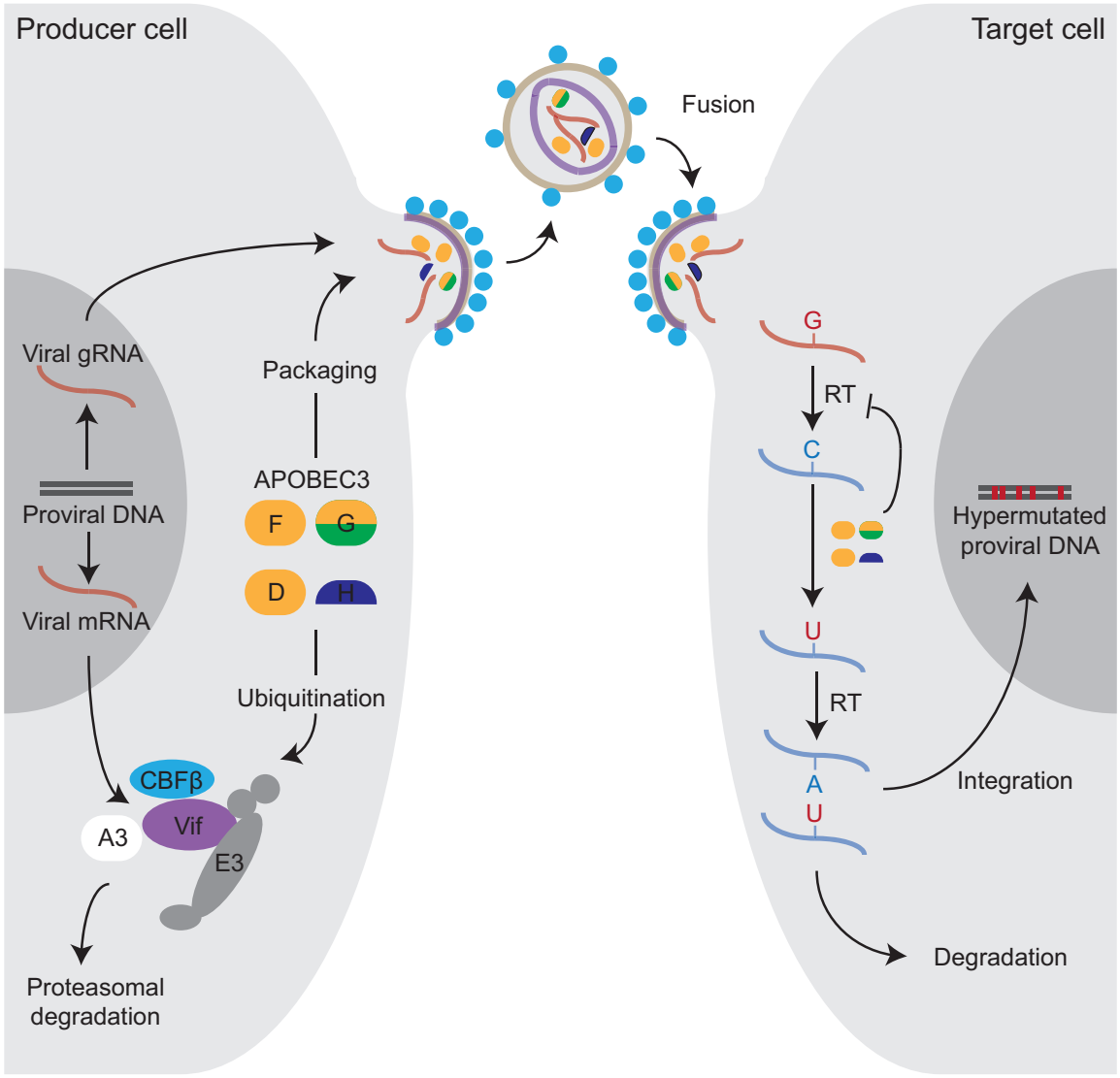

Figure 1-2. Model of A3-mediated restriction of HIV and counteraction by Vif.

The restrictive A3 proteins (D, F, G, and H) package into virions. Upon fusion and initial reverse transcription, A3 proteins mutate the viral cDNA, converting cytosines to uracils. These uracils template for adenines instead of guanines, resulting in non-functional G-to-A hypermutated viral genome. Viral cDNA uracils can also attract DNA repair enzymes and trigger degradation. Vif encoded by HIV-1 forms a complex with CBFβ and E3 ligase to target these cytoplasmic A3 enzymes for ubiquitination and proteasomal degradation.

This figure is adapted from Hultquist et al. (2011) J. Virol. 85:11220-34.

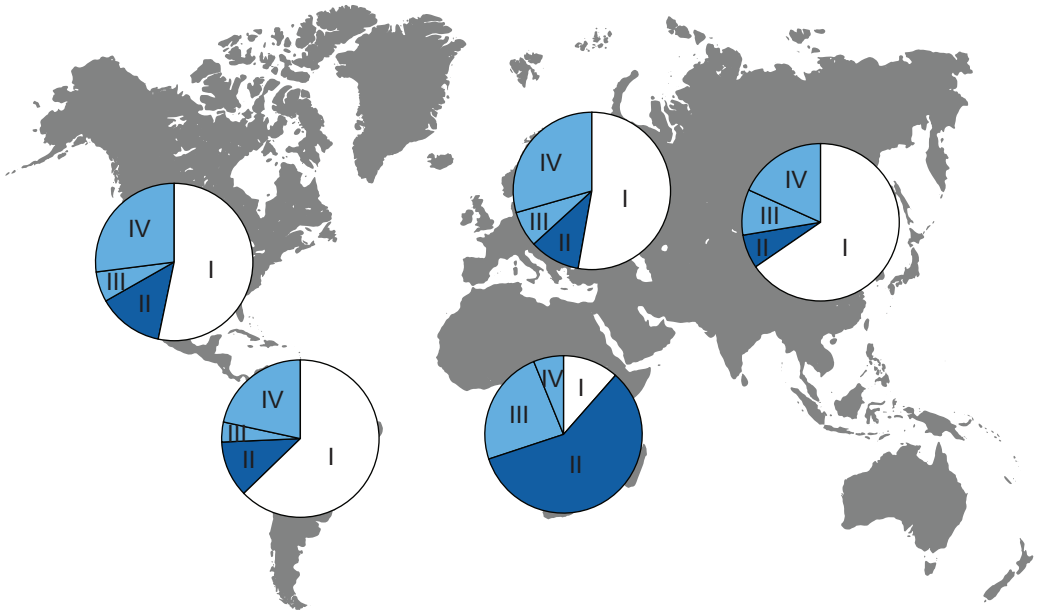

Figure 1-3. Differential distribution of *A3H* haplotypes.

World map with pie charts showing the frequency of major *A3H* haplotypes within each geographic region.

This figure is adapted from Ebrahimi et al. (2018) Nat. Commun. 9:4137.

CHAPTER 2

Simian Immunodeficiency Virus Vif and Human APOBEC3B Interactions Resemble Those between HIV-1 Vif and Human APOBEC3G

Reprinted with permission from: Wang J., N.M. Shaban, A.M. Land, W.L. Brown, & R.S. Harris. (2018) Journal of Virology, 92, e00447-18.

Authors' Contributions

J. Wang, N.M. Shaban, A.M. Land, and R.S. Harris conceived and designed the studies. J. Wang performed all experiments. W.L. Brown provided resources and technical support. J. Wang and R.S. Harris drafted the manuscript with contributions from all authors in figure preparation and revisions.

SUMMARY

HIV-1 Vif is optimized for degrading the restrictive human A3 repertoire and, in general, lentiviral Vif proteins specifically target the restricting A3 enzymes of each host species. However, SIVmac239 Vif elicits a curiously wide range of A3 degradation capabilities that include several human A3s and even human A3B, a non-HIV-1 restricting A3 enzyme. To better understand the molecular determinants of the interaction between SIVmac239 Vif and human A3B, we analyzed an extensive series of mutants. We found that SIVmac239 Vif interacts with the N-terminal domain of human A3B and, interestingly, this occurs within a structural region homologous to the HIV-1 Vif interaction surface of human A3G. An alanine scan of SIVmac239 Vif revealed several residues required for human A3B degradation activity. These residues overlap with HIV-1 Vif surface residues that interact with human A3G, and are distinct from those that engage A3F or A3H. Overall, these studies indicate that the molecular determinants of the functional interaction between human A3B and SIVmac239 Vif resemble those between human A3G and HIV-1 Vif. These studies contribute to growing knowledge of the A3-Vif interaction and may help guide future efforts to disrupt this interaction as an antiviral therapy or exploit the interaction as a novel strategy to inhibit A3B-dependent tumor evolution.

INTRODUCTION

A3 enzymes are single-stranded DNA cytosine deaminases involved in innate immunity against a variety of pathogens including retroviruses and retrotransposons [reviewed by [31-33]]. Up to seven family members, namely A3A, A3B, A3C, A3D, A3F, A3G, and A3H, are expressed in primate cells. Extensive overexpression, separation-of-function, and gain-of-function studies using various model systems including T cell lines and primary T lymphocytes have demonstrated that human A3D, A3F, A3G, and A3H contribute to restricting the replication of Vif-deficient HIV-1. These A3 enzymes package into virions and catalyze C-to-U deamination reactions in viral cDNA upon reverse transcription. This leads to G-to-A hypermutation of the viral genome, greatly affecting its coding capacity and therefore its ability to replicate and transmit. A3 enzymes also elicit varying levels of deaminase-independent restriction activity, which is likely due to a strong affinity for RNA that provides a steric block to reverse transcription.

HIV-1 encodes the accessory protein Vif to counteract A3 enzymes and prevent restriction. Vif hijacks cellular CBF-β to form an E3 ubiquitin ligase complex with CUL5, ELOB, ELOC, and RBX2, which effectively targets restrictive A3 enzymes for polyubiquitination and proteasomal degradation [84, 85, 131-136]. Vif utilizes several conserved residues and motifs to interact with different components of the complex. For instance, the SLQ motif is required for interacting with ELOC, and this is conserved among various strains of HIV-1, HIV-2, and simian immunodeficiency virus (SIV) [87]. The highly conserved zinc-coordinating HCCH motif of Vif is required for the interaction with CUL5 [88]. Moreover, the Vif-CBF-β interaction (also conserved between HIV and SIV)

involves an extensive hydrophobic surface, largely provided by residues within the N-terminal half of Vif [83]. Interestingly, despite these conserved and essential interactions, HIV-1 Vif is still capable of using different regions to target structurally similar A3 proteins (A3F, A3G, and A3H). For instance, the YRHHY motif of HIV-1 Vif is specifically required for A3G interaction and degradation, whereas the DRMR motif is specific for A3F [91, 92]. Residue F39 is essential for the A3H interaction, and changing it to valine results in a separation-of-function protein that degrades A3G and A3F but not A3H [93, 96].

Cross-species comparisons have been instrumental in elucidating molecular determinants of the A3-Vif interaction. This is possible because A3 restriction factors are under positive selection and show considerable variation between species despite overall functional conservation. For instance, human and rhesus macaque A3G are 78% identical and interspecies chimeras showed that D128 is required for the human enzyme to interact with HIV-1 Vif whereas K128 is required for the rhesus macaque enzyme to interact with SIVmac239 Vif [102-105]. Similarly, E289 and E324 are required for the human A3F interaction with HIV-1 Vif and K289 and K324 are required for the interaction with SIVmac239 Vif [89, 97, 98]. These and additional cross-species comparisons have helped to define the A3 protein surfaces involved in these interactions and have led to robust structural models [99, 100, 107, 108, 113], although structures of complete A3-Vif ligase complexes have yet to be determined. In general, rapidly evolving A3 repertoires and far more rapidly evolving lentiviral Vif proteins, selected by strong adaptive immune pressure,

have resulted in present day host-pathogen interactions that are largely but not exclusively species specific.

One clear exception to this rule is SIVmac239 Vif, the Vif protein encoded by a SIV clone that infects rhesus macaques, which degrades all of the restrictive rhesus macaque A3 enzymes as well as multiple human enzymes including A3B and A3G [90, 137, 138]. A functional interaction between SIVmac239 Vif and human A3B is curious because neither the rhesus macaque nor the human enzyme restricts Vif-deficient HIV-1 replication in T cell model systems (SupT11 or CEM-SS) [90, 139]. To shed light on the molecular determinants of this functional interaction we performed mutagenesis studies on both human A3B and SIVmac239 Vif. Using 293T cells as a model system, we found that SIVmac239 Vif exclusively targets the N-terminal domain of human A3B, and particularly residues within the loop 7 region. Based on the various A3-interacting surfaces of HIV-1 Vif, we mutated single amino acid residues of SIVmac239 Vif at corresponding regions. Functional tests of these mutants against human A3B revealed a putative physical interaction surface, which is largely similar to the A3G-interacting region on HIV-1 Vif but distinct from those that engage A3F and A3H.

RESULTS

SIVmac239 Vif mediates degradation of human A3 proteins

Multiple groups have shown that SIVmac239 Vif efficiently degrades both human A3G and A3B, whereas HIV-1 Vif targets human A3G but not A3B [90, 137, 140]. To confirm and extend these results, we performed immunoblots of 293T cells expressing SIVmac239

Vif or HIV-1 IIIB Vif together with A3G or A3B from human or rhesus macaque (**Figure 2-1A**). As a positive control, both Vif proteins promoted the degradation of human A3G, and mutation of the conserved ELOC-binding motif (SLQ-to-AAA) abrogated most of this effect. As reported [90, 141], the Vif SLQ-to-AAA mutant still caused a partial reduction in A3G steady-state levels (*e.g.*, compare lanes 4 and 20 in **Figure 2-1A**). Only SIVmac239 Vif mediated the degradation of rhesus macaque A3G. In contrast, HIV-1 IIIB Vif did not degrade human or rhesus macaque A3B, whereas SIVmac239 Vif efficiently, but not completely, promoted the degradation of both human and rhesus macaque A3B. The abilities of wild-type (WT) SIVmac239 Vif to degrade human A3B and A3G were further demonstrated through a titration experiment, in which SIVmac239 Vif was shown to degrade human A3B in a dose-dependent manner (**Figure 2-1B**). Overall, these results confirm that SIVmac239 Vif elicits a wider range of A3 degradation capabilities that, unlike HIV-1 Vif, are not limited to the A3 enzymes of its host species (**Figure 2-1C**).

SIVmac239 Vif interacts with the N-terminal domain of human A3B

Previous studies on the A3-Vif interaction revealed motifs and single amino acid residues that, when mutated, abrogate the degradation phenotype [65, 89, 97, 98, 101-105, 142]. Most of these studies have focused on HIV-1 Vif and human A3 proteins, such as A3G, A3F, or A3H. For instance, the ^{128}DPD^{130} motif of human A3G has a well-defined role in conferring sensitivity to HIV-1 Vif-mediated degradation and the analogous region of several non-human primate A3G proteins is also required for SIV Vif-mediated degradation [65, 102-105, 143]. The human A3G ^{128}DPD^{130} motif aligns with human A3B

residues ^{128}ERD^{130} (**Figure 2-2A**). To begin to determine how SIVmac239 Vif interacts with human A3B, we asked if the A3B ^{128}ERD^{130} motif is necessary by mutating the glutamic acid and aspartic acid to positively charged lysines. The resulting E128K, D130K, and the double mutant were evaluated by immunoblots of 293T cells expressing WT or mutant A3B together with increasing amount of SIVmac239 Vif or SLQ mutant (representative immunoblot in **Figure 2-2B** and quantification in **Figure 2-2E**). As a positive control, SIVmac239 Vif readily degrades WT human A3B, and this degradation phenotype is reduced by SLQ to AAA. Both single mutants and the E128K D130K double mutant of A3B express at similar levels to WT A3B in the absence of Vif, and these two lysine substitutions alone or combined confer resistance to degradation by WT SIVmac239 Vif. This resistance phenotype is not altered by the SLQ-to-AAA change. These results demonstrate that human A3B and A3G use at least one partly similar surface for interacting with Vif.

E128 and D130 are located on the surface of the N-terminal domain of human A3B [54]. HIV-1 Vif is known to interact exclusively with the N-terminal domain of human A3G [89, 131]. To determine whether this is also the case for A3B, full-length, N-terminal domain, and C-terminal domain constructs were cotransfected into 293T cells with WT SIVmac239 Vif, the SLQ mutant, or empty vector (representative immunoblot in **Figure 2-2C** and quantification in **Figure 2-2F**). As above, WT SIVmac239 Vif leads to decreased levels of full-length A3B, and the degradation phenotype is largely reversed by mutating the SLQ motif. The same trend was observed for the N-terminal domain of A3B, indicating that the N-terminal domain is sensitive to degradation by SIVmac239 Vif. However, the

levels of A3B C-terminal domain are approximately the same when cotransfected with WT versus mutant Vif, indicating that the C-terminal domain is resistant to SIVmac239 Vif. Therefore, analogous to HIV-1 Vif and A3G, SIVmac239 Vif interacts functionally with the N-terminal domain of human A3B.

To identify additional interacting residues within the N-terminal domain of human A3B, we performed a focused alanine scan of the ^{121}RLYYYW^{127} loop region upstream of the ^{128}ERD^{130} motif. The sensitivity of these mutants to SIVmac239 Vif was determined using the cotransfection assay described above. Apart from Y124A and Y125A, all other alanine substitutions affected the steady state levels of the A3B N-terminal domain to varying degrees as demonstrated by the expression levels in the absence of Vif (representative immunoblot in **Figure 2-2D** and quantification in **Figure 2-2G**). Although several of these NTD mutants were expressed at lower than WT levels, immunoblots indicate that amino acid substitutions R122A, L123A, Y126A, and W127A confer resistance to degradation by WT SIVmac239 Vif, while Y124A and Y125A remain sensitive (*e.g.*, compare band intensities for reactions with WT and SLQ mutant Vif for each A3B NTD construct). Taken together, these data show that SIVmac239 Vif requires several residues in N-terminal domain loop 7 for degradation of human A3B.

Mutagenesis of SIVmac239 Vif delineates human A3B-interacting residues

SIVmac239 Vif is more closely related to HIV-2 Vif than HIV-1 Vif, sharing 70% and 25% amino acid identity, respectively (**Figure 2-3A**). To determine critical regions of SIVmac239 Vif required for degradation of human A3B, we constructed single amino acid

mutants targeting potential A3-interacting residues. Several studies have mapped residues in HIV-1 Vif required for interaction with human A3F [99, 100], and these can be grouped into three interacting regions (shaded yellow in **Figure 2-3B-C**). In comparison to WT SIVmac239 Vif, all of the amino acid substitution derivatives informed by A3F-interacting regions 1 and 3 were similarly capable of promoting the degradation of human A3B with the exception of R18A (representative immunoblot in **Figure 2-3D** and quantification in **Figure 2-3G**). In comparison, substitutions in the A3F-interacting region 2, W73A and an insertion of a single Gly after P77 (P77+G), compromised human A3B degradation activity. Moreover, the majority of amino acid substitutions of human A3H-interacting residues [93, 96] such as C40A, C40F, W49A, Q62Δ and G64A retained the ability to degrade human A3B, whereas a minority (W49Δ and W51A/Δ) were compromised (**Figure 2-3E** and quantification in **Figure 2-3G**). These two sets of partial loss of function mutants are discussed below in the context of a structural model.

Interestingly, all SIVmac239 Vif amino acid substitution mutants, which represent A3G interacting residues in HIV-1 Vif [89, 91, 101, 144-146], lost the capacity to degrade human A3B (**Figure 2-3F** and quantification in **Figure 2-3G**). The largest stretch of A3G-interacting amino acids in HIV-1 Vif is ^{40}YRHHY^{44} [89]. Substitutions at any of the analogous positions in SIVmac239 Vif compromised human A3B degradation activity (*i.e.*, P43A, H44A, F45A, K46A, V47A, G48A). An additional A3G-interacting residue in HIV-1 Vif is K26 [91, 144], and substitution of the analogous lysine in SIVmac239 Vif to alanine (K27A), as well as another nearby positively charged residue (K30A), also abrogated human A3B degradation activity. Taken together, these mutagenesis results

indicate that multiple residues in SIVmac239 Vif are required for degrading human A3B, and these are analogous to residues in HIV-1 Vif required for degrading human A3G.

SIVmac239 Vif mutants show differential abilities to counteract human A3B, A3G, A3F, and A3H

To confirm the results from the cotransfection experiments described above and expand the scope of these studies to compare with other human APOBEC3 proteins, we selected three SIVmac239 Vif variants that showed compromised human A3B degradation capabilities and near WT expression levels (K27A, K30A, and H44A), and further tested their abilities to counteract A3-mediated restriction in dose-responsive HIV-1 single-cycle infectivity assays. Although human A3B is not a restriction factor of HIV-1 produced in T lymphocytes, it potently restricts virus produced in 293T cells with or without HIV-1 Vif [90, 140]. We therefore performed single-cycle infectivity assays in 293T cells with Vif-deficient HIV-1 complemented in trans with WT or a mutant SIVmac239 Vif and expressed together with human A3B, A3G, A3F, or A3H haplotype II (infectivity data in **Figure 2-4A**, representative immunoblots in **Figure 2-4B**, and immunoblot quantification in **Figure 2-4C**). Predetermined amounts of each A3 were used in order to reduce viral infectivity to >70% relative to the control reaction and enable proteins to be readily detectable by immunoblot (*i.e.*, no A3 and no Vif reactions). In comparison to these reactions, WT SIVmac239 Vif partly degrades A3B and completely or near completely degrades A3G, A3F, and A3H. As expected, SIVmac239 Vif causes corresponding recoveries in viral infectivity, with partial recovery for reactions with A3B and complete

(or near complete) recovery for those with A3G, A3F, and A3H. In comparison, all three SIVmac239 Vif mutants show a compromised ability to degrade human A3B, resulting in increased A3B packaging and decreased infectivity compared to WT SIVmac239 Vif. When tested against human A3G, the K27A mutant shows drastically compromised degradation and counteraction activities, indicating that this residue is also required for interaction with human A3G. The K30A and H44A substitutions also affect A3G degradation and counteraction, but the infectivity phenotypes are intermediate relative to those caused by WT SIVmac239 Vif and the K27A mutant. The three SIVmac239 Vif mutants retained partial A3F degradation activity but mediated near full recoveries in virus infectivity. In contrast, none of the three substitutions affected the ability of SIVmac239 Vif to degrade A3H, further showing that these mutants are fully active against one A3 enzyme and are likely to be true separation-of-function mutants.

DISCUSSION

The Vif protein encoded by SIVmac239 has been shown previously to have cross-species degradation capabilities against human A3B and A3G [90, 137, 138]. Neither of these activities is likely to contribute to the infection of its host, the rhesus macaque, yet this seemingly vestigial function was acquired and maintained through evolution. The degradation of human A3B by SIVmac239 Vif is particularly intriguing because human A3B is not an HIV-1 restriction factor in human T lymphocytes and is not targeted for degradation by HIV-1 Vif. Here we shed light on the molecular determinants of the cross-species interaction between SIVmac239 Vif and human A3B. We report key interacting

amino acid residues on both Vif and A3B. Our data indicate that SIVmac239 Vif exclusively targets the N-terminal domain of human A3B. Amino acid substitutions E128K D130K within the ^{128}ERD^{130} motif of human A3B, as well as single alanine substitutions of R122, L123, Y126, and W127 on the adjacent loop 7, confer resistance to SIVmac239 Vif mediated degradation. Interestingly, these potential interacting amino acids reside within a region of human A3B that is highly similar to human A3G (^{121}RLYYYWERD^{130} in A3B compared with ^{121}RLYYFWDPD^{130} in A3G), and this conserved loop region of A3G has been implicated by mutagenesis and molecular modeling to interact directly with HIV-1 Vif [113, 147, 148]. In addition, our mutagenesis studies targeting potential A3-interacting residues of SIVmac239 Vif revealed a panel of alterations that abrogated the human A3B-degradation phenotype (*i.e.*, R18A, K27A, K30A, P43A, H44A, F45A, K46A, V47A, G48A, W49Δ, W51A, W51Δ, W73A, and P77+G), suggesting that these residues contribute to the interaction with human A3B. Moreover, the majority of these human A3B-interacting residues map to or near known A3G-interacting regions of HIV-1 Vif (**Figure 2-5**). Testing a subset of these mutants against a panel of human A3 enzymes in infectivity assays confirmed that these substitutions specifically compromise the abilities of SIVmac239 Vif to degrade and counteract human A3B and A3G, to a lesser extent A3F, and not at all A3H. Overall, these results indicate that interaction surfaces are shared between SIVmac239 Vif-human A3B and HIV-1 Vif-human A3G.

Previous studies have demonstrated that the recruitment of CBF-β and other components of the E3 ligase complex, as well as the corresponding interacting residues within Vif, are highly conserved among various primate lentiviral Vif proteins [84, 87, 88,

132, 149, 150]. Therefore, SIVmac239 Vif likely shares an overall similar structure to HIV-1 Vif due to these functional and structural constraints despite low similarity (25%) at amino acid level. This inference is further supported by data showing genetic requirements for A3 protein degradation for the SIVmac239 ELOC-interacting motif (SLQ), predicted CBF-β-interacting residues (W7, W13, and W22), and predicted zinc-coordinating residues (C116) (*e.g.*, SLQ to AAA data in **Figure 2-1** and **Figure 2-2**; W7A, W13A, W22A, and C116A are quantified in **Figure 2-3G**; additional data not shown). Therefore, the human A3B-interacting residues of SIVmac239 Vif can be illustrated by highlighting the corresponding residues on the HIV-1 Vif crystal structure (**Figure 2-5A**). The resulting image suggests that the A3B-interacting residues cluster within a surface that is similar to the human A3G-interacting surface of HIV-1 Vif, and potentially even spanning a slightly larger surface area (compare **Figure 2-5A** and **Figure 2-5B**).

There are several possible explanations for why a functional interaction occurs between SIVmac239 Vif and human A3B in the absence of an apparent contemporary physiological context. One possibility is that the ability to degrade primate A3B arose as a necessary counterdefense in an ancestral simian lentivirus and that this activity has been maintained by a subset of present-day viruses including SIVmac239 Vif. This idea is supported by reports showing human A3B degradation by HIV-2 Vif (49) and by several different SIVsm Vif proteins (31). This functional relationship is also consistent with the relatively recent origin of SIVmac, which is thought to have occurred in captivity by cross-species transmission from a sooty mangabey (50). An alternative, albeit less likely explanation, is that the functional interaction between SIVmac239 Vif and human A3B

may be due to molecular mimicry with the Vif-binding region of A3G, which based on cross-species comparisons has a long evolutionary history of lentivirus restriction (40). This alternative is supported by strong conservation of negative charge at amino acid position 130 (D in human A3B, human A3G, and almost all primate equivalents including the sooty mangabey homologs). However, this alterative is refuted by divergence at amino acid position 128, which is variable among primates A3B and A3G enzymes. For instance, position 128 is a positively charged lysine in rhesus macaque A3G and a negatively charged aspartate in human A3G, whereas the corresponding position in rhesus macaque and human A3B is a negatively charged glutamate. Further studies are needed such as a full matrix of cross-species virus/host comparisons to fully distinguish between these alternatives and additional possibilities such as Vif functional promiscuity within SIVmac/sm viral lineages.

Understanding the molecular interactions between SIVmac239 Vif and human A3B may also lead to the development of novel cancer therapies. Human A3B has been shown to cause mutations in multiple types of cancer and contribute to the development of drug resistance in mouse models [39, 117, 118]. A3B is therefore likely to have a major role in driving tumor evolution and has become both a diagnostic and a therapeutic target. We previously proposed using SIVmac239 Vif as a molecular probe to interrogate A3B function *in vivo* [137] but a direct application of this idea is complicated by promiscuous A3 degradation activity. Therefore, a better understanding of the interactions between SIVmac239 Vif and human A3B may help to engineer the requisite specificity for such an application. Indeed, our data show that the human A3B-interacting surface on SIVmac239

Vif is likely quite distinct and separable from the human A3F- or A3H-interacting surfaces. However, the large overlap between the human A3B- and A3G-interacting surfaces on SIVmac239 Vif is still a formidable hurdle toward engineering perfect specificity. Nevertheless, the fact that three Vif mutants did not counter A3B and A3G identically suggests that this goal may be achieved with additional studies and particularly with comparative structural studies of multiple different Vif-A3 complexes.

MATERIALS AND METHODS

A3 expression constructs

The constructs expressing huA3G (NM021822), huA3B (NM004900), rhA3G (AY331716), and rhA3B (JF714485) with carboxy(C)-terminal 3× hemagglutinin (HA) tags in pcDNA3.1(+) vector (Invitrogen) have been reported [90]. The pcDNA3.1(+) constructs expressing C-terminally 3×HA-tagged NTD and CTD of huA3B have also been described [151]. Mutants of human A3B (R122A, L123A, Y124A, Y125A, Y126A, W127A, E128K, D130K, and E128K D130K) were created by site-directed mutagenesis using forward primers 5'-ACC ATC TCT GCC GCC GCC CTC TAC TAC TAC TG-3', 5'-TCT CTG CCG CCC GCG CCT ACT ACT ACT GGG-3', 5'-TCT GCC GCC CGC CTC GCC TAC TAC TGG GAA AG-3', 5'-GCC GCC CGC CTC TAC GCC TAC TGG GAA AGA GA-3', 5'-CCG CCC GCC TCT ACT ACG CCT GGG AAA GAG ATT ACC-3', 5'-GCC CGC CTC TAC TAC TAC GCG GAA AGA GAT TAC CGA AG-3', 5'-GCC TCT ACT ACT ACT GGA AAA GAG ATT ACC GAA GG-3', 5'-CTA CTA CTA CTG GGA AAG AAA GTA CCG AAG GGC GCT CTG C-3', 5'-CGC CTC TAC TAC TAC

TGG AAA AGA AAG TAC CGA AGG GCG CTC TGC-3' and corresponding reverse primers, respectively, verified by DNA sequencing, and used for transient expression in 293T cells. The constructs expressing untagged huA3F (NM145298) and huA3H haplotype II (FJ376614.1) in pcDNA3.1(+) vector have been reported [141, 152].

Vif expression constructs

The lentiviral Vif proteins from HIV-1 IIIB (EU541617) and SIVmac239 (AY588946) were codon-optimized (GenScript Corporation) and expressed with a C-terminal MYC tag from pVR1012 [141]. Mutants of SIVmac239 Vif (W7A, W13A, P16A, E17A, R18A, R21A, W22A, K27A, K30A, K38A, C40A, C40F, P43A, H44A, F45A, K46A, V47A, G48A, W49A, W49Δ, W51A, W51Δ, Q62Δ, F64A, W73A, P77+G, C116A, R173A, D174A, N175A, R176A, R177A, and G178A) were created by site-directed mutagenesis using forward primers 5'-GAG GAA GAG AAG CGG GCG ATC GCA GTG CCT AC-3', 5'-ATC GCA GTG CCT ACC GCG CGC ATT CCA GAG AG-3', 5'-CTA CCT GGC GCA TTG CAG AGA GGC TCG A-3', 5'-TGG CGC ATT CCA GCG AGG CTC GAG AGG-3', 5'-GGC GCA TTC CAG AGG CGC TCG AGA GGT GGC-3', 5'-CCA GAG AGG CTC GAG GCG TGG CAT AGC CTC AT-3', 5'-AGA GAG GCT CGA GAG GGC GCA TAG CCT CAT CAA G-3', 5'-GAG AGG TGG CAT AGC CTC ATC GCG TAC CTT AAA TAT AAG ACC AA-3', 5'-GCA TAG CCT CAT CAA GTA CCT TGC ATA TAA GAC CAA AGA CCT GCA G-3', 5'-AGA CCA AAG ACC TGC AGG CAG TGT GCT ATG TGC CCC-3', 5'-CAA AGA CCT GCA GAA AGT GGC CTA TGT GCC CCA TTT TAA G-3', 5'-AAA GAC CTG CAG AAA GTG TTC TAT GTG CCC CAT

TTT AAG-3', 5'-CAG AAA GTG TGC TAT GTG GCC CAT TTT AAG GTG G-3', 5'-AAA GTG TGC TAT GTG CCC GCT TTT AAG GTG GGA TGG GC-3', 5'-GTG CTA TGT GCC CCA TGC TAA GGT GGG ATG GGC C-3', 5'-AAG TGT GCT ATG TGC CCC ATT TTG CGG TGG GAT GGG C-3', 5'-GTG CCC CAT TTT AAG GCG GGA TGG GCC TGG-3', 5'-CCC ATT TTA AGG TGG CAT GGG CCT GGT GGA C-3', 5'-GCC CCA TTT TAA GGT GGG AGC GGC CTG GTG G-3', 5'-GCC CCA TTT TAA GGT GGG AGC CTG GTG GA-3', 5'-GGT GGG ATG GGC CGC GTG GAC CTG TTC C-3', 5'-GGT GGG ATG GGC CTG GAC CTG TTC CA-3', 5'-GTG ATT TTT CCC TTG GAG GGC TCC CAC CTG-3', 5'-CCT TGC AGG AGG CCT CCC ACC TGG A-3', 5'-GGA AGT TCA GGG ATA CGC GCA CCT GAC TCC TGA G-3', 5'-TGG CAC CTG ACT CCT GGA GAG AAA GGC TGG CTG-3', 5'-CTC CAC ATA CTT CCC CGC TTT CAC CGC CGG TGA G-3', 5'-GAA GCA GTG GCG CGC CGA TAA CCG GCG C-3', 5'-GTG GCG CCG CGC TAA CCG GCG CG-3', 5'-AGC AGT GGC GCC GCG ATG CCC GGC GCG G-3', 5'-GGC GCC GCG ATA ACG CGC GCG GGC TG-3', 5'-CCG CGA TAA CCG GGC CGG GCT GAG GAT G-3', 5'-ATA ACC GGC GCG CGC TGA GGA TGG C-3' and corresponding reverse primers, respectively, verified by DNA sequencing, and used for transient expression in 293T cells.

Cell lines

293T cells were maintained in Dulbecco's modified Eagle medium (DMEM) containing 10% fetal bovine serum (FBS) and 0.5% penicillin-streptomycin (P/S). CEM-GFP cells were maintained in RPMI medium with 15% FBS and 0.5% P/S.

Vif degradation experiments

293T cells were transfected with pcDNA3.1(+)-A3-HA or empty vector, along with pVR1012-Vif-MYC or empty vector, using polyethyleneimine (PEI; Polysciences, Inc.) The following amounts of A3 and Vif expression constructs were transfected: 200 ng A3 and 200 ng Vif for **Figure 2-1A**, 100 ng A3B, 200 ng A3G and 25, 50, or 100 ng Vif for **Figure 2-1B**, 200 ng A3 and 200 or 400 ng Vif for **Figure 2-2B** and **2D**, 200 ng A3 and 200, 300, or 400 ng Vif for **Figure 2-2C** and **Figure 2-3**. After 48 hours, cells were harvested for immunoblot analysis.

Immunoblotting experiments

Cell and virus particle lysates were prepared by resuspension of washed cell pellets directly in 2.5× Laemmli sample buffer. Proteins were separated using discontinuous sodium dodecyl sulfate polyacrylamide gel electrophoresis (SDS-PAGE) and transferred to polyvinylidene difluoride (PVDF) membranes (Millipore). HA-tagged A3 proteins were detected using monoclonal mouse anti-HA (BioLegend). Human A3F was detected using a polyclonal rabbit anti-A3F serum 675 created by contracted immunization of animals (Covance) with a peptide corresponding to the last 30 residues of the protein. A3H proteins were detected using previously generated monoclonal mouse anti-A3H (P1D8) [142]. MYC-tagged Vif proteins were detected using polyclonal rabbit anti-MYC (Sigma-Aldrich). Tubulin was detected using a monoclonal mouse anti-α-Tubulin antibody (Covance). HIV-1 Gag was detected using monoclonal mouse anti-HIV-1 p24 (NIH AIDS

Reagent Program) [153]. Immunoblots were quantified using ImageJ.

HIV single-cycle infection with replication-proficient virus

The single-cycle infection assay was carried out as described [90]. 293T cells were transfected (TransIT-LT1; Mirus) with 1 μg of a Vif-deficient HIV proviral expression construct along with 0, 25, or 50 ng of a Vif expression construct and 25 ng of an A3 expression construct. After 48 hours, CEM-GFP HIV-1 reporter cells were infected with virus-containing supernatants, and cell and virus particle lysates were prepared for immunoblotting.

Flow cytometry

HIV-infected CEM-GFP cells were prepared for flow cytometry by fixation using 4% paraformaldehyde in phosphate-buffered saline (PBS). GFP fluorescence was measured on a BD FACS Canto II flow cytometer. Data were analyzed using FlowJo flow cytometry analysis software (version 8.8.6). The fraction of GFP+ cells among all live cells was quantified for each sample.

Sequence alignments and structural images

All amino acid sequences were aligned using Clustal Omega. The amino acid sequences of human A3B, human A3G, HIV-1 IIIB Vif, HIV-2 ROD Vif, SIVmac239 Vif correspond to Genbank accession numbers NM004900, NM021822, EU541617, P04595, and AY588946, respectively. The secondary structure elements of human A3B-NTD, human

A3B-CTD, and human A3G-CTD were annotated based on reported crystal structures [51, 52, 54]. The secondary structural elements of human A3G-NTD were predicted based on a crystal structure of the homologous rhesus macaque A3G-NTD [53]. Structural images were generated with PyMOL (pymol.org).

ADDITIONAL CONTRIBUTIONS

We thank D. Salamango for comments on the manuscript, and B. Wei and J. Lalli for assistance with plasmid constructions. This work was supported by NIAID R37 AI064046 and NCI R21 CA206309. J.W. received partial salary support from an Interdisciplinary Doctoral Fellowship from the University of Minnesota Graduate School. R.S.H. is the Margaret Harvey Schering Land Grant Chair for Cancer Research, a Distinguished McKnight University Professor, and an Investigator of the Howard Hughes Medical Institute.

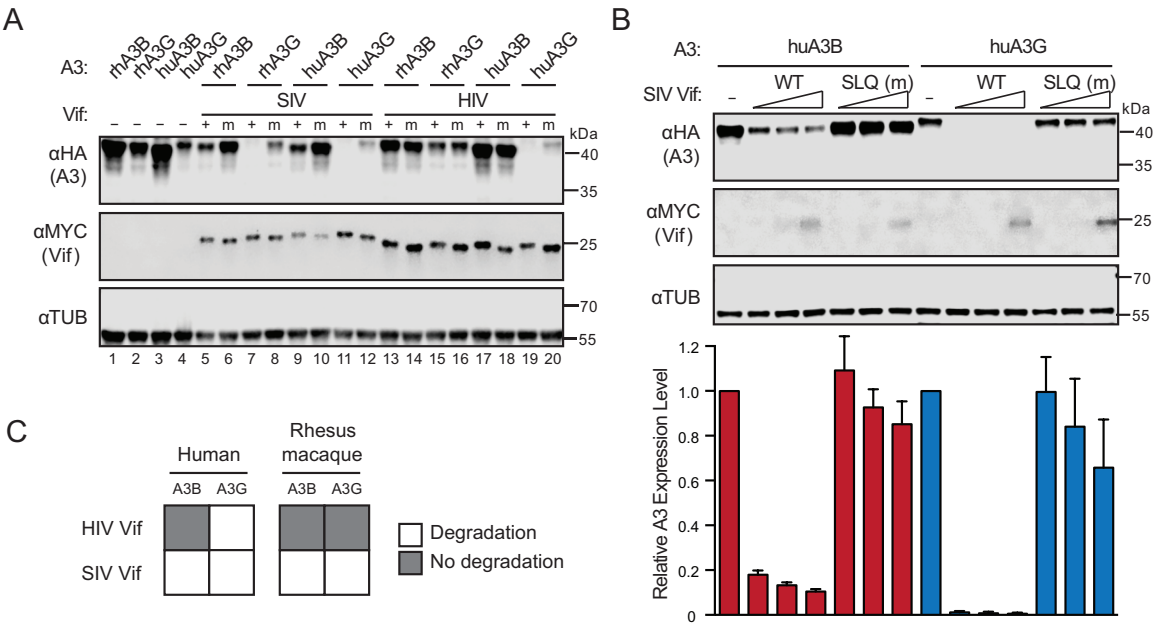

Figure 2-1. SIVmac239 Vif degrades both human A3B and A3G.

(**A**) Immunoblots of 293T cells expressing the indicated rhesus macaque (rh) or human (hu) A3 enzymes together with SIVmac239 Vif, HIV-1 IIIB Vif or SLQ-AAA mutant (m) derivatives. A3 enzymes were detected using an anti-HA antibody for a C-terminal HA epitope tag. Vif was detected using an anti-MYC antibody for a C-terminal MYC epitope tag, and anti-tubulin-alpha was used as a loading control.

(**B**) Bar graphs for quantification (bottom) of immunoblots (top and not shown) of 293T cells expressing fixed amounts of the indicated human A3 enzymes together with an empty vector control (-) or varying amounts of SIVmac239 Vif (WT) or a SLQ-AAA mutant (m) derivative (analyzed with the same antibodies as panel A). A3 expression levels were determined by quantifying band intensities normalized to those of the corresponding Vif-null condition. Each error bar represents the standard deviation of three biological replicates.

(**C**) Schematic summarizing the immunoblot results from panels A and B. Open squares represent a functional Vif-A3 interaction evidenced by A3 degradation.

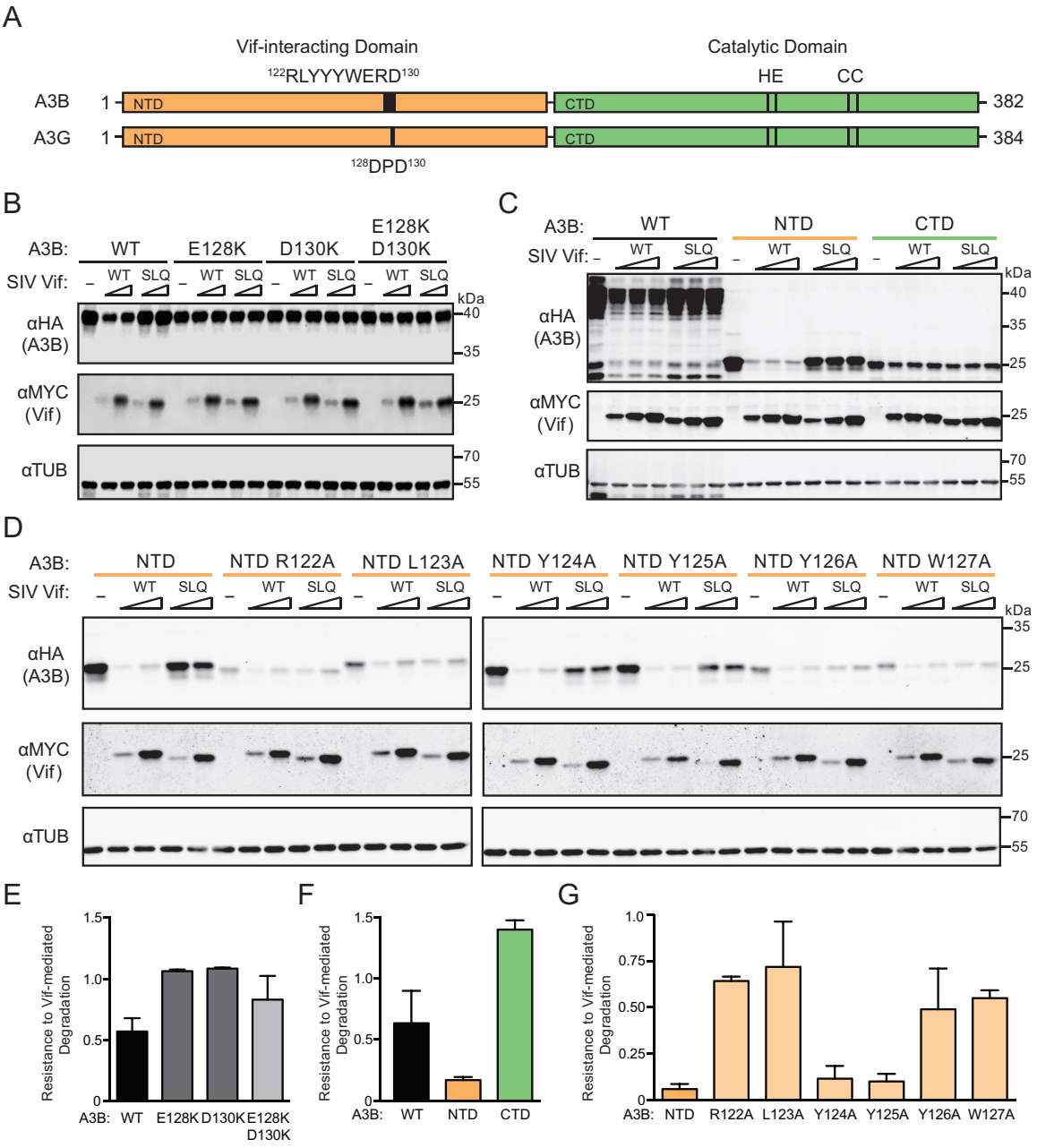

Figure 2-2. SIVmac239 Vif interacts with the N-terminal domain of human A3B.

(**A**) A schematic of human A3B and A3G with N- and C-terminal halves shaded orange and green, respectively. N-terminal Vif-interacting amino acids and C-terminal catalytic domain residues are labeled.

(**B**) Immunoblots of 293T cells expressing full-length human A3B, WT or the indicated mutants, together with SIVmac239 Vif or a SLQ-AAA derivative (SLQ). A3B was detected using an anti-HA antibody for a C-terminal HA epitope tag. Vif was detected using an anti-MYC antibody for a C-terminal MYC epitope tag, and anti-tubulin-alpha was used as a loading control.

(**C**) Immunoblots of 293T cells expressing full-length human A3B (WT), the N-terminal half (NTD), or the C-terminal half (CTD) together with an empty vector (-), SIVmac239 Vif, or a SLQ-AAA derivative. Analyzed with the same antibodies as panel B.

(**D**) Immunoblots of 293T cells expressing the N-terminal half of human A3B (NTD) or the indicated single amino acid substitution mutants together with an empty vector (-), SIVmac239 Vif, or a SLQ-AAA derivative. Analyzed with the same antibodies as panel B.

(**E**, **F**, and **G**) Quantification of data in panels B, C, and D, respectively. The A3B level of each immunoblot lane was first normalized to tubulin, and then resistance-to-degradation values were calculated as the normalized A3B level in the presence of WT SIVmac239 Vif relative to SIVmac239 Vif SLQ mutant. Each histogram bar reports the mean +/- the difference between two independent reactions (panels E and G) or the mean +/- the standard deviation of three independent reactions (panel F).

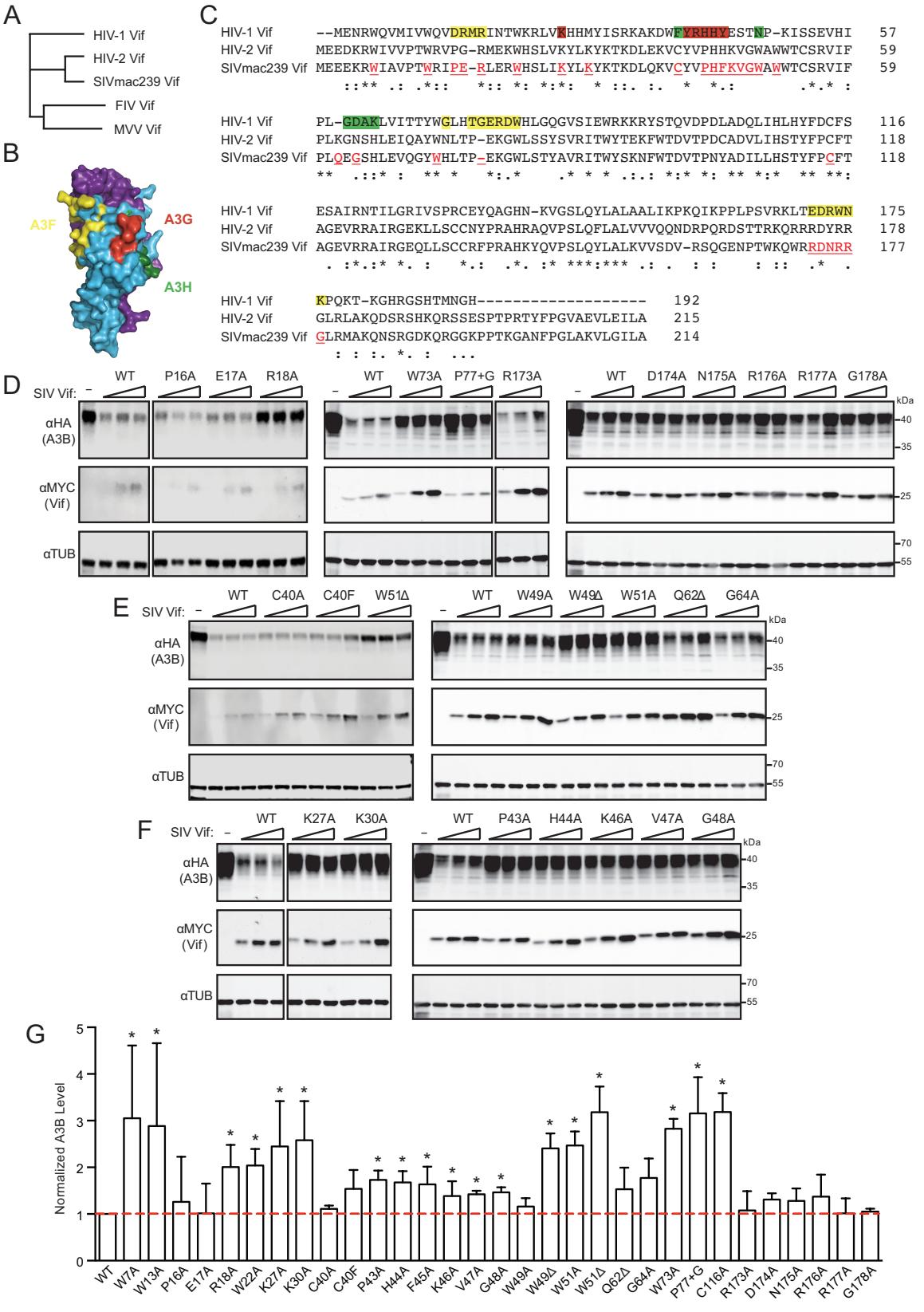
A
HIV-1 Vif
HIV-2 Vif
SIVmac239 Vif
FIV Vif
MVV Vif
B
A3F
A3G
A3H
C
HIV-1 Vif --MENRWQVMIVWQVDRMRINTWKRLVKHHMYISRKAKDWFYRHHYESTNP-KISSEVHI 57
HIV-2 Vif MEEDKRWIVVPTWRVPG-RMEKWHSLVKYLKYKTKDLEKVCYVPHHKVGWAWWTCSRVIF 59
SIVmac239 Vif MEEEKRWIAVPTWRIPE-RLERWHSLIKYLKYKTKDLQKVCYVPHFKVGWAWWTCSRVIF 59
HIV-1 Vif PL-GDAKLVITTYWGLHTGERDWHLGQGVSIEWRKKRYSTQVDPDLADQLIHLHYFDCFS 116
HIV-2 Vif PLKGNSHLEIQAYWNLTP-EKGWLSSYSVRITWYTEKFWTDVTPDCADVLIHSTYFPCFT 118
SIVmac239 Vif PLQEGSHLEVQGYWHLTP-EKGWLSTYAVRITWYSKNFWTDVTPNYADILLHSTYFPCFT 118
HIV-1 Vif ESAIRNTILGRIVSPRCEYQAGHN-KVGSLQYLALAALIKPKQIKPPLPSVRKLTEDRWN 175
HIV-2 Vif AGEVRRAIRGEKLLSCCNYPRAHRAQVPSLQFLALVVVQQNDRPQRDSTTRKQRRRDYRR 178
SIVmac239 Vif AGEVRRAIRGEQLLSCCRFPRAHKYQVPSLQYLALKVVSDV-RSQGENPTWKQWRRDNRR 177
HIV-1 Vif KPQKT-KGHRGSHTMNGH------------------- 192
HIV-2 Vif GLRLAKQDSRSHKQRSSESPTPRTYFPGVAEVLEILA 215
SIVmac239 Vif GLRMAKQNSRGDKQRGGKPPTKGANFPGLAKVLGILA 214
D
SIV Vif:
WT P16A E17A R18A
WT W73A P77+G R173A
WT D174A N175A R176A R177A G178A
αHA (A3B)
αMYC (Vif)
αTUB
kDa
40
35
25
70
55
E
SIV Vif:
WT C40A C40F W51Δ
WT W49A W49Δ W51A Q62Δ G64A
αHA (A3B)
αMYC (Vif)
αTUB
kDa
40
35
25
70
55
F
SIV Vif:
WT K27A K30A
WT P43A H44A K46A V47A G48A
αHA (A3B)
αMYC (Vif)
αTUB
kDa
40
35
25
70
55
G
Normalized A3B Level
0
1
2
3
4
5
WT W7A W13A P16A E17A R18A W22A K27A K30A C40A C40F P43A H44A F45A K46A V47A G48A W49A W49Δ W51A W51Δ Q62Δ G64A W73A P77+G C116A R173A D174A N175A R176A R177A G178A

Figure 2-3. Human A3B degradation capabilities of SIVmac239 Vif and mutant derivatives.

(**A**) A phylogenetic tree showing the relationship between SIVmac239 Vif, HIV-1 IIIB Vif, and related lentiviral Vif proteins.

(**B**) Schematic of HIV-1 Vif (blue) and CBF-β (purple) highlighting known A3F (yellow), A3G (red), and A3H (green) interacting amino acid residues (Vif-CBF-β structure from pdb 4N9F).

(**C**) Amino acid sequence alignment of HIV-1 IIIB Vif, HIV-2 ROD Vif, and SIVmac239 Vif. Established A3F, A3G, and A3H interacting residues of HIV-1 Vif are highlighted with the same colors as in panel B. Asterisks and colons indicate identical and similar residues, respectively. Red-shaded and underlined SIVmac239 Vif residues were targeted by site-directed mutagenesis.

(**D**-**F**) Immunoblots of 293T cells expressing full-length human A3B and an empty vector (-) or three different amounts of SIVmac239 Vif (WT) or the indicated mutant derivative. A3B was detected using an anti-HA antibody for a C-terminal HA epitope tag. Vif was detected using an anti-MYC antibody for a C-terminal MYC epitope tag, and anti-tubulin-alpha was used as a loading control.

(**G**) Quantification of immunoblots in Figures 2-3D-F and additional data not shown. The A3B level of each lane was first normalized using the loading control, tubulin, and then against the A3B levels in the presence of WT SIVmac239 Vif. Each histogram bar reports mean +/- the standard deviation of at least three independent reactions. The asterisks (*) represent statistically significant differences from WT ($p \leq 0.05$, two-sample t-test). Red

dashed line indicates normalized A3B levels of 1, in the presence of WT SIVmac239 Vif.

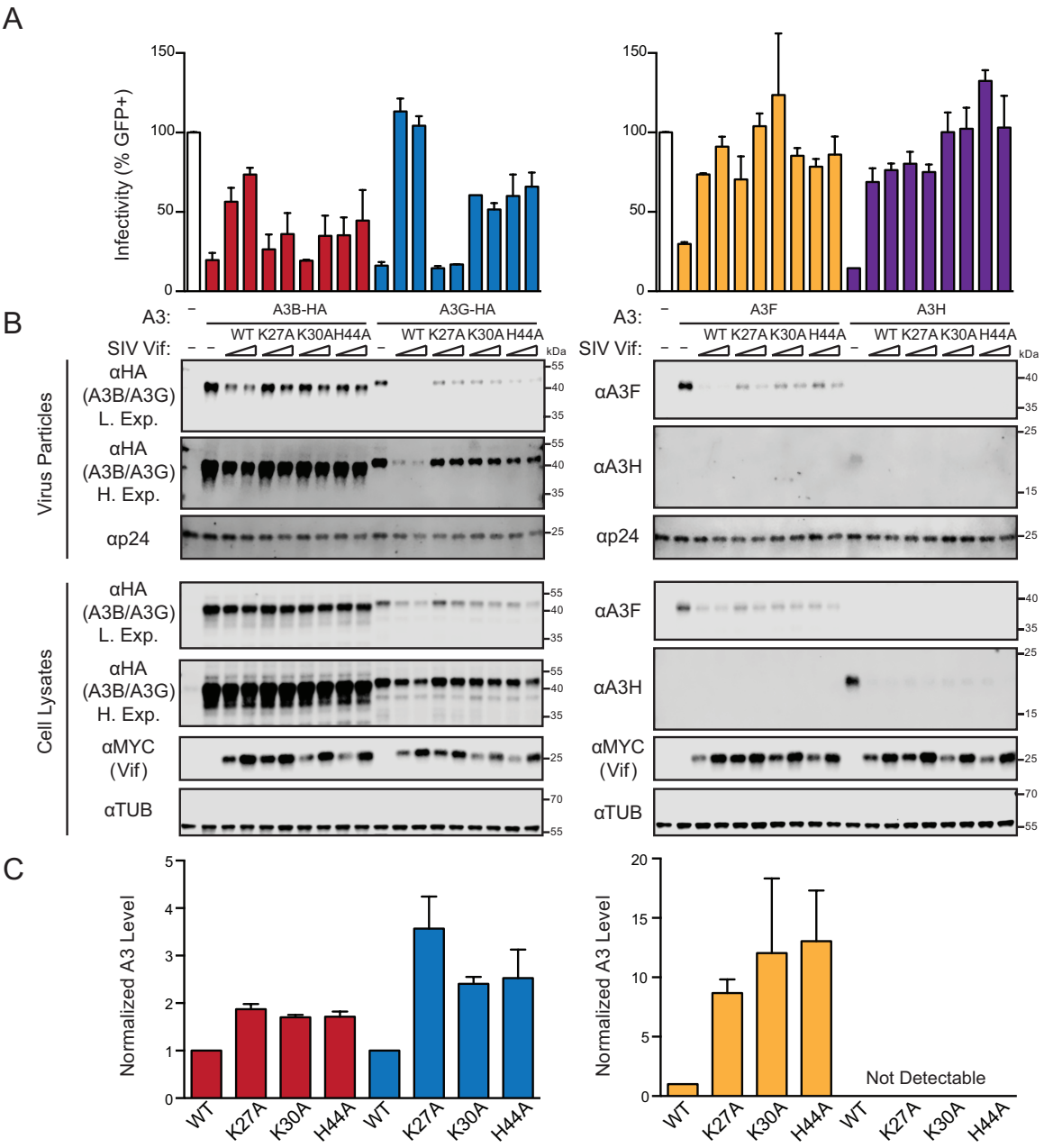

Figure 2-4. The abilities of SIVmac239 Vif and mutant derivatives to counteract restriction by human A3B, A3G, A3F, and A3H.

(**A**) Bar graphs depicting relative infectivity of virus particles produced from 293T cells expressing the indicated A3 and Vif constructs. Infectivity is measured as the percentage of infected/fluorescent CEM-GFP reporter cells, and values are normalized to those of the

A3-null condition (open bars, duplicated to position above the relevant lanes of the corresponding immunoblots). Each histogram bar represents the mean of two separate CEM-GFP infections, and the error bars represent the difference between these two values. The data on the left and right are from the same representative experiment, and are only separated due to the necessity of requiring two separate immunoblots to analyze all of the reactions.

(**B**) Immunoblots of virus particles and 293T cell lysates expressing the indicated constructs. A3B and A3G enzymes from virus particles and cell lysates were detected using an anti-HA antibody for a C-terminal HA epitope tag. A3F and A3H enzymes from virus particles and cell lysates were detected using specific anti-A3F and anti-A3H antibodies, respectively. Vif from cell lysates was detected using an anti-MYC antibody for a C-terminal MYC epitope tag. Anti-tubulin-alpha and anti-p24 (Gag) are loading controls for cell lysates and virus particles, respectively.

(**C**) Quantification of virus particles immunoblot data in Figure 2-4B. The color scheme matches that in panel A with A3B, A3G, A3F, and A3G represented by red, blue, orange, and purple, respectively. The A3 level of each lane was first normalized using the loading control, tubulin, and then against the A3 levels in the presence of WT SIVmac239 Vif. Each histogram bar reports mean +/- the difference between two independent reactions.

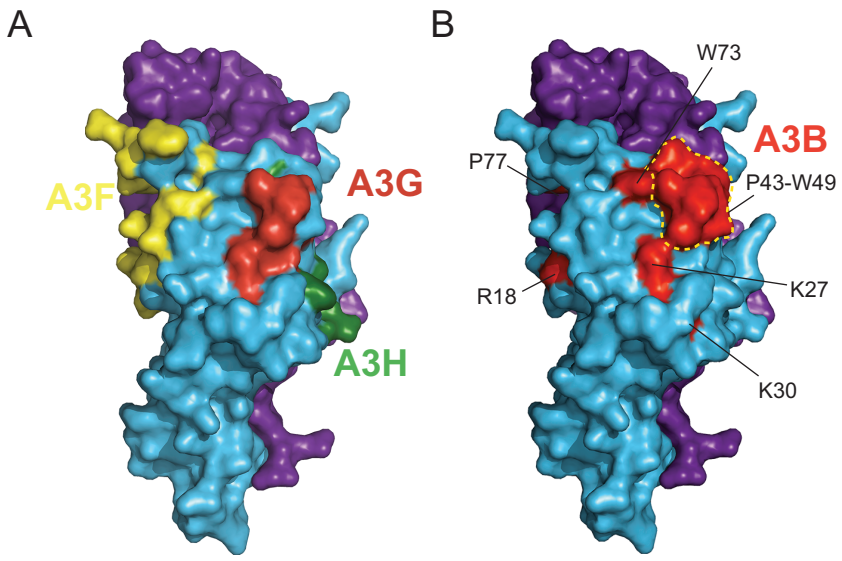

Figure 2-5. Structural depiction of the human A3B interacting region of SIVmac239 Vif.

(**A**) A larger representation of the schematic in Figure 2-3B showing HIV-1 Vif (blue) and CBF-β (purple), and highlighting known A3F (yellow), A3G (red), and A3H (green) interacting amino acid residues (pdb 4N9F).

(**B**) Human A3B-interacting residues of SIVmac239 Vif highlighted upon the HIV-1 Vif (blue)-CBF-β (purple) x-ray crystal structure (pdb 4N9F). The red-shaded, A3B-interacting region (R18, K27, K30, P43-W49, W51, W73, and P77) largely overlaps with the red-shaded, A3G-interacting region in panel A.

CHAPTER 3

The Role of RNA in HIV-1 Vif-Mediated Degradation of APOBEC3H

Adapted from submitted manuscript: Wang J., K. Shi, J.T. Becker, K.V. Lauer, D.J. Salamango, H. Aihara, R.S. Harris, & N.M. Shaban. (2019) The role of RNA in HIV-1-mediated degradation of APOBEC3H

Authors' Contributions

J. Wang, N.M. Shaban. and R.S. Harris conceived and designed the studies. J. Wang performed Vif degradation experiments and split GFP studies. N.M. Shaban and K. Shi purified and crystallized A3H. K. Shi determined the structure. J.T. Becker performed live cell imaging experiments. J. Wang, J.T. Becker, K.V. Lauer, N.M. Shaban, D.J. Salamango and N.M. Shaban created DNA constructs. R.S. Harris, H. Aihara and N.M. Shaban supervised the project. J. Wang, R.S. Harris, and N.M. Shaban drafted the manuscript with contributions from all authors in figure preparation and revisions.

SUMMARY

A3H is unique among family members by dimerization through cellular and viral duplex RNA species. RNA binding is required for localization of A3H to the cytoplasmic compartment, for efficient packaging into nascent HIV-1 particles, and ultimately for effective virus restriction activity. Here we compared WT human A3H and RNA binding mutants to ask whether RNA may be a factor in the functional interaction with HIV-1 Vif. We used x-ray crystallography, immunoblotting, live cell imaging, and split green fluorescence protein (GFP) reconstitution approaches to assess the capability of HIV-1 Vif to promote the degradation of WT A3H in comparison to RNA binding mutants. The results combined to show that RNA is not strictly required for Vif-mediated degradation of A3H, and that RNA and Vif are likely to bind this single domain DNA cytosine deaminase on physically distinct surfaces. However, a subset of the results also indicated that the A3H degradation process may be affected by A3H protein structure, subcellular localization, and differences in the constellation of A3H interaction partners suggesting additional factors may also influence the fate and functionality of this host-pathogen interaction.

INTRODUCTION

The human APOBEC3 family consists of seven members, namely A3A, A3B, A3C, A3D, A3F, A3G, and A3H (reviewed by [31-33]). These enzymes have all exhibited ssDNA cytosine deamination activity in a variety of assays and are expressed at varying levels in the cytoplasmic compartment of different cell types. At least five of these deaminases, A3C-H, are expressed in CD4-positive T lymphocytes and capable of restricting the replication of HIV-1 through deamination-dependent and deamination-independent mechanisms. Virus restriction minimally requires nucleic acid binding activity in order to enter viral particles (RNA), deaminate viral cDNA replication intermediates (DNA), and impede reverse transcription (RNA and DNA). The virion infectivity factor, Vif, provides the primary A3 counterdefense mechanism for HIV-1 and related lentiviruses (reviewed by [31-33]). Vif heterodimerizes with the cellular transcription co-factor CBF-β and nucleates the assembly of an E3 ubiquitin ligase complex that directly binds and targets A3 proteins for polyubiquitination and proteasomal degradation [84, 85, 131-136]. Mutagenesis studies have shed light on some of the molecular determinants of the A3-Vif interaction. For instance, residue F39 of Vif is specifically required for interacting with A3H because changing it to valine results in a separation-of-function variant that still degrades A3G and A3F but no longer degrades A3H [93, 96]. For A3H, α3 and α4 helices have been implicated in binding to Vif with D121K on α4 conferring resistance to HIV-1 Vif-mediated degradation [106-108, 127, 128, 154].

RNA has multiple roles in the antiviral activities of A3 enzymes. First, RNA binding is a key determinant in cytoplasmic localization of several A3 family members

[151, 155-160]. The clearest example is human A3H where disruption of RNA binding residues causes a simultaneous disruption of cytoplasmic localization [50, 159]. Similar observations have been made for various A3G and A3F mutants but the precise RNA binding mechanism has yet to be determined for these related enzymes [47, 151, 161]. Second, RNA binding is required for the packaging of A3G, A3F, and A3H into viral particles and subsequent antiviral activity [50, 62-72]. In particular, CLIP-seq (cross-linking immunoprecipitation coupled to next generation sequencing) experiments with A3F, A3G, and A3H have indicated preferential binding to viral RNA over cellular RNA, which is likely to facilitate packaging into virions [71]. Last, but not least, a proportion of the DNA deaminase-independent activities of A3F, A3G, and A3H can be attributed to the RNA binding properties of these enzymes exerting a steric block to DNA synthesis by the viral reverse transcriptase [50, 75-82].

A3H crystal structures have combined to demonstrate an evolutionarily conserved dimerization mechanism mediated by duplex RNA [42, 49, 50]. Multiple structural elements in A3H create an extensive, positively charged patch that binds strongly to duplex RNA. For human A3H, the RNA binding region is comprised of amino acids in loop 1 (L1 R18), loop 7 (L7 H114 and W115), and α-helix 6 (α6 R171, A172, R175, R176, and R179) [50]. Amino acid substitutions of several of these residues (R18E, H114A, W115A, A172E, RR175/6EE, and R179E) cause perturbations in cytoplasmic localization, encapsidation, and Vif-deficient HIV-1 restriction [50, 159]. Moreover, a human A3H triple mutant, R115A, R175E, and R176E, has all of these activities compromised and is monomeric with compromised RNA binding ability [50].

Here, we investigated the role of RNA in HIV-1 Vif-mediated degradation of human A3H. First, x-ray crystallography was used to determine the structure of a monomeric, RNA-binding defective variant of human A3H (triple mutant above plus a catalytic glutamate substitution). Second, immunoblots of cellular extracts were used to compare the Vif-susceptibility of WT A3H and a panel of RNA binding mutants. Third, live cell imaging approaches were used to quantify the kinetics of Vif-mediated degradation of WT A3H versus select RNA binding mutants. Finally, a split GFP reconstitution system was used to show that HIV-1 Vif is not capable of disrupting RNA-mediated A3H dimerization in living cells. Overall, the results of these experiments support a model in which Vif targets a surface on A3H that is distinct from the RNA-binding region.

RESULTS

Structure of an A3H mutant defective in binding RNA

The x-ray structures of human, chimpanzee, and pig-tailed macaque A3H revealed a novel dimerization mechanism in which two monomers are united by binding to opposing sides of the same duplex RNA [42, 49, 50] (*e.g.*, human A3H in **Figure 3-1A**). Several residues in A3H loop 1, loop 7, and helix 6 combine to strongly bind duplex RNA, including W115 from each protomer that stacks with the RNA nucleobases. Mutating these residues results in monomeric enzymes defective in RNA binding and, surprisingly, hyperactive for ssDNA cytosine deamination [50]. For instance, a triple mutant with W115A in loop 7 and R175E and R176E in helix 6 showed a monomeric size exclusion profile and a large increase in ssDNA deaminase activity [50] (conservation shown in **Figure 3-1B**). This triple mutant

combines mutations that have previously been shown to cause defects in cytoplasmic localization, packaging into nascent HIV-1 particles, and restricting the infectivity of Vif-deficient HIV-1 virions, which are all metrics of A3H RNA binding activity [50].

To better understand these A3H RNA binding activities and assess potential relevance in the interaction with HIV-1 Vif, we sought to determine the structure of a triple mutant of A3H haplotype II (residues 1-183) that no longer binds RNA. This construct includes three amino acid substitution mutations that combine to prevent RNA binding, W115A, R175E, and R176E, as well as a substitution of the catalytic glutamate E56A to prevent toxicity in *E. coli* [50]. A His6-SUMO-A3H mutant construct was expressed in *E. coli* and purified using metal affinity and size-exclusion chromatography. The protein was immediately screened for crystallization and a structure was determined at 3.2 Angstroms (structural statistics in **Table 3-1**). The overall structure of this monomeric construct is similar to the RNA bound form of A3H (superposition in **Figure 3-1C**). Core structural elements and many of the loop regions adopted near-identical conformations. In comparison, the loop 1, loop 7, helix 4 (connected to loop 7), and helix 6 regions adopted slightly different positions. For instance, helix 4 was tilted by several degrees. This slightly different conformation may be relevant to binding HIV-1 Vif, which prior studies have shown interacts with amino acids in A3H helices 3 and 4 including D121 [106-108] (positions shaded yellow in **Figure 3-1D**; considered again below in **Discussion**).

A subset of A3H RNA-binding residues are required for functional interaction with Vif

Most naturally occurring A3H variants including haplotype II are sensitive to Vif-mediated degradation [93, 94, 96, 106, 127, 128, 142]. The WT construct used here is A3H haplotype II splice variant 1-183. To ask whether RNA binding-defective proteins are susceptible or resistant to Vif-mediated degradation, a panel of mutants was co-transfected into 293T cells with 0.5 μg or 1.0 μg of HIV-1 LAI Vif (WT) or a degradation-defective mutant (F39V) and, after a 48-hour incubation, protein levels were analyzed by immunoblotting whole cell extracts (representative blots in **Figure 3-2A** with quantification in **2B**). As controls, expression of WT Vif decreases levels of WT A3H as well as those of an A3H E56A catalytic mutant by approximately 50%, and Vif F39V is defective in WT A3H degradation (similar to previous observations [50, 127]). As an additional control, A3H D121K resists degradation as evidenced by similar band intensities with WT Vif and the F39V mutant (again similar to previous observations [106, 108]).

In comparison, A3H RNA binding-defective mutants showed either Vif-sensitive or Vif-resistant phenotypes. These different phenotypes were even observed for mutants within the same surface region of the protein. For instance, A3H helix 6 mutants A172E, R175E, and R179E showed a WT-like Vif sensitivity, whereas R176E appeared fully resistant to Vif-mediated degradation (representative blots in **Figure 3-2A** with quantification in **2B**). A3H loop 7 mutants, H114A and W115A, showed completely resistant phenotypes, whereas A3H loop 1 R18E retained a WT-like Vif sensitivity. Based on single mutant phenotypes, not surprisingly, the monomeric A3H triple mutant was also

resistant to Vif-mediated degradation and this property was unchanged by adding an E56A catalytic glutamate substitution. Similar results were obtained for the Vif protein of a different HIV-1 strain (IIIB) with previously demonstrated hyperfunctional amino acid substitutions [96] showing strong degradation of WT A3H and little degradation activity with the monomeric A3H triple mutant (**Figure 3-2C**). These additional results are notable because the hyperfunctional Vif protein caused degradation of almost all cellular A3H and even showed partial activity against A3H D121K (all results in this panel are in comparison to a Vif variant, hypo, that has F39V as above and no A3H degradation activity as reported previously [94, 96]). These results are summarized by color coding phenotypes of these mutants on the surface of the 3-dimensional structure of A3H with RNA (**Figure 3-2D**).

RNA-binding mutants of A3H are degraded less efficiently by HIV-1 Vif

We next used live cell fluorescent video microscopy to measure the degradation kinetics of fluorescently-tagged A3H at a single-cell level during HIV-1 infection. HeLa cell lines stably expressing WT or mutant A3H fused to the C-terminus of a yellow fluorescent protein (YFP-A3H) were generated and then infected with a replication-defective HIV-1 construct that, following integration into host cell genomic DNA, expresses mCherry as a reporter protein (MOI = 0.5). WT A3H and the Vif-resistant derivative D121K variant each localized to cytoplasmic and nucleolar compartments, as reported [50, 82, 154, 159, 162]. The RNA binding-defective A3H triple mutant showed compromised cytoplasmic localization and appeared predominantly nuclear, also as reported [50, 159]. As expected, WT LAI Vif expressed from the virus at the same time as the mCherry marker caused the

degradation of WT A3H (representative image in **Figure 3-3A**). The WT YFP-A3H fluorescence intensity declined at a relative rate of approximately 10% per hour (**Figure 3-3C**). In comparison, both the YFP-A3H-D121K control and the RNA binding-defective triple mutant were resilient to degradation by LAI Vif (representative image in **Figure 3-3A** and quantification in **3C**). As an additional control, infection of the same cells with an HIV-1 construct encoding Vif-F39V did not cause a reduction in fluorescence of any forms of A3H (images not shown; quantification summarized in **Figure 3-3C**). These single-cell results are consistent with the immunoblot data described above using LAI Vif and untagged WT A3H.

Additional live cell fluorescent imaging experiments were done with a set of HIV-1 NL4-3 mCherry reporter viruses encoding either Hyper- or Hypo-Vif (variants described above and, notably, NL4-3 Vif and IIIB Vif have identical amino acid sequences). We observed that HIV-1 NL4-3 mCherry Hyper-Vif not only degraded WT YFP-A3H, as expected, but it also triggered the degradation of YFP-A3H-D121K and the YFP-A3H-triple mutant, albeit with slower kinetics (representative image in **Figure 3-3B** and quantification in **3C**). Infection by HIV-1 NL4-3 mCherry Hypo-Vif did not reduce levels of any form of A3H (**Figure 3-3C**). These single cell imaging results were confirmed by flow cytometric quantification of the median fluorescent intensity (MFI) of the YFP (A3H) signal in infected cells 48 hours post-infection (**Figure 3-3D**). Taken together, these real-time imaging data showed that the A3H RNA binding-defective mutant is less susceptible to HIV-1 Vif-mediated degradation compared to WT A3H. However, it can still be

degraded by HIV-1 NL4-3 derived Hyper-Vif (but not Hypo-Vif), suggesting that the RNA-binding defective mutant of A3H may still be capable of interacting with Hyper-Vif.

A split GFP system to study A3H dimerization in living cells

To be able to study A3H dimerization in living cells, a split fluorescence system was designed in which one A3H protomer was N-terminally tagged with GFP β-strands 1-10 (GFP1-10) and the second with GFP β-strand 11 (GFP11) plus an extended flexible linker. Based on prior reports with other proteins including various homo- and hetero-dimerization partners (reviewed in [163, 164]) and structural data from our group and others [42, 49, 50], efficient GFP reconstitution would only be expected following A3H dimerization through duplex RNA (schematic in **Figure 3-4A**). Indeed, a robust GFP signal was observed in both the cytoplasmic compartment and in nucleoli following co-transfection of 293T cells with these constructs (**Figure 3-4B-C**). By flow cytometry, more than 70% of transfected mCherry-positive cells (co-transfection marker) were GFP-positive with MFI more than 20-fold higher than negative controls (**Figure 3-4C**). Moreover, transfection of either construct alone failed to emit fluorescence (not shown), and similarly tagged A3A constructs also failed to reconstitute strong GFP signal (**Figure 3-4B-C**). The latter negative result was expected because A3A is monomeric in living cells and, even under most conditions *in vitro*, A3A behaves as a monomeric protein [44, 165, 166] (although A3A dimerization has been reported under some *in vitro* conditions [48]). As further validation of the robustness of this system, A3H-D121K yielded strong GFP signal similar to WT A3H, and the RNA binding-defective triple mutant (W115A, R175E, R176E)

was indistinguishable from A3A (**Figure 3-4B-C**). These results indicated that the split GFP reconstitution system can be used as a quantitative measure of A3H dimerization in living cells.

Vif overexpression does not interfere with A3H-mediated dimerization

We next asked whether HIV-1 IIIB Vif N48H, previously reported to degrade WT A3H but not cause cell cycle arrest [95, 167], is capable of interfering with A3H dimerization using the split GFP system. In one scenario, Vif may bind to A3H regardless of its dimerization status, and if so, the GFP fluorescence signal should be unaffected by the presence of Vif (top schematic in **Figure 3-5A**). Alternatively, Vif may intercept A3H prior to binding RNA, prevent dimerization, and lead to diminished GFP fluorescence reconstitution (bottom schematic in **Figure 3-5A**).

To distinguish between these possibilities, 293T cells were co-transfected with the same panel of split GFP constructs as above together with Vif N48H or an empty vector control. Each reaction also included an mCherry expression vector as a transfection control. Following a 32-hour incubation period, one set of reactions was treated for 16 hours with MG132 and the parallel set was untreated, and then all reactions were analyzed in parallel by immunoblotting and flow cytometry (**Figure 3-5B-C**). Similar to results presented above in Fig. 2, in the absence of MG132, Vif triggered a reduction in WT A3H levels but did not affect the A3H RNA binding-defective triple mutant (W115A R175E R176E) or Vif-resistant A3H-D121K. This result is supported by flow cytometry where an MFI

reduction of 4-fold was observed (representative flow cytometry histograms in **Figure 3-5C** and duplicate experiments averaged in the bar graph in the top part of **Figure 3-5B**).

MG132 was included in the experiment to prevent A3H proteasomal degradation and facilitate quantification of the dimerization phenotype. Interestingly, the dimerization potential of WT A3H was unaffected by Vif under these conditions, as evidenced by statistically indistinguishable MFIs (representative flow cytometry histograms in **Figure 3-5C** and duplicate experiments averaged in the bar graph in the top part of **Figure 3-5B**). It is worth noting that the lack of GFP reconstitution by the A3H triple mutant is likely due to a failure to dimerize through RNA and not to lower expression levels, because MG132 treatment caused an increase in steady-state levels of this mutant to near those of WT A3H [49] (compare lanes 3, 7, 11, and 15 in **Figure 3-5B**) and its GFP MFI remained approximately 10-fold lower (representative flow cytometry histograms in **Figure 3-5C** and duplicate experiments averaged in the bar graph in the top part of **Figure 3-5B**). These results combined to indicate that the dimerization status of A3H is unlikely to be affected by the functional interaction with Vif.

DISCUSSION

RNA plays essential roles in the dimerization, subcellular localization, and antiviral functions of A3H. Here we address whether the RNA bound by A3H has a role in HIV-1 Vif-mediated degradation. Immunoblot results with a panel of RNA binding mutants were somewhat inconclusive with some A3H mutants resisting Vif and others maintaining WT levels of sensitivity (**Figure 3-2**). The Vif-resistance of an RNA binding-defective triple

mutant of A3H was confirmed by imaging A3H degradation in living cells, but observations with a hyper-functional Vif variant indicated that even this mutant could be targeted for degradation (albeit at an approximately 4-fold slower rate than WT A3H; **Figure 3-3**). A split GFP system enabled asking whether Vif might compete with the same surface as RNA and interfere with A3H dimerization (**Figure 3-4**). These results favored a model in which the Vif and RNA binding surfaces of A3H are physically distinct. For instance, even under conditions of proteasome inhibition to prevent A3H degradation, Vif did not have the capability to alter the dimerization potential of WT A3H.

The overall resistance of the RNA binding-deficient A3H triple mutant (W115A R175E R176E) may be due to the slightly different angle of α helix 4 as observed in the new monomeric A3H crystal structure (**Figure 3-1**). As confirmed here and demonstrated in prior studies, α helix 4 including residue D121 is essential for A3H degradation by HIV-1 Vif [106-108, 127, 128, 154]. However, the hyper-Vif variant could still trigger the degradation of the D121K mutant suggesting that this Vif protein may have a greater conformational flexibility and/or recognize a slightly different overall surface than the Vif proteins from HIV-1 IIIB/NL4-3 and HIV-1 LAI. Subcellular localization and/or as-yet-unidentified binding partners might also play a role in the observed resistance of the subset of RNA binding mutants to Vif-mediated degradation. For instance, cytoplasmic A3H was degraded at a faster rate than nucleolar A3H (*e.g.*, residual nucleolar A3H is evident in **Figure 3-3A-B** in the presence of WT Vif and hyper-Vif, respectively). Moreover, several of the RNA binding mutants, including the triple mutant, tended to accumulate at higher levels in the nuclear compartment including the nucleoli, and this mislocalization likely

also contributed to the overall degree of Vif resistance (particularly in immunoblots of whole cell lysates). Taken together with our prior localization studies, the RNA binding mutants that are more nuclear also tend to be more resistant to Vif (and those that are cytoplasmic are more sensitive) [50, 159]. It is therefore reasonable to postulate that the binding of Vif to CBF-β immediately post-translation and the assembly of a large >200 kDa E3 ligase complex hinders Vif from accessing the nuclear compartment.

These results are also sensible from practical and evolutionary perspectives. Recent structural, biophysical, and functional studies have indicated that duplex RNA is required for A3H to package into assembling viral particles and also for deamination-independent restriction of virus replication [42, 49, 50, 168]. The massive molar excess of structured RNA in cells would make it difficult for Vif to compete for the same binding surface of A3H. Therefore, it is likely that the HIV-1 Vif protein evolved to avoid competition with RNA and bind a distinct A3H surface. Thus, Vif may have evolved the potential to degrade both monomeric as well as RNA-dimerized forms of cellular A3H and thereby maintain the upper hand in counteracting restriction.

MATERIALS AND METHODS

A3 expression constructs

The constructs expressing intron-containing WT, E56A, H114A, W115A, R175E, R176E, W115A/R175E/R176E, R18E, A172E, and R179E huA3H haplotype II in pcDNA3.1(+) (Invitrogen) have been reported [50]. Other mutants of A3H (D121K and E56A/W115A/R175E/R176E) within the same backbone were made by site-directed

mutagenesis and verified by Sanger sequencing (primer sequences available on request). The A3H triple mutant (W115A/R175E/R176E) was subcloned into pESUMO vector using restriction enzymes Bsa1 and Xba1. Retroviral transduction vectors encoding YFP fused to A3H (haplotype II) and mutants were generated by subcloning SYFP2 from SYFP2-C1 (Addgene #22878) into pcDNA3.1 plasmids containing A3H using NheI and KpnI restriction cut sites followed by transfer into MigR1-derived simple retroviral vector using MluI and MfeI cut sites. The split GFP system used in this study was based on a previous system [169] with minor modifications. A gblock (IDT) encoding GFP β-strand 11 (GFP11) followed by a 27 amino-acid flexible linker was ordered and cloned into the previously reported pcDNA3.1(+) construct of WT A3H protein to the N-termini [50]. A ClaI restriction site was added in between GFP11 and the linker. GFP β-strand 1-10 (GFP1-10) was PCR amplified and cloned in place of GFP11 to make the GFP1-10 construct.

HIV-1 and Vif expression constructs

The lentiviral Vif protein from HIV-1 IIIB (EU541617) was codon optimizted (GenScript Corp) and cloned into pVR1012 with a C-terminal HA tag using SalI and BamHI. The Vif protein from HIV-1 LAI (1102247D) was cloned into pVR1012 with a C-terminal HA tag using SalI and NotI. F39V mutant of HIV-1 LAI Vif, Hypo-variant (F39V), N48H, and Hyper-variant (N48H, GDAK60-63EKGE) of HIV-1 IIIB Vif were made by site-directed mutagenesis and verified by Sanger sequencing (primer sequences available on request). HIV-1 NL4-3 mCherry reporter viruses were generated by subcloning Hypo- and Hyper-Vif encoding segments from IIIB infectious molecular clones [139] into a NL4-3 E-R-

mCherry full-length reporter virus plasmid [170] using AgeI and SalI cut sites. HIV-1 LAI mCherry reporter viruses were generated by transferring the mCherry reporter cassette from pRGH (NIH ARP #12427) into a previously described LAI infectious molecular clone using BlpI and XhoI cut sites. LAI F39V was generated by site-directed mutagenesis. All plasmids were confirmed by restriction digestion and Sanger sequencing.

Protein expression and purification

His-SUMO-A3H (E56A, W115A, R175E, R176E) plasmid was transformed into BL21 (DE3) cells for protein expression. 2xYT media with 100 μg/mL of ampicillin was inoculated with transformed bacteria and grown to OD 0.8-1. Approximately 30 minutes prior to induction, cultures were supplemented with 50 μM zinc-sulfate, cooled to 16ºC, and protein expression was induced overnight with 0.5 mM IPTG. The next day, cultures were spun down at 3800xg for 20 minutes. Pellets were resuspended in lysis buffer (20 mM Hepes pH 7.5, 1M NaCl, 5 mM imidazole, 100 μg/μl RNase A), and the resuspension was sonicated twice in an ice-bath (Branson Sonifier Output cycle, 50, Duty cycle 50). The lysate was centrifuged at 12,000 xg for 30 minutes to remove cellular debris. The supernatant was collected and bound to Talon Cobalt Resin (Clontech), washed extensively with wash buffer (20 mM Hepes pH 7.5, 1M NaCl, 5 mM imidazole), and eluted with elution buffer (20 mM Hepes pH 7.5, 1M NaCl, 250 mM imidazole). The fractions containing protein were pooled and purified further using an S200 16/600 column (GE Healthcare) equilibrated in 20 mM Tris-HCl pH 8 and 500 mM NaCl. Fractions were

collected, 10 mM DTT was added, and purified protein samples were concentrated to ~10mg/ml.

Protein crystallization and structure determination

His-SUMO-A3H (E56A, W115A, R175E, R176E) was crystalized in 20% PEG 3350,200 mM potassium fluoride, using the sitting drop vapor diffusion method. Prior to crystal tray set up, trace amounts of Ulp1 protease was added to the protein aliquot to remove the His-SUMO tag. Untagged A3H triple mutant is prone to precipitation, and adding protease immediately before crystal tray set up kept the protein in solution long enough to set up the trays. Crystals were cryoprotected in ~20% ethylene glycol, mounted on nylon loops, and flash frozen in liquid nitrogen. Diffraction data was collected at the APS synchrotron beamline and processed with XDS software [171]. Molecular replacement using the structure of human A3H (pdb 6B0B) as a search model was performed in PHASER. Model building and structure refinement was done using COOT [172] and Phenix [173], respectively.

Cell lines

293T cells were maintained at 37°C and 5% CO_2 in Dulbecco's modified Eagle medium (DMEM) containing 10% fetal bovine serum (FBS) and 1% penicillin-streptomycin (P/S). HeLa cells (ATCC) were maintained at 37°C and 5% CO_2 in DMEM supplemented with 10% FBS, 1% P/S, and 1% GlutaMAX.

Vif degradation experiments

293T cells were transfected with WT or mutant pcDNA3.1(+)-A3H, along with 500 or 1000 ng pVR1012- HIV-1 LAI Vif WT/F39V-HA (**Fig. 2a**), or 50 or 100 ng pVR1012-HIV-1 IIIB Hyper-/Hypo-Vif (**Fig. 2c**) or empty vector, using Transit-LT1 (Mirus). The following amounts of A3H were transfected: 25 ng of WT, D121K, E56A, H114A, R175E, R18E, and A172E, 100 ng of R179E, and 200 ng of W115A, R176E, W115A/R175E/R176E, and E56A/ W115A/R175E/R176E. Empty vector is added to equalize the amounts of total DNA. After 48 hours, cells were harvested for immunoblot analysis.

Immunoblotting experiments

Cell lysates were prepared by resuspension of washed cell pellets directly in 2.5× Laemmli sample buffer. Proteins were separated using discontinuous sodium dodecyl sulfate polyacrylamide gel electrophoresis (SDS-PAGE) and transferred to polyvinylidene difluoride (PVDF) membranes (Millipore). HA-tagged A3 proteins were detected using monoclonal mouse anti-HA (BioLegend #MMS-101P). A3H proteins were detected using polyclonal rabbit anti-A3H (Novus #NBP1-91682). Tubulin was detected using a monoclonal mouse anti-α-Tubulin antibody (Covance #MMS-489P). Immunoblots were quantified using ImageStudio.

Live cell fluorescent imaging

Reporter viruses were produced in 293T cells by co-transfection with VSV-G to generate pseudo-typed single cycle infectious virus. Viral inoculum was harvested at 48 hours post-transfection and passed through a 0.45-μm syringe filter. HeLa YFP-A3H stable cells were plated at 20,000 cells per well of an ibidi μ-well slide (ibidi GmbH) in 200 μL of Fluorobrite DMEM (Thermo Fisher Scientific) supplemented with 10% FBS, 1% GlutaMAX, 1% P/S, and 100 mM HEPES. Cells were infected at a MOI of 0.5 infectious units per cell with 2 μg/mL polybrene. Live cell fluorescent video microscopy was performed as previously described [170] beginning at 12 hours after addition of virus and a multi-color image was captured every 60 minutes (mCherry, YFP, and DAPI) for up 40 hours post-infection. All images were processed and analyzed using FIJI/ImageJ2 [174]. Briefly, regions of interest (ROIs) were drawn around whole single cells based on YFP-A3H image and around nuclei of those cells based on DAPI in every frame of live cell movies. Cytoplasmic fluorescence was quantified by subtracting nuclear from whole cell integrated density (IntDen). The cytoplasmic YFP and whole cell mCherry fluorescence were normalized to each single cell's value at the beginning of each movie. Rate of change in YFP (showing YFP-A3H degradation) was quantified for the period 5 hours following detection of mCherry.

Split GFP experiments

293T cells were transfected with 100 ng GFP1-10 plasmids, 25 ng GFP11 plasmids, 500 ng of HIV-1 IIIB Vif N48H-HA or empty vector, and 100 ng mCherry plasmid. Cells were

treated with MG132 at a final concentration of 2 μM at 32 hours and subjected to analyses by fluorescence imaging, flow cytometry, and immunoblotting at 48 hours post-transfections. Cells were treated with NucBlue live cell stain (Invitrogen) at 37°C for 30 min for DAPI (4',6'-diamidino-2-phenylindole) staining prior to imaging. Images were collected using a Nikon inverted Ti-E deconvolution microscope. A fraction of the cells was resuspended in phosphate-buffered saline (PBS) with 1 mM ethylenediaminetetraacetic acid (EDTA) in preparation for flow cytometry. GFP and mCherry fluorescence was measured on a BD FACS Canto II flow cytometer. Data were analyzed using FlowJo flow cytometry analysis software (version 8.8.6). The fraction of GFP+ cells and median fluorescence intensity (MFI) of all transfected (mCherry-positive) cells was quantified for each sample. The remaining cells were prepared for immunoblotting.

Sequence alignments.

All amino acid sequences were aligned using Clustal Omega. The amino acid sequences of human A3H, chimpanzee A3H, and pig-tailed macaque A3H correspond to GenBank accession numbers ACK77775.1, 5Z98_A, and MF509624, respectively.

Accession numbers.

Coordinates and structure factors for the monomeric A3H x-ray structure have been deposited in the Protein Data Bank with accession number 6P92.

ADDITIONAL CONTRIBUTIONS

This work was supported by NIAID R37 AI064046 (to R.S.H.), NIGMS R01 GM118000 (to R.S.H. and H.A.), and NIGMS R01 GM118047 (to H.A.). This work is based upon research conducted at the Northeastern Collaborative Access Team (NE-CAT) beamlines, which are funded by the NIH (NIGMS P30 GM124165). The Pilatus 6M detector on 24-ID-C beamline is funded by a NIH-ORIP HEI grant (S10 RR029205). This research used resources of the Advanced Photon Source, a U.S. Department of Energy (DOE) Office of Science User Facility operated for the DOE Office of Science by Argonne National Laboratory under Contract No. DE-AC02-06CH11357. J.W. received partial salary support from the University of Minnesota Graduate School, Interdisciplinary Doctoral Fellowship. D.J.S. received partial salary support from the University of Minnesota Craniofacial Research Training (MinnCResT) program (NIH T90DE022732). R.S.H. is the Margaret Harvey Schering Land Grant Chair for Cancer Research, a Distinguished University McKnight Professor, and an Investigator of the Howard Hughes Medical Institute. The following reagent was obtained through the NIH AIDS Reagent Program, Division of AIDS, NIAID, NIH: pRGH-WT (#12427) from Ivan Sadowski and Viviana Simon. Microscopy imaging and analysis was performed at the University Imaging Centers, University of Minnesota.

Table 1. Data collection and refinement statistics.

Data collection	
Resolution range (Å)	86.8 - 3.2 (3.3 - 3.2)
Space group	$P2_12_12_1$
Unit cell	
a,b,c (Å)	39.99 109.06 143.45
Total reflections	52479 (5458)
Unique reflections	10453 (1001)
Multiplicity	5.0 (5.1)
Completeness (%)	96.1 (91.8)
Mean I/sigma(I)	6.7 (1.4)
R-merge (%)	18.0 (1.47)
CC1/2	0.995 (0.460)
Refinement	
Total	10347 (999)
Reflections for R-free	500 (46)
R-work (%)	27.8 (41.6)
R-free (%)	32.5 (38.2)
Number of non-hydrogen atoms	4362
macromolecules	4351
ligands	7
solvent	4
Protein residues	530
r.m.s.d.	
Bond lengths (Å)	0.002
Bond angles (°)	0.53
Ramachandran plot	
Favored (%)	95.58
Allowed (%)	4.42
Outliers (%)	0.00
Average B-factor	114.16
macromolecules	114.28
ligands	67.71
solvent	64.63

Statistics for the highest-resolution shell are shown in parentheses.

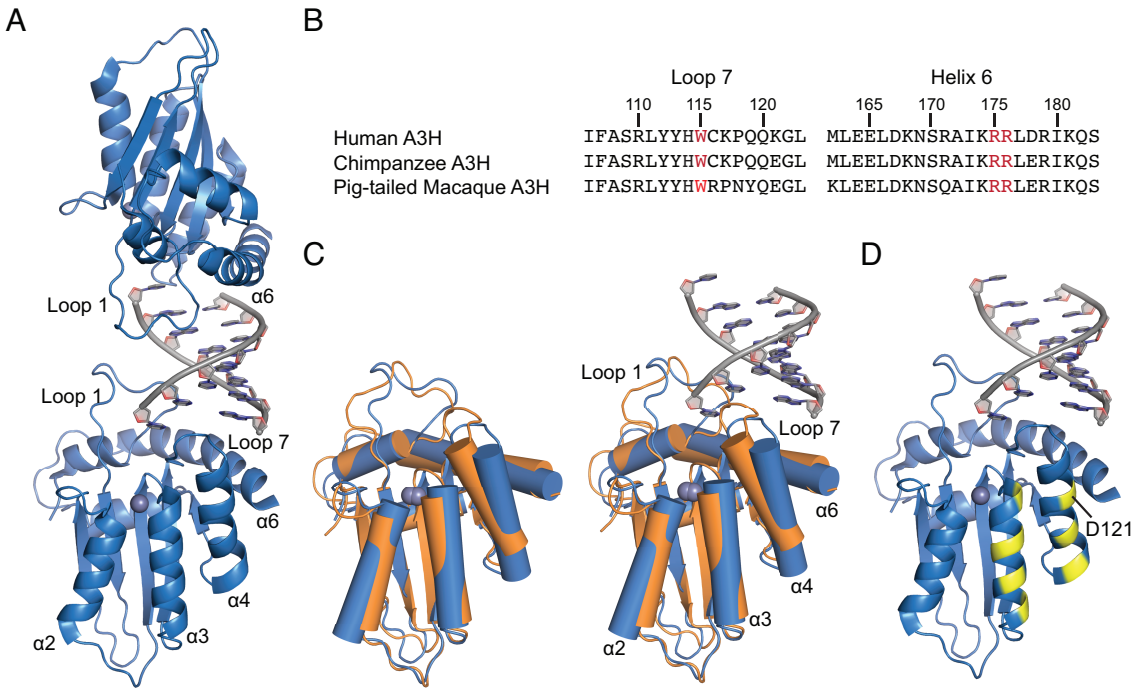

Figure 3-1. Structure of an RNA binding-defective variant of human A3H.

(**A**) X-ray structure of human A3H in complex with duplex RNA showing loop 1, loop 7, and α-helix 6 interacting with duplex RNA (ribbon schematic of pdb 6B0B).

(**B**) Partial amino acid sequence alignment of the loop 7 and α-helix 6 regions of human (pdb 6B0B), chimpanzee (pdb 5Z98), and pig-tailed macaque (pdb 5W3V) A3H proteins. Conserved RNA-interacting residues W115, R175, and R176 are highlighted in red.

(**C**) Superposition of the monomeric RNA binding-defective A3H mutant (E56A, W115A, R175E, R176E) in orange with a single A3H protomer (with/without RNA) in blue from the previously determined dimeric structure (pdb 6B0B).

(**D**) A3H structure with yellow highlights for previously identified Vif-interacting residues including D121. The orientation is similar to those in the bottom of panel A and panel C to facilitate comparisons.

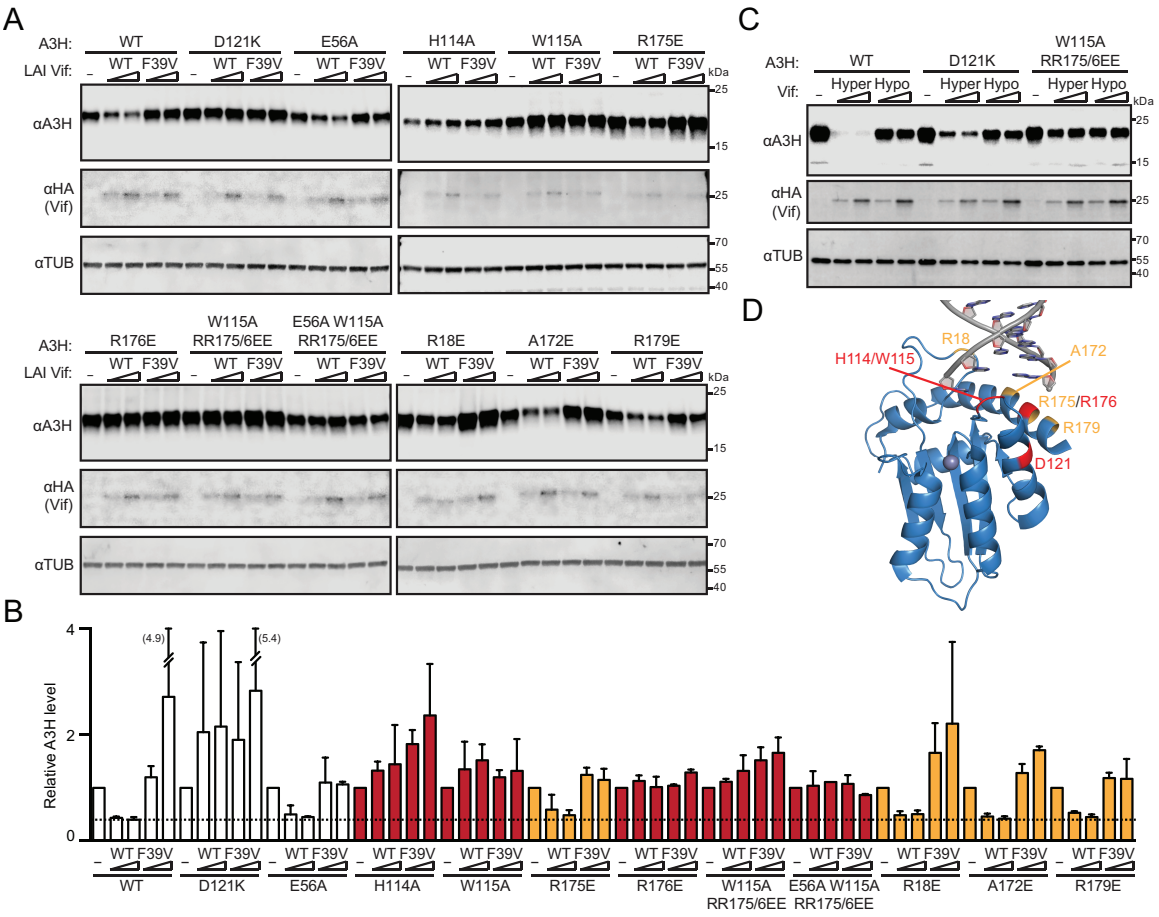

Figure 3-2. Vif susceptibility of human A3H RNA binding mutants.

(**A**) Immunoblots of 293T cells expressing WT A3H or the indicated mutants, together with empty vector (-), HIV-1 LAI Vif, or a F39V derivative. A3H was detected using an anti-A3H antibody and Vif was detected using an anti-HA antibody. Anti-α-tubulin was used as a loading control.

(**B**) A bar graph quantifying immunoblot data from panel A and from an independent experiment (not shown). The A3H level for each construct is normalized to that of the corresponding empty vector control. The mean and difference between two independent experiments are shown. The dashed line represents level of sensitivity of WT A3H to Vif.

(**C**) Immunoblots of 293T cells expressing WT A3H or the indicated mutants, together with empty vector (-), HIV-1 IIIB-derived Hyper Vif (F39, H48, EKGE60-63) or Hypo Vif (V39, N48, GDAK60-63) with the same antibodies as in panel A.

(**D**) A structural depiction of human A3H residues required (red) or dispensable (orange) for functional interaction with HIV-1 Vif.

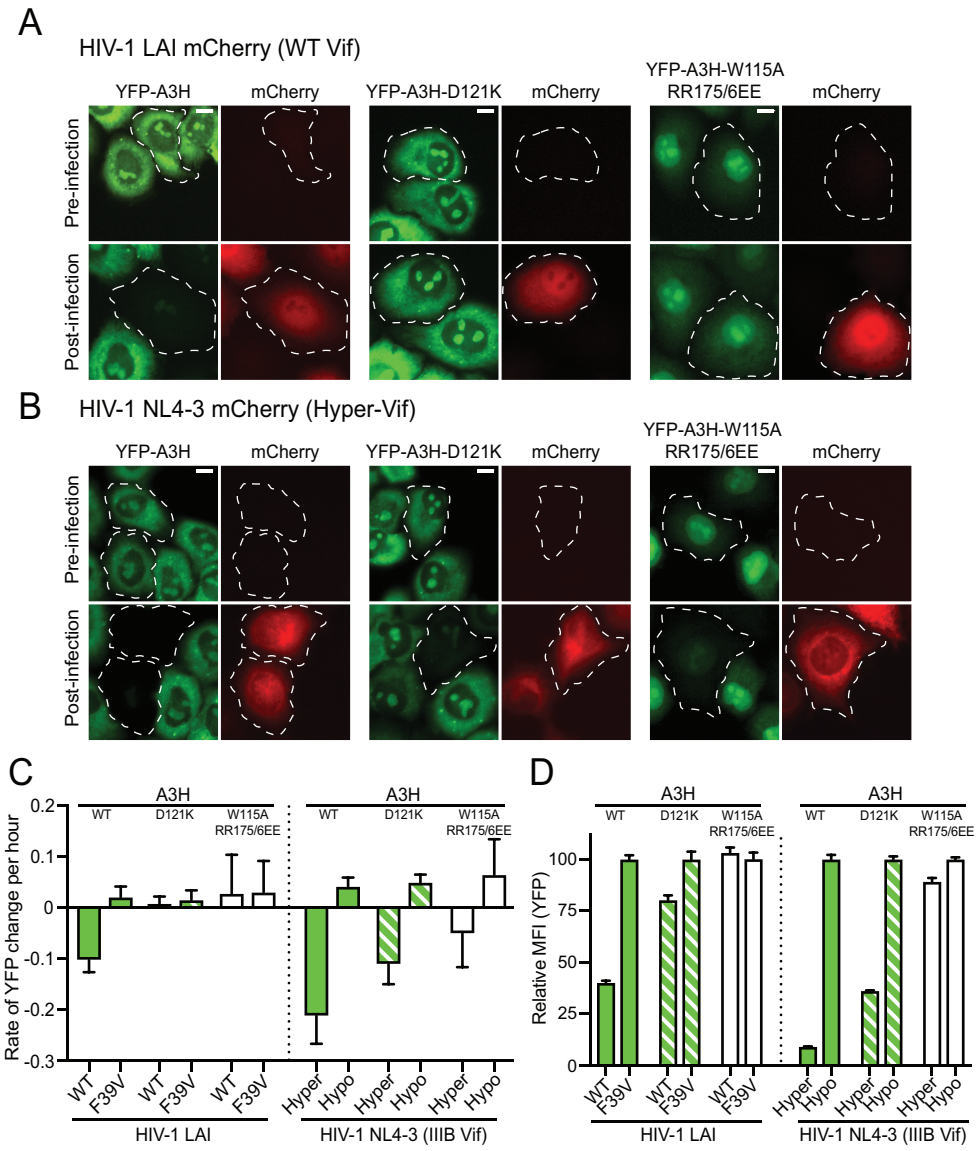

Figure 3-3. The degradation kinetics of human A3H and key mutants.

(**A**) Representative images of HeLa cells stably expressing WT or mutant A3H fused to the C-terminus of a YFP before infection or 25-hour post-infection with an HIV-1 LAI mCherry reporter virus (WT Vif ; MOI = 0.5). Parallel cultures were also infected with a reporter virus expressing LAI Vif F39V as a negative control (images not shown). Cells

circled with dashed lines became infected as evidenced by mCherry expression. The scale bar at the upper right corner represents 10 μm.

(**B**) Representative images of HeLa cells stably expressing WT or mutant A3H fused to the C-terminus of a YFP before infection or 16-hour post-infection with an HIV-1 NL4-3 mCherry reporter virus (Hyper-Vif; MOI = 0.5). Parallel cultures were also infected with a reporter virus expressing Hypo-Vif as a negative control (images not shown). Cells circled with dashed became infected as evidenced by mCherry expression. The scale bar at the upper right corner represents 10 μm.

(**C**) Quantification of the rate of A3H degradation (change in YFP fluorescence) of a minimum of 10 infected cells representing each of the indicated conditions (mean +/- SD).

(**D**) Flow cytometry quantification of the relative MFI of YFP-A3H in HeLa cells infected under the same conditions as panels A-B. Data were normalized by setting the post-infection MFI of each Vif F39V or Hypo-Vif reaction to 100%.

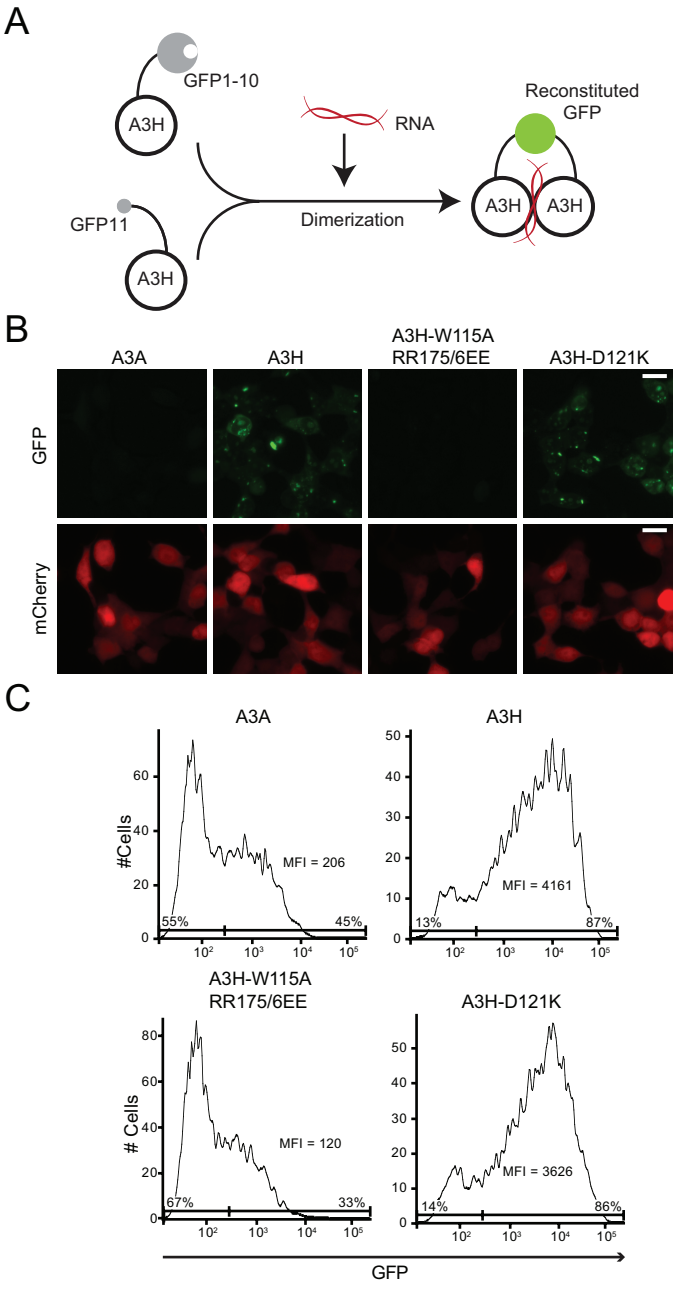

Figure 3-4. A split GFP system to study A3H dimerization in living cells.

(**A**) A schematic of the split GFP system for A3H dimerization. One A3H construct is fused to GFP β-strand 1-10 (GFP1-10) and the other to β-strand 11 (GFP11). GFP Reconstitution occurs upon duplex RNA-mediated dimerization of A3H.

(**B**) Representative fluorescent microscopy images of 293T cells expressing split GFP constructs of the indicated A3s. A mCherry plasmid was included as a co-transfection control. The scale bar represents 20 μm.

(**C**) Flow cytometry profiles of the same cells as in panel B. The MFI is shown for the whole mCherry-positive population, and the percentages of GFP-negative and GFP-positive cells are included at the bottom left and right, respectively (gates based on untransfected 293T cells analyzed in parallel).

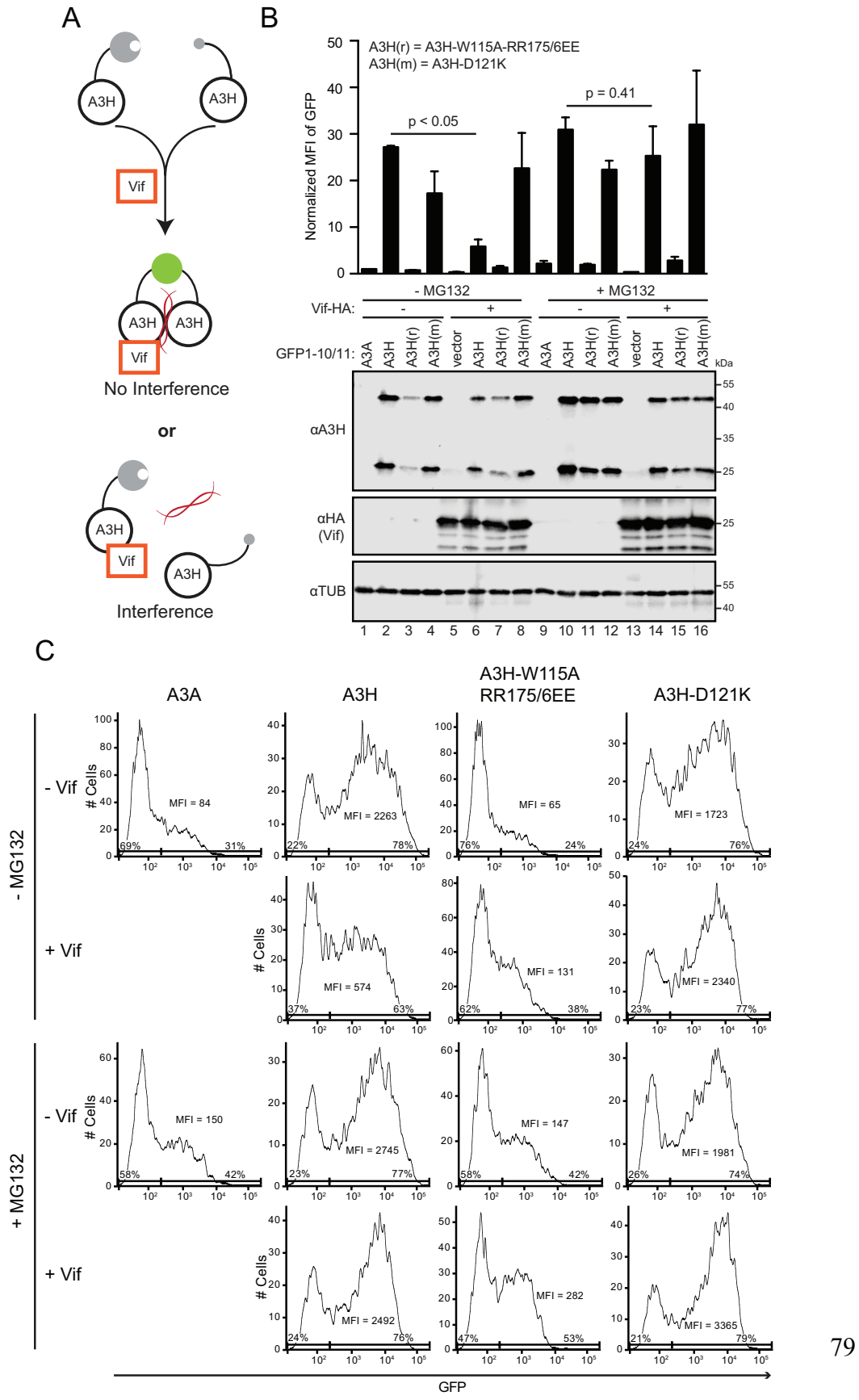
A
A3H
A3H
Vif
A3H
A3H
Vif
No Interference
or
A3H
Vif
A3H
Interference
B
A3H(r) = A3H-W115A-RR175/6EE
A3H(m) = A3H-D121K
Normalized MFI of GFP
p < 0.05
p = 0.41
- MG132
+ MG132
Vif-HA:
GFP1-10/11:
A3A
A3H
A3H(r)
A3H(m)
vector
kDa
αA3H
αHA (Vif)
αTUB
1 2 3 4 5 6 7 8 9 10 11 12 13 14 15 16
C
A3A
A3H
A3H-W115A RR175/6EE
A3H-D121K
- MG132
+ MG132
- Vif
+ Vif
# Cells
MFI = 84
MFI = 2263
MFI = 65
MFI = 1723
MFI = 574
MFI = 131
MFI = 2340
MFI = 150
MFI = 2745
MFI = 147
MFI = 1981
MFI = 2492
MFI = 282
MFI = 3365
GFP

Figure 3-5. Vif does not interfere with A3H dimerization in the split GFP system.

(**A**) Models for Vif interaction with A3H. The top schematic depicts Vif binding to a distinct surface on A3H (predicted to have no interference in GFP reconstitution), whereas the bottom schematic depicts Vif competing with RNA for A3H (interference in GFP reconstitution).

(**B**) Immunoblots of 293T cells expressing A3A, A3H, or the indicated A3H mutants, together with empty vector (-) or HIV-1 IIIB Vif N48H +/- MG132. A3H was detected using an anti-A3H antibody and Vif was detected using an anti-HA antibody. Anti-α-tubulin was used as a loading control. A bar graph is shown above the immunoblots for quantification of flow cytometry data from panel C and from an independent experiment not shown. The MFI level of cells of each indicated condition is normalized to A3A in the absence of Vif or MG132. The mean and difference between two independent experiments are shown.

(**C**) Flow cytometry profiles of 293T cells expressing the indicated A3 and Vif construct (+/- MG132). Each profile is labeled as in Figure 3-4c.

CHAPTER 4

The Impact of Stable and Unstable APOBEC3H Haplotypes on HIV-1 Transmission

Adapted from manuscript in preparation: Wang J., B.J. Hoium, A.M. Land, E.W. Refsland, E.M. Luengas, R.D. Mackelprang, W.L. Brown, M. Emerman, J. Lingappa, & R.S. Harris (2019) The impact of stable and unstable APOBEC3H haplotypes on HIV-1 transmission.

Authors' Contributions

J. Wang performed all experiments, wrote and revised the manuscript, and designed all figures except as follows. B.J. Hoium performed a fraction of vif genotyping. A.M. Land performed an initial round of viral RNA isolation. E.W. Refsland and E.M Luengas isolated genomic DNA from dried blood spot specimens. R.D. Mackelprang performed statistical power calculations that aided in the experimental design. W.L. Brown provided technical support. J. Lingappa provided primary patient samples. M. Emermen, J. Lingappa, R.S. Harris contributed to experimental designs and manuscript preparation. All authors contributed to manuscript revision.

SUMMARY

Human A3H is highly polymorphic with more than ten reported haplotypes and four splice variants. Amino acid variations at five positions define haplotypes and dictate protein stability. Stable proteins such as haplotype II contribute to HIV-1 restriction in T lymphocytes but can be counteracted by fully functional Vif variants. A3H haplotype II has a 60% allele frequency in African populations, and haplotypes that are undetectable at the protein level (III/IV) has a frequency of approximately 25%. In contrast, other populations less frequently express stable A3H with approximately 10% allele frequency of A3H haplotype II. We tested the hypothesis that stable A3H enzymes provide a transmission barrier to HIV-1 isolates harboring less-than-fully functional Vif alleles. We determined the *A3H* and viral *vif* genotypes of a large cohort of African HIV-1 serodiscordant couples and showed that stable A3H is unlikely to be a general protective factor in HIV-1 acquisition on the populational level. However, stable A3H enzymes may still serve positive roles in slowing virus spread and disease progression.

INTRODUCTION

At least four members of the human APOBEC3 (A3) family of single-stranded cytosine deaminases are involved in innate immunity against HIV-1 (reviewed by [31-33]). These A3 enzymes (A3D, A3F, A3G, and A3H) package into virions and target single-stranded viral cDNA substrates. They catalyze deamination reactions, mutating viral cytosines to uracils, which leads to G-to-A hypermutations in the viral genome. Some A3 proteins also demonstrate deaminase-independent restriction activities, likely forming a physical blockade to reverse transcription [50, 75-82]. HIV-1 encodes the accessory protein Vif to counteract restriction by A3 enzymes and rescue viral infectivity. Vif recruits a cellular co-factor, CBF-β, to nucleate an E3 ubiquitin ligase complex, which targets restrictive A3 enzymes for polyubiquitination and proteasomal degradation [84, 85, 131-136].

A3H is the most polymorphic member of the A3 subfamily with more than ten reported haplotypes and four splice variants [126-129]. Different haplotypes of A3H are dictated by amino acid variances at five positions (15, 18, 105, 121, and 178), with position 15 and 105 being critical for protein stability and activity (**Table 4-1**). A3H proteins with an asparagine at position 15 (N15) and an arginine at 105 (R105), such as haplotype II, are expressed stably and capable of potent anti-viral activity [94, 96, 126, 129, 175]. In contrast, haplotypes with a deletion of N15 (Δ15), such as III/IV, regardless of residue identity at position 105 results in proteins that are undetectable by immunoblot and lack of anti-viral activity [126, 128, 129]. A3H haplotype I with N15 and glycine at 105 (G105) is hypomorphic, with 3 to 4-fold lower steady state expression levels in comparison to

haplotype II and altered subcellular localization but the protein itself is equally active [122, 129, 162].

Not all naturally occurring Vif variants can counteract restriction by stable A3H. Previous studies comparing various laboratory strains and natural isolates of HIV-1 Vif have shown that amino acid position 39, 48, and 60 to 63 are specifically important for the ability of Vif to degrade A3H [93-96]. Vif proteins with phenylalanine or tyrosine at position 39 can mediate the degradation of A3H, and changing this residue to valine or nine other less frequently observed residues results in separation-of-function variants that degrade A3G and A3F but not A3H [93, 94]. Histidine at position 48 also enables Vif to mediate the degradation of A3H, whereas changing this residue to asparagine compromises this function [93, 95]. Having amino acids EKGE at position 60 to 63 enhances the function of Vif to degrade A3H but these residues are not strictly required [96, 126]. Hereon, Vif proteins that degrade both A3H and A3G will be referred to as *hyper-functional* and those that fail to degrade A3H, yet still degrade A3G, will be called *hypo-functional*.

In geographic regions of world such as sub-Saharan Africa where stable A3H is more common, clinical HIV-1 isolates tend to harbor *vif* alleles predicted to encode hyper-functional proteins (F39) [96, 126, 129]. In contrast, in regions of the globe such as Asia with higher frequencies of unstable and hypomorphic *A3H* haplotypes, hypo-functional *vif* alleles are predicted to occur more frequently (V39) [96, 126, 129]. These differential global distributions suggest a potential ongoing genetic conflict between human A3H (stable/unstable) and HIV-1 Vif (hyper/hypofunctional).

These global trends and mechanistic studies (above) led us to hypothesize that stable A3H serves as a transmission barrier within the human population by protecting individuals (sexual partners) against acquisition of HIV-1 harboring a hypo-functional *vif* allele from patients with unstable *A3H* haplotypes (transmission scenarios depicted in **Figure 4-1A**). To test this idea, we determined the *A3H* genotypes of an existing cohort of 597 heterosexual sub-Saharan African couples who were initially discordant for HIV-1 status (*i.e.*, upon the initiation of these original clinical studies, one person was infected as evidenced by serologic analysis and his/her partner was not). Over the course of these studies, which were originally designed for other reasons. [176-178], a subset of the patients transmitted the virus to their partners. Our retrospective cohort was assembled with a ratio of 1 transmission event to 2 non-transmission events in order to provide as much statistical power as possible to be able to determine potential reason(s) for non-transmission. Once patient and partner genotyping studies were complete, we further determined HIV-1 *vif* genotypes from a subgroup of couples in which the index patient has unstable A3H and his/her partner has stable A3H. Overall, at least at the population level, these analyses show that stable A3H is unlikely to be an HIV-1 transmission barrier.

RESULTS

A3H genotyping of a large cohort of serodiscordant couples

The *A3H* genotypes of a previously characterized large HIV-1 serodiscordant heterosexual couple cohort was analyzed by DNA sequencing [178, 179]. This cohort was established through recruitment of HIV-1 serodiscordant couples from 7 countries in Eastern and

Southern Africa. Longitudinal blood-spot, serum, and peripheral blood mononuclear cell (PBMC) specimens have been collected and preserved from the participants during periodic clinical visits within a period of five years. HIV-1 transmission and seroconversion occurred for a fraction of the participating couples. In these cases, genetic sequencing of *env* and *gag* gene regions was used to confirm the transmission linkage within the couple. A total of 597 couples was selected for inclusion in our study, with 1/3 having transmission events and the remainder remaining free of transmission (n = 199 and 398, respectively). The 199 seroconverted couples represent all of the transmission events that occurred during the course of prior studies with longitudinal samples available from both the index patient and the recipient partner. A total of 398 serodiscordant couples were chosen randomly to provide a 99% power to detect a 3-fold reduced risk of HIV-1 acquisition.

The genomic DNA of each individual was purified from archived blood-spot specimens (IRB 1003E78700). Because A3H amino acid positions 15 and 105 can be used to predict protein stability, the corresponding genomic DNA region spanning exons 2 and 3 was amplified by PCR, enzymatically cleaned-up using exonuclease I and shrimp alkaline phosphatase, and sequenced. The Sanger sequence chromatograms were analyzed to determine *A3H* genotypes at these two positions (**Figure 4-1B**). Asparagine 15 (N15) is encoded by AAC, and its reverse-complementary sequence is GTT. A chromatogram with clean GTT peaks therefore identified individuals homozygous for N15 (N15/N15). In contrast, chromatograms lacking GTT peaks identified individuals with homozygous deletions of N15 (Δ15/Δ15), and chromatograms with mixed peaks downstream of this

codon revealed heterozygotes (N15/Δ15). A3H position 105 can be an arginine (R105, encoded by CGC) or glycine (G105, encoded by GGC). The single base pair difference between these two codons in exon 3 was distinguished using a similar PCR sequencing approach.

We determined the *A3H* genotype at amino acid positions 15 and 105 for all 1194 individuals with the exception of 31 mostly due to low quality DNA (**Table 4-2**). The allele frequencies for N15 and Δ15 are 61.5% and 38.5%, and those for R105 and G105 are 88% and 12%, respectively. These frequencies are consistent with the reported global distributions of *A3H* haplotypes, which indicated that haplotype II (with N15 and R105) is the most common allele in sub-Saharan Africa [122, 129, 130]. We subsequently predicted A3H protein stability from these genotyped individuals. Individuals homozygous for N15 and R105 (N15/N15 with R105/R105) have both *A3H* alleles encoding stably expressed protein. Individuals heterozygous for position 15 or 105 (*i.e.* N15/N15 with R105/G105, and N15/Δ15 with R105/R105) express at least one copy of stable A3H. These individuals described above are considered as having stable A3H. In contrast, individuals that are homozygous for Δ15 (Δ15/Δ15 with any combinations at 105) express only unstable A3H. Because of the hypomorphic phenotype of A3H haplotype I, 20 individuals that are homozygous for haplotype I (N15/N15 with G105/G105) or heterozygous for haplotype I and unstable A3H (N15/Δ15 with G105/G105) are excluded. Another 102 individuals with N15/Δ15 and G105/R105 were also excluded due to insufficient information to associate the alleles. Overall, the cohort is enriched for individuals with stable A3H (n = 874) rather than unstable A3H (n = 167). After exclusion of couples with unidentified, hypomorphic,

or ambiguous *A3H* genotypes, we obtained a total of 474 couples with clear stable or unstable *A3H* alleles.

The transmission rate of each A3H stable/unstable scenario was calculated using these patient and partner *A3H* genotypes (**Table 4-3**). In the majority of couples, both the index patient and the partner expressed stable A3H (n = 241) and the transmission rate was 32.0%. The transmission rate in couples where the index patient has stable A3H and the partner unstable A3H was slightly higher at 36.5% (n = 159). The transmission rates for these two scenarios were not statistically different (p = 0.39, Fisher's exact test). However, the critical comparison that tests our central hypothesis is the transmission frequencies for couples with infected individuals with unstable A3H haplotypes to partners with stable versus unstable haplotypes. Unexpectedly, the unstable-to-stable and unstable-to-unstable transmission rates were similar, 33.8% (n = 65) and 33.3% (n = 9), respectively. These rates are also not different statistically (p = 1.0, Fisher's exact test) indicating stable A3H is unlikely to be a major transmission barrier.

Genotyping *vif* for index patients with unstable A3H

However, the viral *vif* genotype is an equally important factor in determining transmission rates, and viral sources for index cases were unknown. In other words, there was no way to know the *A3H* genotypes of the patients that infected the index patients in our cohort but, based on our genotyping and prior reports (1000 genomes), there was at least a 50% chance of this being stable A3H [122, 129]. Thus, there was an equally high probability that the HIV-1 isolate in our infected patients had been subjected recently to selective

pressure from stable A3H and may have retained A3H counteraction activity despite an unstable index patient *A3H* genotype. Therefore, to address this issue, we determined the *vif* genotypes of the virus in each infected unstable A3H patient to predict their functionality against stable A3H (*i.e.*, determine whether each Vif was hypo- or hyper-functional against stable A3H and then revisit the transmission question).

Total RNA was isolated from 500 μl of virus-containing serum from index patients, reverse transcribed, and subjected to high-fidelity PCR (workflow in **Figure 4-2**). The *vif* gene was amplified using nested PCR with two sets of degenerate primers recognizing adjacent regions in *pol* and *vpr*. The amplicons containing patient *vif* were purified and cloned into pJET vectors. Due to the likelihood of diversity in each virus population, a minimum of 10 *vif* clones were sequenced for each patient. Within the unstable-to-stable scenario, we were able to determine the *vif* genotypes of 23 out of 43 index patients from the non-transmission subgroup, as well as 15 out of 21 patients from the transmission subgroup (excluding a transmission event with mismatched virus). Numbers were reduced due to specimen unavailability and, in some instances, low quality RNA. Nevertheless, based on prior studies, Vif proteins with Y39 or F39 were predicted to be hyper-functional, whereas Vif proteins with any other residues at this position were predicted to be hypo-functional [93, 94, 96]. Moreover, if an index patient yielded even a single Vif sequence with Y39 or F39, then his/her viral Vif was deemed hyper-functional. Using these guidelines, the majority of index patient viral isolates in the transmission subgroup had a predicted hyper-functional Vif. And, surprisingly, the non-transmission subgroup had a

similar predicted Vif functionality (57% versus 60% hyper-functional, respectively; p = 1.0, Fisher exact test; **Table 4-4**).

DISCUSSION

Stable haplotypes of A3H encode proteins that are potent restriction factors of HIV-1 and can only be counteracted by hyper-functional Vif proteins. Global distributions of *A3H* haplotypes and predicted Vif functionality suggest an adaptation of the viral Vif to overcome the protection of stable A3H. Here we hypothesized that stable A3H is a transmission barrier to HIV-1 harboring a hypo-functional *vif* allele. We analyzed the *A3H* genotypes of a large African serodiscordant couple cohort (with a fraction of seroconcordant couples) to show that the majority of this population consists of individuals with stable A3H. Combining the A3H genotypes and transmission status of these couples, we determined the transmission rate from an index patient with unstable A3H to a partner with stable A3H, and we showed that it is approximately the same to an unstable-to-unstable scenario. We also genotyped the *vif* isolated from the patients within the unstable-to-stable subgroups and predicted function of the encoded protein based on previously reported position 39. We discovered that the predicted fractions of hypo-functional Vif is approximately 40% in both the transmission and non-transmission couples within this subgroup. With a large fraction of the virus expressing hypo-functional Vif and nevertheless the lack of protection of stable A3H in transmissions within this cohort, we conclude that stable A3H is unlikely a transmission barrier on the populational level.

The lack of transmission from one individual to another can be attributed to a variety of reasons, such as the lack of exposure and natural resistance. Previous characterizations of this serodiscordant couple cohort has indicated that 14% of the individuals within this cohort have persistently high HIV-1 exposure and remained uninfected [180]. This suggests that a small fraction of the individuals may exhibit one or multiple natural resistance mechanisms that protect them from HIV-1 acquisition. Some previously studied biological factors that contribute to natural resistance include the polymorphisms in chemokine receptor CCR5 (Δ32 residues) and differences in human leukocyte antigens (HLA) [181-184]. Due to the small number of naturally resistant individuals and the wide variety of potential factors behind the resistance, it is possible that the contribution of stable A3H in protection from HIV-1 acquisition is overshadowed by insufficient exposure and other natural factors on the populational level. Therefore, we propose an experiment in which we obtain peripheral blood mononuclear cells (PBMCs) from the uninfected stable-A3H partner and infect them with HIV-1 harboring the hypo-functional Vif from the infected index patient (**Figure 4-3**). In parallel, we test a hyper-functional derivative of the patient Vif converted using mutagenesis or adaptation and infect the same PBMCs. If conversion of the Vif functionality granted the virus the ability to infect the previously uninfectable PBMCs, the stable A3H is likely the transmission barrier in this case. Otherwise, if the PBMCs remain uninfectable, another factor or multiple factors may be responsible for the resistance.

It is possible that stable A3H may play a role later during HIV-1 infection. We have observed that stable A3H is up-regulated upon HIV-1 infection, but the expression level

does not reach its peak until 10 days post-infection in primary T lymphocytes [96]. Therefore, it is possible that stable A3H, rather than blocking the transmission, helps to protect the host by restricting viral replication and slowing disease progression after establishment of the infection. This possibility is supported by a previous study showing that HIV-1 patients with stable A3H have significantly lower viral load and higher CD4 counts than those with unstable A3H [94]. Another study comparing HIV-1 infected patients, long-term non-progressors, and healthy controls within the Japanese population have also found lower risk of disease progression in individuals with stable A3H [185]. Further longitudinal studies are needed to determine if stable A3H provides additional benefits to the life expectancy of HIV-1 infected patients undergoing anti-retroviral therapies.

MATERIALS AND METHODS

A3H genotyping

Genomic DNA was isolated from dried blood spots using the Gentra Puregene (Qiagen) protocol with a modified lysis step (based on [186]). Paper containing dried blood spot was punched into a tube and incubated with lysis solution (1 M Tris pH8.0, 0.5 M EDTA, 4 M NaCl, 20% SDS, 0.3 mg/mL proteinase K) at 56°C for at least 2 hours before being removed. A 313 or 310 base-pair amplicon containing the N15 or Δ15 position was amplified using primers RSH5902 (5'-CCG AAA CAT TCC GCT TAC AG-3') and RSH5905 (5'-AAC TGG GCC ACT CAG ATC C-3'). A 269 base-pair amplicon containing the R105 or G105 position was amplified using primers RSH16871 (5'-GAA

AAA GTG CCA TGC AGA AAT TTG CTT T-3') and RSH16872 (5'-CTG GGA AGC CCA TGA CCT CC-3'). Both were amplified using Taq (Denville) at 94°C for 5 min, followed by 13 cycles of 94°C for 45 sec, 68°C for 30 sec, and 72°C for 1.5 min, subsequently 22 cycles of 94°C for 45 sec, 55°C for 30 sec, and 72°C for 1 min, and final elongation at 72°C for 10 min. The crude PCR reaction was incubated with exonuclease I (NEB) and recombinant shrimp alkaline phosphatase (NEB) at 37°C for 30 min and inactivated at 95°C for 10 min. The enzymatically cleaned-up 15 and 105 amplicons were sequenced using the RSH5905 and RSH16871 respectively and analyzed using Sequencher.

vif genotyping

Viral RNA was isolated from approximately 500 μL of each patient serum sample using the QIAamp viral RNA mini kit (Qiagen) and reverse transcribed using Transcriptor reverse transcriptase (Roche) and random DNA hexamers as the primer. The amplicons containing the open-reading frame of *vif* was first amplified using primers RSH9754 (5'-GAA AGG TGA AGG GGC ART AR-3') and RSH9755 (5'-TCT TAT TAK RGC TTC AAC TCC-3') with Phusion high-fidelity polymerase (NEB). The reaction was incubated at 98°C for 30 sec, 30 cycles of 98°C for 10 sec, 60°C for 20 sec, and 72°C for 1 min, and followed by 72°C for 10 min. It was subsequently amplified using primers RSH9756 (5'-CCN AGA AGR AAA GYA AAR ATC A-3') and RSH9757 (5'-AGG AAA RTG TCT NAC AGC YTC-3') with Phusion. The reaction was incubated at the same thermal cycles except with 10 additional cycles. The PCR product was purified using 1% agarose gel and extracted using the GeneJET gel extraction kit (Thermo Scientific). Purified amplicons

containing *vif* was cloned into pJET1.2 vectors using the CloneJET PCR cloning kit (Thermo Scientific), transformed and amplified in E. coli (DH10B), miniprepped, and sequenced using RSH2313 (5'-CGA CTC ACT ATA GGG AGA GCG GC-3') and RSH2314 (5'-AAG AAC ATC GAT TTT CCA TGG CAG-3'). The sequencing results were analyzed using Sequencher and ApE.

ADDITIONAL CONTRIBUTIONS

This work was supported by NIAID R37 AI064046. J.W. received partial salary support from the University of Minnesota Graduate School, Interdisciplinary Doctoral Fellowship. R.S.H. is the Margaret Harvey Schering Land Grant Chair for Cancer Research, a Distinguished University McKnight Professor, and an Investigator of the Howard Hughes Medical Institute.

Table 4-1. Common human *A3H* haplotypes.

A3H haplotype	Amino acid position and variant					Protein stability
	15	**18**	**105**	**121**	**178**	
I	N	R	G	K	E	Hypomorphic
II	N	R	R	D	D	Stable
III	Δ	R	R	D	D	Unstable
IV	Δ	L	R	D	D	Unstable

Table 4-2. *A3H* genotyping results.

A3H genotype		All subjects	
15	**105**	**n**	**Frequency**
N/N	R/R	293	0.25
N/N	G/R	125	0.10
N/N	G/G	17	0.01
N/Δ	R/R	456	0.38
N/Δ	G/R	102	0.09
N/Δ	G/G	3	< 0.01
Δ/Δ	R/R	157	0.13
Δ/Δ	G/R	8	0.01
Δ/Δ	G/G	2	< 0.01
Unknown		31	
Total		**1194**	

Table 4-3. Transmission rates of couples with different *A3H* genotypes.

A3H genotypes	Total	Transmission	Non-transmission	Transmission rate
Stable-to-stable	241	77	164	32.0%
Stable-to-unstable	159	58	101	36.5%
Unstable-to-stable	65	22	43	33.8%
Unstable-to-unstable	9	3	6	33.3%

Table 4-4. Predicted functionality of Vif isolated from the unstable-to-stable subgroups.

Transmission status	Total	Hyper-functional	Hypo-functional	Unknown	%Hypo-functional
Non-transmission	43	13	10	20	43%
Transmission	21	9	6	6	40%

Hyper-functional Vif is predicted based on at least one clone of Vif having F39 or Y39. Hypo-functional Vif is predicted when all clones of Vif have amino acid other than F or Y at position 39.

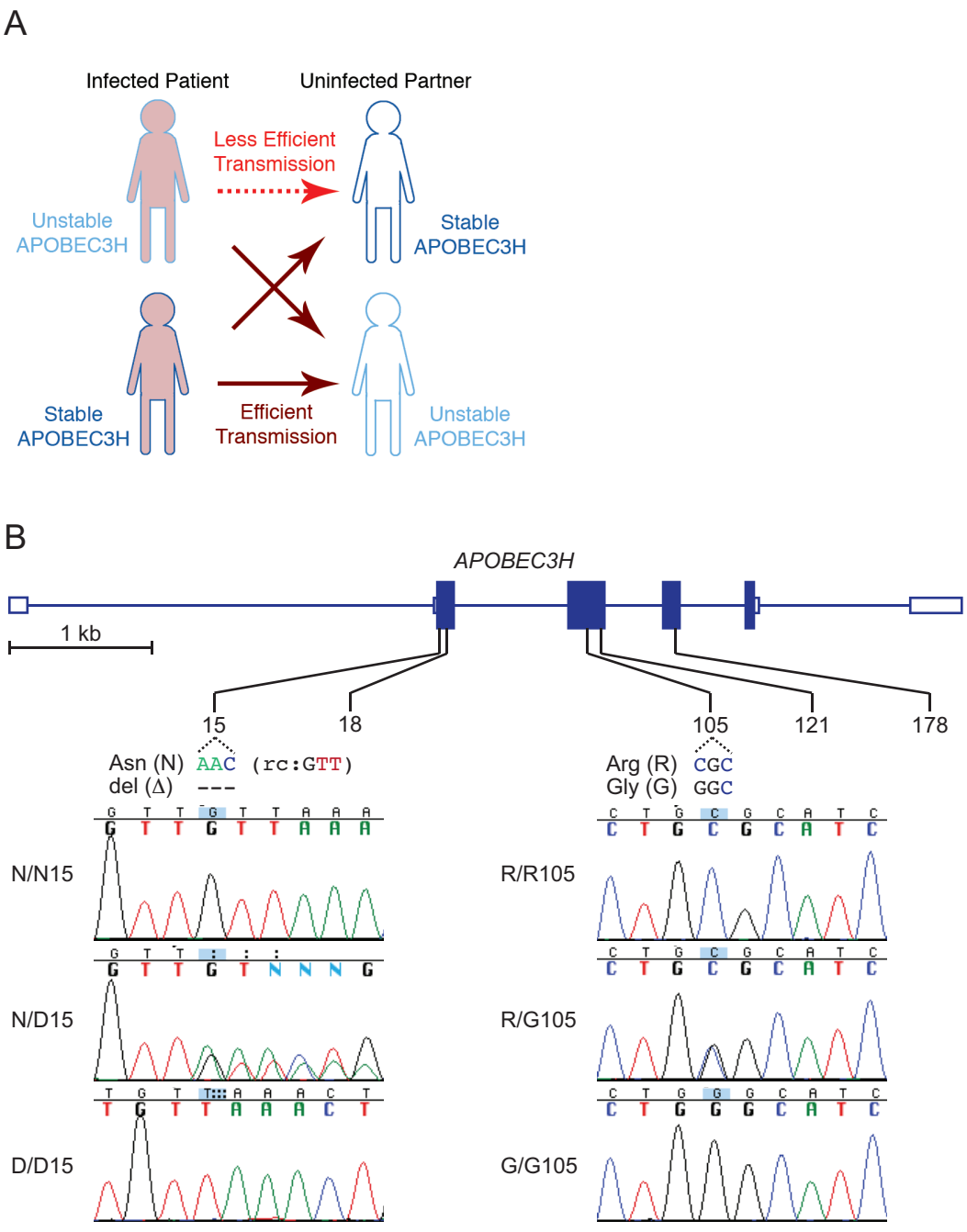

Figure 4-1. The potential role of A3H as a transmission barrier to HIV-1 acquisition. (**A**) A schematic showing stable A3H as a transmission barrier to HIV-1 acquisition from partner with unstable A3H.

(**B**) A schematic of the human *A3H* gene showing locations of critical amino acid positions 15 and 105 that dictate the stability of the encoded proteins (top). Representative sequence chromatograms of individuals with indicated *A3H* genotypes (bottom).

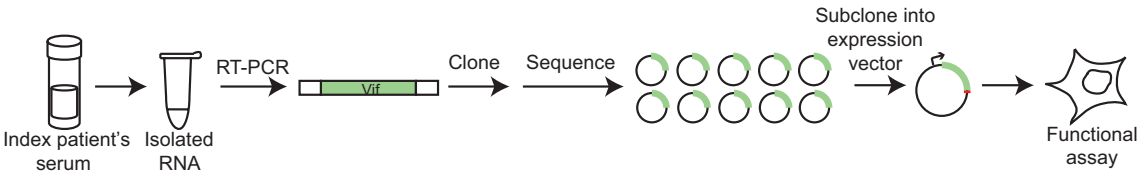

Figure 4-2. Determining the Vif functionality in unstable-to-stable subgroup.

A schematic showing the workflow of Vif genotyping and functional assay.

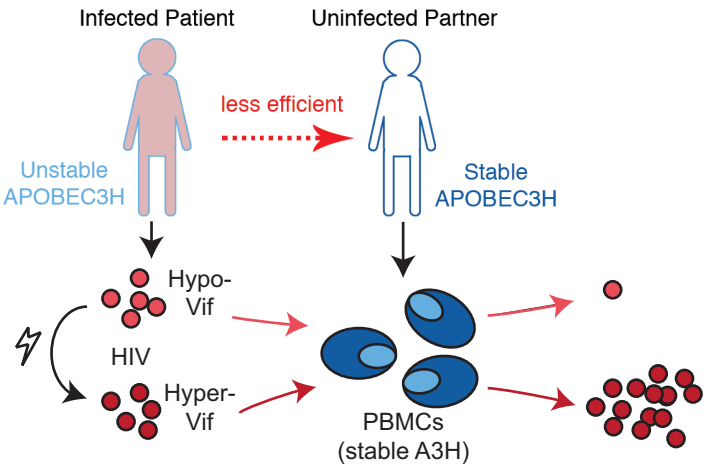

Figure 4-3. Schematic of the PBMC experiment to test stable A3H as a transmission barrier.

See text for details. Lightning symbol represents mutations to restore the A3H degradation function of Vif.

CHAPTER 5

Conclusions and Discussion

CONCLUSIONS

Efficient HIV-1 infection of human cells requires neutralization or evasion of a variety of host restriction factors. Restoring these innate immune defense mechanisms is a largely under-explored area of HIV research. An especially appealing target is the human A3 family of DNA cytosine deaminases, with at least four members having potent anti-HIV-1 activity. These enzymes are all capable of directly hypermutating the viral genome and ablating pathogenesis. HIV-1 counteracts this restriction mechanism using Vif, which directly binds to restrictive A3 proteins and mediates their degradation. More than a decade of scientific research on A3 and Vif has elucidated a range of molecular determinants and cofactors required for the functional interaction between the two (see **Chapter 1**). Many of the discoveries were enabled by loss-of-function studies, molecular modeling and structural determinations of a single protein or a partial complex [40, 42-54, 65, 89, 92-108, 113, 142, 145, 147, 187, 188], despite the lack of direct biophysical information of the A3-Vif interface (co-structure of Vif with any A3). My thesis research is focused on understanding the dynamic interplay between human A3 enzymes and lentiviral Vif, both in terms of the molecular determinants and implications for HIV-1 transmission within the human population.

The functional interactions between a lentiviral Vif and the host A3 proteins are largely species-specific. One exception to this rule is SIVmac239 Vif, which exhibits degradation activity against multiple human A3 enzymes, including human A3B that does not normally restrict HIV-1 or SIV. To understand this interface, we performed mutagenesis studies on both human A3B and SIVmac239 Vif, and revealed amino acid

determinants for this functional interaction (see **Chapter 2**). Our results demonstrated that the putative physical interface is largely similar to the HIV-1 Vif interface responsible for A3G degradation.

RNA binding, in addition to DNA binding and editing activity, has integral roles in the antiviral activities of A3 proteins. It is required for multiple A3 proteins' ability to localize into the cytoplasm and package into virions [151, 155-160] [50, 62-72]. Recent discoveries of human and other primate A3H crystal structures revealed an evolutionarily conserved duplex RNA-mediated dimerization mechanism, as well as A3H amino acid residues involved in this interaction [42, 49, 50]. Mutating some of the RNA-binding residues results in altered localization and reduced HIV-1 virion packaging. We determined the x-ray crystal structure of an RNA binding-defective A3H variant with amino acid substitutions W115A, R175E, and R176E (see **Chapter 3**). These mutations abrogate RNA binding and result in a monomeric A3H protein. We subsequently investigated the role of RNA in the A3H-Vif interaction by testing the susceptibility of A3H RNA binding-defective mutants to Vif using degradation assay and fluorescence live cell imaging. A subset of the A3H mutants including the monomeric triple mutant are resistant to Vif. However, using a split GFP system, we show that Vif does not interfere with A3H dimerization in living cells. Therefore, Vif and RNA likely binds to A3H physically distinct surfaces.

The *A3H* gene is highly variable in the human population with differential geographical distribution of haplotypes. The African populations are enriched with haplotype II (> 50% frequency) that encodes stably expressed proteins with potent antiviral

activity [94, 96, 126, 129, 175]. A hypomorphic allele of *A3H* (haplotype I) that lacks antiviral activity is predominant in the other geographic regions of the world [122, 129, 162]. Only a fraction of HIV-1 isolates harbors hyper-functional *vif* allele that counteracts stable A3H, suggesting that stable A3H can potentially protect the host from acquisition of viruses lacking a hyper-functional Vif [94, 96]. To test this hypothesis, we determined the *A3H* and *vif* genotypes of a large to patient cohort and analyzed their associations with transmission status (see **Chapter 4**). On the populational level, we did not observe protection of stable A3H from transmission statistically, suggesting that A3H haplotype II is unlikely an intraspecies transmission barrier.

DISCUSSION

The promiscuity of SIVmac239 Vif in targeting multiple human A3 proteins may have its roots in an ancestral lentiviral Vif activity. A Prior study have indicated that HIV-1 and HIV-2 Vif proteins interact with human A3G using different residues [188]. In particular, the YRHHY motif of HIV-1 Vif is required and G48 is dispensable for human A3G degradation, whereas HIV-2 Vif has the opposite requirements [188]. Interestingly, here we show that SIVmac239 Vif residues within both the YRHHY motif as well as G48 are required for degrading human A3B (**Figure 2-3**). The ability of SIVmac239 Vif to target a non-restricting A3 protein of a foreign species may be due to the retention of an ancestral function. For instance, an ancestral Vif may have been able to target a wide range of A3 proteins using a single conserved surface, as proposed in the "Wobble Model" [100, 189]. Over time, each lentiviral Vif had the potential to adapt step-wise (wobble) to use more

distinct surfaces to target different A3 proteins, and at the same time become more specific for each restrictive A3 enzyme. HIV-1 Vif exemplifies a highly evolved Vif, while SIVmac239 Vif protein's promiscuity may be a remnant of such an ancestral Vif function. It would be interesting in future studies to ask if SIVmac239 and SIVsm have similar functional requirements for A3B antagonism, as the Vif proteins of several SIVsm isolates have clear human A3B degradation activity [137].

Studying the role of RNA in A3H-Vif interaction has led to a working model in which Vif and RNA bind to separate solvent-exposed surfaces of A3H. This may be advantageous for the virus, as Vif can potentially mediate the degradation of both monomeric and dimeric A3H simultaneously. This dimeric degradation may allow Vif to more efficiently target the cellular A3H pool. However, it is unclear why a fraction of A3H RNA binding-defective mutants are resistant to Vif. We speculate that the altered localization of these mutants might play a role in hindering degradation by Vif, as A3H proteins in the cytoplasmic compartments are degraded more rapidly than those in nucleoli (**Figure 3-3A-B**). This may be due to the differential mobility of A3H and Vif-CBF-β-E3 ligase complex in different subcellular compartments, allowing Vif to more readily interact with A3H in cytoplasm than in nuclear compartments. Another possible explanation is that the binding of an unknown (protein or nucleic acid) nuclear retention factor to A3H affects the A3H-Vif interaction. The identity of such retention factor and the determinants of its interaction with A3H remain questions to be answered.

The nucleic acid sequences of the RNA bound by primate A3H were not resolved clearly by any of the x-ray structures [42, 49, 50]. Therefore, it is unclear whether A3H

recognize a specific RNA sequence and/or a secondary structure such as the stem of a stem-loop motif. A previous CLIP-seq study highlighted hotspots on the HIV-1 genome bound by overexpressed A3H in both cells and virions, indicating that the LTR regions are preferred [71]. These are regions of the HIV-1 gRNA with conserved secondary structures [190]. A comprehensive study identifying the RNA molecules bound by endogenous A3H in the absence and presence of HIV-1 infection is necessary to elucidate the role of RNA in A3H biology.

Although stable A3H has been implicated as an interspecies barrier [116], it is unlikely an intraspecies transmission barrier on the populational level. However, the differential geographical distribution of the *A3H* and HIV-1 *vif* genetic variations suggest viral adaptation to a selective pressure to counteract A3H (**Figure 1-3**). Therefore, the presence of stable A3H may still serve as a "hurdle" that grants fitness advantages to viruses encoding hyper-functional Vif proteins. This is consistent with previous studies suggesting that stable A3H plays a role in slowing disease progression in HIV-1-infected individuals [94, 185]. However, an intriguing question is whether the viruses reverse back to encode hypo-functional Vif in the absence of stable A3H, *i.e.* "de-adapt". This would suggest a fitness cost in retaining function against A3H in sacrifice of another function. A previous study implicated a conflict between Vif's function in mediating A3H degradation and inducing cell cycle arrest, since these functions require different amino acids at the same solvent-exposed positions [167]. How the latter increases the fitness of the virus remains unclear. However, it is possible, as this would suggest, that HIV-1 Vif might have reached a limit in its optimization as a multi-functional protein.

CLOSING REMARKS

Tremendous amount of progress has been made in understanding the biology of HIV-1 from the past decades of research, but unfortunately, viral eradication is still impossible. As such a "successful" virus, HIV-1 designate at least three out of its nine genes to encode proteins as counterdefenses against human restriction factors. Understanding the host-pathogen interactions may shed light on novel therapeutic approaches to restore the functionality of these powerful restriction factors.

My thesis research contributes to the growing knowledge of A3-Vif interaction, from elucidating the molecular determinants of a cross-species interface, to investigating the role of RNA in the A3H-Vif interaction, and finally determining whether A3H can be an intraspecies transmission barrier.

A lot more questions remain to be answered. I hope every step we make forward is leading us closer to a cure that is surely to come.

BIBLIOGRAPHY

[1] Freed EO. HIV-1 gag proteins: diverse functions in the virus life cycle. Virology. 1998;251:1-15.

[2] Chinen J, Shearer WT. Molecular virology and immunology of HIV infection. J Allergy Clin Immunol. 2002;110:189-98.

[3] Fanales-Belasio E, Raimondo M, Suligoi B, Butto S. HIV virology and pathogenetic mechanisms of infection: a brief overview. Ann Ist Super Sanita. 2010;46:5-14.

[4] Sundquist WI, Krausslich HG. HIV-1 assembly, budding, and maturation. Cold Spring Harb Perspect Med. 2012;2:a006924.

[5] Frankel AD, Young JA. HIV-1: fifteen proteins and an RNA. Annu Rev Biochem. 1998;67:1-25.

[6] Checkley MA, Luttge BG, Freed EO. HIV-1 envelope glycoprotein biosynthesis, trafficking, and incorporation. J Mol Biol. 2011;410:582-608.

[7] Munro JB, Mothes W. Structure and dynamics of the native HIV-1 Env trimer. J Virol. 2015;89:5752-5.

[8] Ward AB, Wilson IA. The HIV-1 envelope glycoprotein structure: nailing down a moving target. Immunol Rev. 2017;275:21-32.

[9] Debaisieux S, Rayne F, Yezid H, Beaumelle B. The ins and outs of HIV-1 Tat. Traffic. 2012;13:355-63.

[10] Pugliese A, Vidotto V, Beltramo T, Petrini S, Torre D. A review of HIV-1 Tat protein biological effects. Cell Biochem Funct. 2005;23:223-7.

[11] Romani B, Engelbrecht S, Glashoff RH. Functions of Tat: the versatile protein of human immunodeficiency virus type 1. J Gen Virol. 2010;91:1-12.

[12] Hope TJ. The ins and outs of HIV Rev. Arch Biochem Biophys. 1999;365:186-91.

[13] Pollard VW, Malim MH. The HIV-1 Rev protein. Annu Rev Microbiol. 1998;52:491-532.

[14] Li L, Li HS, Pauza CD, Bukrinsky M, Zhao RY. Roles of HIV-1 auxiliary proteins in viral pathogenesis and host-pathogen interactions. Cell Res. 2005;15:923-34.

[15] Briggs JA, Wilk T, Welker R, Krausslich HG, Fuller SD. Structural organization of authentic, mature HIV-1 virions and cores. EMBO J. 2003;22:1707-15.

[16] German Advisory Committee Blood SAoPTbB. Human immunodeficiency virus (HIV). Transfus Med Hemother. 2016;43:203-22.

[17] Mogensen TH, Melchjorsen J, Larsen CS, Paludan SR. Innate immune recognition and activation during HIV infection. Retrovirology. 2010;7:54.

[18] Engelman A, Cherepanov P. The structural biology of HIV-1: mechanistic and therapeutic insights. Nat Rev Microbiol. 2012;10:279-90.

[19] Ambrose Z, Aiken C. HIV-1 uncoating: connection to nuclear entry and regulation by host proteins. Virology. 2014;454-455:371-9.

[20] Arhel N. Revisiting HIV-1 uncoating. Retrovirology. 2010;7:96.

[21] Hu WS, Hughes SH. HIV-1 reverse transcription. Cold Spring Harb Perspect Med. 2012;2.

[22] Le Grice SF. Human immunodeficiency virus reverse transcriptase: 25 years of research, drug discovery, and promise. J Biol Chem. 2012;287:40850-7.

[23] Craigie R, Bushman FD. HIV DNA integration. Cold Spring Harb Perspect Med. 2012;2:a006890.

[24] Harris RS, Hultquist JF, Evans DT. The restriction factors of human immunodeficiency virus. J Biol Chem. 2012;287:40875-83.

[25] Malim MH, Bieniasz PD. HIV restriction factors and mechanisms of evasion. Cold Spring Harb Perspect Med. 2012;2:a006940.

[26] Grutter MG, Luban J. TRIM5 structure, HIV-1 capsid recognition, and innate immune signaling. Curr Opin Virol. 2012;2:142-50.

[27] Nisole S, Stoye JP, Saib A. TRIM family proteins: retroviral restriction and antiviral defence. Nat Rev Microbiol. 2005;3:799-808.

[28] Stremlau M, Owens CM, Perron MJ, Kiessling M, Autissier P, Sodroski J. The cytoplasmic body component TRIM5alpha restricts HIV-1 infection in Old World monkeys. Nature. 2004;427:848-53.

[29] Li YL, Chandrasekaran V, Carter SD, Woodward CL, Christensen DE, Dryden KA, et al. Primate TRIM5 proteins form hexagonal nets on HIV-1 capsids. Elife. 2016;5.

[30] Nakayama EE, Shioda T. TRIM5alpha and species tropism of HIV/SIV. Front Microbiol. 2012;3:13.

[31] Desimmie BA, Delviks-Frankenberrry KA, Burdick RC, Qi DF, Izumi T, Pathak VK. Multiple APOBEC3 restriction factors for HIV-1 and one Vif to rule them all. J Mol Biol. 2014;426:1220-45.

[32] Harris RS, Dudley JP. APOBECs and virus restriction. Virology. 2015;479:131-45.

[33] Nakano Y, Aso H, Soper A, Yamada E, Moriwaki M, Juarez-Fernandez G, et al. A conflict of interest: the evolutionary arms race between mammalian APOBEC3 and lentiviral Vif. Retrovirology. 2017;14.

[34] Perez-Caballero D, Zang T, Ebrahimi A, McNatt MW, Gregory DA, Johnson MC, et al. Tetherin inhibits HIV-1 release by directly tethering virions to cells. Cell. 2009;139:499-511.

[35] Rosa A, Chande A, Ziglio S, De Sanctis V, Bertorelli R, Goh SL, et al. HIV-1 Nef promotes infection by excluding SERINC5 from virion incorporation. Nature. 2015;526:212-7.

[36] Usami Y, Wu Y, Gottlinger HG. SERINC3 and SERINC5 restrict HIV-1 infectivity and are counteracted by Nef. Nature. 2015;526:218-23.

[37] Jarmuz A, Chester A, Bayliss J, Gisbourne J, Dunham I, Scott J, et al. An anthropoid-specific locus of orphan C to U RNA-editing enzymes on chromosome 22. Genomics. 2002;79:285-96.

[38] Refsland EW, Harris RS. The APOBEC3 family of retroelement restriction factors. Curr Top Microbiol. 2013;371:1-27.

[39] Burns MB, Lackey L, Carpenter MA, Rathore A, Land AM, Leonard B, et al. APOBEC3B is an enzymatic source of mutation in breast cancer. Nature. 2013;494:366-70.

[40] Shi K, Carpenter MA, Banerjee S, Shaban NM, Kurahashi K, Salamango DJ, et al. Structural basis for targeted DNA cytosine deamination and mutagenesis by APOBEC3A and APOBEC3B. Nat Struct Mol Biol. 2017;24:131-9.

[41] LaRue RS, Andresdottir V, Blanchard Y, Conticello SG, Derse D, Emerman M, et al. Guidelines for naming nonprimate APOBEC3 genes and proteins. J Virol. 2009;83:494-7.

[42] Bohn JA, Thummar K, York A, Raymond A, Brown WC, Bieniasz PD, et al. APOBEC3H structure reveals an unusual mechanism of interaction with duplex RNA. Nat Commun. 2017;8:1021.

[43] Bohn MF, Shandilya SM, Albin JS, Kouno T, Anderson BD, McDougle RM, et al. Crystal structure of the DNA cytosine deaminase APOBEC3F: the catalytically active and HIV-1 Vif-binding domain. Structure. 2013;21:1042-50.

[44] Byeon IJ, Ahn J, Mitra M, Byeon CH, Hercik K, Hritz J, et al. NMR structure of human restriction factor APOBEC3A reveals substrate binding and enzyme specificity. Nat Commun. 2013;4:1890.

[45] Holden LG, Prochnow C, Chang YP, Bransteitter R, Chelico L, Sen U, et al. Crystal structure of the anti-viral APOBEC3G catalytic domain and functional implications. Nature. 2008;456:121-4.

[46] Kitamura S, Ode H, Nakashima M, Imahashi M, Naganawa Y, Kurosawa T, et al. The APOBEC3C crystal structure and the interface for HIV-1 Vif binding. Nat Struct Mol Biol. 2012;19:1005-10.

[47] Kouno T, Luengas EM, Shigematsu M, Shandilya SM, Zhang J, Chen L, et al. Structure of the Vif-binding domain of the antiviral enzyme APOBEC3G. Nat Struct Mol Biol. 2015;22:485-91.

[48] Kouno T, Silvas TV, Hilbert BJ, Shandilya SMD, Bohn MF, Kelch BA, et al. Crystal structure of APOBEC3A bound to single-stranded DNA reveals structural basis for cytidine deamination and specificity. Nat Commun. 2017;8:15024.

[49] Matsuoka T, Nagae T, Ode H, Awazu H, Kurosawa T, Hamano A, et al. Structural basis of chimpanzee APOBEC3H dimerization stabilized by double-stranded RNA. Nucleic Acids Res. 2018;46:10368-79.

[50] Shaban NM, Shi K, Lauer KV, Carpenter MA, Richards CM, Salamango D, et al. The antiviral and cancer genomic DNA deaminase APOBEC3H is regulated by an RNA-mediated dimerization mechanism. Mol Cell. 2018;69:75-86.e9.

[51] Shandilya SM, Nalam MN, Nalivaika EA, Gross PJ, Valesano JC, Shindo K, et al. Crystal structure of the APOBEC3G catalytic domain reveals potential oligomerization interfaces. Structure. 2010;18:28-38.

[52] Shi K, Carpenter MA, Kurahashi K, Harris RS, Aihara H. Crystal structure of the DNA deaminase APOBEC3B catalytic domain. J Biol Chem. 2015;290:28120-30.

[53] Xiao X, Li SX, Yang H, Chen XS. Crystal structures of APOBEC3G N-domain alone and its complex with DNA. Nat Commun. 2016;7:12193.

[54] Xiao X, Yang H, Arutiunian V, Fang Y, Besse G, Morimoto C, et al. Structural determinants of APOBEC3B non-catalytic domain for molecular assembly and catalytic regulation. Nucleic Acids Res. 2017;45:7494-506.

[55] Logue EC, Bloch N, Dhuey E, Zhang R, Cao P, Herate C, et al. A DNA sequence recognition loop on APOBEC3A controls substrate specificity. PLoS One. 2014;9:e97062.

[56] Rathore A, Carpenter MA, Demir Ö, Ikeda T, Li M, Shaban NM, et al. The local dinucleotide preference of APOBEC3G can be altered from 5'-CC to 5'-TC by a single amino acid substitution. J Mol Biol. 2013;425:4442-54.

[57] Zhang W, Du J, Yu K, Wang T, Yong X, Yu XF. Association of potent human antiviral cytidine deaminases with 7SL RNA and viral RNP in HIV-1 virions. J Virol. 2010;84:12903-13.

[58] Conticello SG, Thomas CJF, Petersen-Mahrt SK, Neuberger MS. Evolution of the AID/APOBEC family of polynucleotide (deoxy)cytidine deaminases. Mol Biol Evol. 2005;22:367-77.

[59] Harris RS, Liddament MT. Retroviral restriction by APOBEC proteins. Nat Rev Immunol. 2004;4:868-77.

[60] LaRue RS, Jonsson SR, Silverstein KA, Lajoie M, Bertrand D, El-Mabrouk N, et al. The artiodactyl APOBEC3 innate immune repertoire shows evidence for a multi-functional domain organization that existed in the ancestor of placental mammals. BMC Mol Biol. 2008;9:104.

[61] Münk C, Willemsen A, Bravo IG. An ancient history of gene duplications, fusions and losses in the evolution of APOBEC3 mutators in mammals. BMC Evol Biol. 2012;12:71.

[62] Apolonia L, Schulz R, Curk T, Rocha P, Swanson CM, Schaller T, et al. Promiscuous RNA binding ensures effective encapsidation of APOBEC3 proteins by HIV-1. PLoS Pathog. 2015;11:e1004609.

[63] Bogerd HP, Cullen BR. Single-stranded RNA facilitates nucleocapsid: APOBEC3G complex formation. RNA. 2008;14:1228-36.

[64] Cen S, Guo F, Niu M, Saadatmand J, Deflassieux J, Kleiman L. The interaction between HIV-1 Gag and APOBEC3G. J Biol Chem. 2004;279:33177-84.

[65] Huthoff H, Malim MH. Identification of amino acid residues in APOBEC3G required for regulation by human immunodeficiency virus type 1 Vif and virion encapsidation. J Virol. 2007;81:3807-15.

[66] Khan MA, Kao S, Miyagi E, Takeuchi H, Goila-Gaur R, Opi S, et al. Viral RNA is required for the association of APOBEC3G with human immunodeficiency virus type 1 nucleoprotein complexes. J Virol. 2005;79:5870-4.

[67] Schafer A, Bogerd HP, Cullen BR. Specific packaging of APOBEC3G into HIV-1 virions is mediated by the nucleocapsid domain of the gag polyprotein precursor. Virology. 2004;328:163-8.

[68] Svarovskaia ES, Xu H, Mbisa JL, Barr R, Gorelick RJ, Ono A, et al. Human apolipoprotein B mRNA-editing enzyme-catalytic polypeptide-like 3G (APOBEC3G) is incorporated into HIV-1 virions through interactions with viral and nonviral RNAs. J Biol Chem. 2004;279:35822-8.

[69] Wang T, Tian C, Zhang W, Luo K, Sarkis PT, Yu L, et al. 7SL RNA mediates virion packaging of the antiviral cytidine deaminase APOBEC3G. J Virol. 2007;81:13112-24.

[70] Wang T, Tian C, Zhang W, Sarkis PT, Yu XF. Interaction with 7SL RNA but not with HIV-1 genomic RNA or P bodies is required for APOBEC3F virion packaging. J Mol Biol. 2008;375:1098-112.

[71] York A, Kutluay SB, Errando M, Bieniasz PD. The RNA binding specificity of human APOBEC3 proteins resembles that of HIV-1 nucleocapsid. PLoS Pathog. 2016;12:e1005833.

[72] Zennou V, Perez-Caballero D, Gottlinger H, Bieniasz PD. APOBEC3G incorporation into human immunodeficiency virus type 1 particles. J Virol. 2004;78:12058-61.

[73] Donahue JP, Levinson RT, Sheehan JH, Sutton L, Taylor HE, Meiler J, et al. Genetic analysis of the localization of APOBEC3F to human immunodeficiency virus type 1 virion cores. J Virol. 2015;89:2415-24.

[74] Song C, Sutton L, Johnson ME, D'Aquila RT, Donahue JP. Signals in APOBEC3F N-terminal and C-terminal deaminase domains each contribute to encapsidation in HIV-1 virions and are both required for HIV-1 restriction. J Biol Chem. 2012;287:16965-74.

[75] Bélanger K, Langlois MA. RNA-binding residues in the N-terminus of APOBEC3G influence its DNA sequence specificity and retrovirus restriction efficiency. Virology. 2015;483:141-8.

[76] Bishop KN, Verma M, Kim EY, Wolinsky SM, Malim MH. APOBEC3G inhibits elongation of HIV-1 reverse transcripts. PLoS Pathog. 2008;4:e1000231.

[77] Gillick K, Pollpeter D, Phalora P, Kim EY, Wolinsky SM, Malim MH. Suppression of HIV-1 infection by APOBEC3 proteins in primary human CD4(+) T cells is

associated with inhibition of processive reverse transcription as well as excessive cytidine deamination. J Virol. 2013;87:1508-17.

[78] Iwatani Y, Chan DS, Wang F, Maynard KS, Sugiura W, Gronenborn AM, et al. Deaminase-independent inhibition of HIV-1 reverse transcription by APOBEC3G. Nucleic Acids Res. 2007;35:7096-108.

[79] Kobayashi T, Koizumi Y, Takeuchi JS, Misawa N, Kimura Y, Morita S, et al. Quantification of deaminase activity-dependent and -independent restriction of HIV-1 replication mediated by APOBEC3F and APOBEC3G through experimental-mathematical investigation. J Virol. 2014;88:5881-7.

[80] Morse M, Huo R, Feng Y, Rouzina I, Chelico L, Williams MC. Dimerization regulates both deaminase-dependent and deaminase-independent HIV-1 restriction by APOBEC3G. Nat Commun. 2017;8:597.

[81] Newman EN, Holmes RK, Craig HM, Klein KC, Lingappa JR, Malim MH, et al. Antiviral function of APOBEC3G can be dissociated from cytidine deaminase activity. Curr Biol. 2005;15:166-70.

[82] Ooms M, Majdak S, Seibert CW, Harari A, Simon V. The localization of APOBEC3H variants in HIV-1 virions determines their antiviral activity. J Virol. 2010;84:7961-9.

[83] Guo Y, Dong L, Qiu X, Wang Y, Zhang B, Liu H, et al. Structural basis for hijacking CBF-beta and CUL5 E3 ligase complex by HIV-1 Vif. Nature. 2014;505:229-33.

[84] Jäger S, Kim DY, Hultquist JF, Shindo K, LaRue RS, Kwon E, et al. Vif hijacks CBF-beta to degrade APOBEC3G and promote HIV-1 infection. Nature. 2011;481:371-5.

[85] Zhang W, Du J, Evans SL, Yu Y, Yu XF. T-cell differentiation factor CBF-beta regulates HIV-1 Vif-mediated evasion of host restriction. Nature. 2011;481:376-9.

[86] Stanley BJ, Ehrlich ES, Short L, Yu Y, Xiao Z, Yu XF, et al. Structural insight into the human immunodeficiency virus Vif SOCS box and its role in human E3 ubiquitin ligase assembly. J Virol. 2008;82:8656-63.

[87] Yu YK, Xiao ZX, Ehrlich ES, Yu XH, Yu XF. Selective assembly of HIV-1 Vif-Cul5-ElonginB-ElonginC E3 ubiquitin ligase complex through a novel SOCS box and upstream cysteines. Gene Dev. 2004;18:2867-72.

[88] Luo K, Xiao ZX, Ehrlich E, Yu YK, Liu BD, Zheng S, et al. Primate lentiviral virion infectivity factors are substrate receptors that assemble with cullin 5-E3 ligase through a HCCH motif to suppress APOBEOG. Proc Natl Acad Sci U S A. 2005;102:11444-9.

[89] Russell RA, Pathak VK. Identification of two distinct human immunodeficiency virus type 1 Vif determinants critical for interactions with human APOBEC3G and APOBEC3F. J Virol. 2007;81:8201-10.

[90] Hultquist JF, Lengyel JA, Refsland EW, LaRue RS, Lackey L, Brown WL, et al. Human and rhesus APOBEC3D, APOBEC3F, APOBEC3G, and APOBEC3H demonstrate a conserved capacity to restrict Vif-deficient HIV-1. J Virol. 2011;85:11220-34.

[91] Chen G, He Z, Wang T, Xu R, Yu XF. A patch of positively charged amino acids surrounding the human immunodeficiency virus type 1 Vif SLVx4Yx9Y motif influences its interaction with APOBEC3G. J Virol. 2009;83:8674-82.

[92] Russell RA, Smith J, Barr R, Bhattacharyya D, Pathak VK. Distinct domains within APOBEC3G and APOBEC3F interact with separate regions of human immunodeficiency virus type 1 Vif. J Virol. 2009;83:1992-2003.

[93] Binka M, Ooms M, Steward M, Simon V. The activity spectrum of Vif from multiple HIV-1 subtypes against APOBEC3G, APOBEC3F, and APOBEC3H. J Virol. 2012;86:49-59.

[94] Ooms M, Brayton B, Letko M, Maio SM, Pilcher CD, Hecht FM, et al. HIV-1 Vif adaptation to human APOBEC3H haplotypes. Cell Host Microbe. 2013;14:411-21.

[95] Ooms M, Letko M, Binka M, Simon V. The resistance of human APOBEC3H to HIV-1 NL4-3 molecular clone is determined by a single amino acid in Vif. PLoS One. 2013;8:e57744.

[96] Refsland EW, Hultquist JF, Luengas EM, Ikeda T, Shaban NM, Law EK, et al. Natural polymorphisms in human APOBEC3H and HIV-1 Vif combine in primary T lymphocytes to affect viral G-to-A mutation levels and infectivity. PLoS Genet. 2014;10:e1004761.

[97] Albin JS, LaRue RS, Weaver JA, Brown WL, Shindo K, Harjes E, et al. A single amino acid in human APOBEC3F alters susceptibility to HIV-1 Vif. J Biol Chem. 2010;285:40785-92.

[98] Land AM, Shaban NM, Evans L, Hultquist JF, Albin JS, Harris RS. APOBEC3F determinants of HIV-1 Vif sensitivity. J Virol. 2014;88:12923-7.

[99] Nakashima M, Ode H, Kawamura T, Kitamura S, Naganawa Y, Awazu H, et al. Structural insights into HIV-1 Vif-APOBEC3F interaction. J Virol. 2015;90:1034-47.

[100] Richards C, Albin JS, Demir O, Shaban NM, Luengas EM, Land AM, et al. The binding interface between human APOBEC3F and HIV-1 Vif elucidated by genetic and computational approaches. Cell Rep. 2015;13:1781-8.

[101] Smith JL, Pathak VK. Identification of specific determinants of human APOBEC3F, APOBEC3C, and APOBEC3DE and African green monkey APOBEC3F that interact with HIV-1 Vif. J Virol. 2010;84:12599-608.

[102] Bogerd HP, Doehle BP, Wiegand HL, Cullen BR. A single amino acid difference in the host APOBEC3G protein controls the primate species specificity of HIV type 1 virion infectivity factor. Proc Natl Acad Sci U S A. 2004;101:3770-4.

[103] Mangeat B, Turelli P, Liao S, Trono D. A single amino acid determinant governs the species-specific sensitivity of APOBEC3G to Vif action. J Biol Chem. 2004;279:14481-3.

[104] Schrofelbauer B, Chen D, Landau NR. A single amino acid of APOBEC3G controls its species-specific interaction with virion infectivity factor (Vif). Proc Natl Acad Sci U S A. 2004;101:3927-32.

[105] Xu H, Svarovskaia ES, Barr R, Zhang Y, Khan MA, Strebel K, et al. A single amino acid substitution in human APOBEC3G antiretroviral enzyme confers resistance to HIV-1 virion infectivity factor-induced depletion. Proc Natl Acad Sci U S A. 2004;101:5652-7.

[106] Zhen A, Wang T, Zhao K, Xiong Y, Yu XF. A single amino acid difference in human APOBEC3H variants determines HIV-1 Vif sensitivity. J Virol. 2010;84:1902-11.

[107] Nakashima M, Tsuzuki S, Awazu H, Hamano A, Okada A, Ode H, et al. Mapping region of human restriction factor APOBEC3H critical for interaction with HIV-1 Vif. J Mol Biol. 2017;429:1262-76.

[108] Ooms M, Letko M, Simon V. The structural interface between HIV-1 Vif and human APOBEC3H. J Virol. 2017;91:e02289.

[109] Gao F, Bailes E, Robertson DL, Chen Y, Rodenburg CM, Michael SF, et al. Origin of HIV-1 in the chimpanzee Pan troglodytes troglodytes. Nature. 1999;397:436-41.

[110] Plantier JC, Leoz M, Dickerson JE, De Oliveira F, Cordonnier F, Lemee V, et al. A new human immunodeficiency virus derived from gorillas. Nat Med. 2009;15:871-2.

[111] Gao F, Yue L, White AT, Pappas PG, Barchue J, Hanson AP, et al. Human infection by genetically diverse SIVSM-related HIV-2 in west Africa. Nature. 1992;358:495-9.

[112] Duggal NK, Emerman M. Evolutionary conflicts between viruses and restriction factors shape immunity. Nat Rev Immunol. 2012;12:687-95.

[113] Letko M, Booiman T, Kootstra N, Simon V, Ooms M. Identification of the HIV-1 Vif and human APOBEC3G protein interface. Cell Rep. 2015;13:1789-99.

[114] Krupp A, McCarthy KR, Ooms M, Letko M, Morgan JS, Simon V, et al. APOBEC3G polymorphism as a selective barrier to cross-species transmission and emergence of pathogenic SIV and AIDS in a primate host. PLoS Pathog. 2013;9:e1003641.

[115] Etienne L, Bibollet-Ruche F, Sudmant PH, Wu LI, Hahn BH, Emerman M. The role of the antiviral APOBEC3 gene family in protecting chimpanzees against lentiviruses from monkeys. PLoS Pathog. 2015;11:e1005149.

[116] Zhang Z, Gu Q, de Manuel Montero M, Bravo IG, Marques-Bonet T, Häussinger D, et al. Stably expressed APOBEC3H forms a barrier for cross-species transmission of simian immunodeficiency virus of chimpanzee to humans. PLoS Pathog. 2017;13:e1006746.

[117] Burns MB, Temiz NA, Harris RS. Evidence for APOBEC3B mutagenesis in multiple human cancers. Nat Genet. 2013;45:977-83.

[118] Law EK, Sieuwerts AM, LaPara K, Leonard B, Starrett GJ, Molan AM, et al. The DNA cytosine deaminase APOBEC3B promotes tamoxifen resistance in ER-positive breast cancer. Sci Adv. 2016;2:e1601737.

[119] Cheng AZ, Yockteng-Melgar J, Jarvis MC, Malik-Soni N, Borozan I, Carpenter MA, et al. Epstein-Barr virus BORF2 inhibits cellular APOBEC3B to preserve viral genome integrity. Nat Microbiol. 2019;4:78-88.

[120] Kidd JM, Newman TL, Tuzun E, Kaul R, Eichler EE. Population stratification of a common APOBEC gene deletion polymorphism. PLoS Genet. 2007;3:e63.

[121] Wen WX, Soo JS, Kwan PY, Hong E, Khang TF, Mariapun S, et al. Germline APOBEC3B deletion is associated with breast cancer risk in an Asian multi-ethnic cohort and with immune cell presentation. Breast Cancer Res. 2016;18:56.

[122] Refsland EW, Stenglein MD, Shindo K, Albin JS, Brown WL, Harris RS. Quantitative profiling of the full APOBEC3 mRNA repertoire in lymphocytes and tissues: implications for HIV-1 restriction. Nucleic Acids Res. 2010;38:4274-84.

[123] Wittkopp CJ, Adolph MB, Wu LI, Chelico L, Emerman M. A single nucleotide polymorphism in human APOBEC3C enhances restriction of lentiviruses. PLoS Pathog. 2016;12:e1005865.

[124] Anderson BD, Ikeda T, Moghadasi SA, Martin AS, Brown WL, Harris RS. Natural APOBEC3C variants can elicit differential HIV-1 restriction activity. Retrovirology. 2018;15:78.

[125] An P, Bleiber G, Duggal P, Nelson G, May M, Mangeat B, et al. APOBEC3G genetic variants and their influence on the progression to AIDS. J Virol. 2004;78:11070-6.

[126] OhAinle M, Kerns JA, Li MM, Malik HS, Emerman M. Antiretroelement activity of APOBEC3H was lost twice in recent human evolution. Cell Host Microbe. 2008;4:249-59.

[127] Harari A, Ooms M, Mulder LC, Simon V. Polymorphisms and splice variants influence the antiretroviral activity of human APOBEC3H. J Virol. 2009;83:295-303.

[128] Wang X, Abudu A, Son S, Dang Y, Venta PJ, Zheng YH. Analysis of human APOBEC3H haplotypes and anti-human immunodeficiency virus type 1 activity. J Virol. 2011;85:3142-52.

[129] Ebrahimi D, Richards CM, Carpenter MA, Wang J, Ikeda T, Becker JT, et al. Genetic and mechanistic basis for APOBEC3H alternative splicing, retrovirus restriction, and counteraction by HIV-1 protease. Nat Commun. 2018;9:4137.

[130] OhAinle M, Kerns JA, Malik HS, Emerman M. Adaptive evolution and antiviral activity of the conserved mammalian cytidine deaminase APOBEC3H. J Virol. 2006;80:3853-62.

[131] Conticello SG, Harris RS, Neuberger MS. The Vif protein of HIV triggers degradation of the human antiretroviral DNA deaminase APOBEC3G. Curr Biol. 2003;13:2009-13.

[132] Yu X, Yu Y, Liu B, Luo K, Kong W, Mao P, et al. Induction of APOBEC3G ubiquitination and degradation by an HIV-1 Vif-Cul5-SCF complex. Science. 2003;302:1056-60.

[133] Marin M, Rose KM, Kozak SL, Kabat D. HIV-1 Vif protein binds the editing enzyme APOBEC3G and induces its degradation. Nat Med. 2003;9:1398-403.

[134] Sheehy AM, Gaddis NC, Malim MH. The antiretroviral enzyme APOBEC3G is degraded by the proteasome in response to HIV-1 Vif. Nat Med. 2003;9:1404-7.

[135] Stopak K, de Noronha C, Yonemoto W, Greene WC. HIV-1 Vif blocks the antiviral activity of APOBEC3G by impairing both its translation and intracellular stability. Mol Cell. 2003;12:591-601.

[136] Mariani R, Chen D, Schrofelbauer B, Navarro F, Konig R, Bollman B, et al. Species-specific exclusion of APOBEC3G from HIV-1 virions by Vif. Cell. 2003;114:21-31.

[137] Land AM, Wang J, Law EK, Aberle R, Kirmaier A, Krupp A, et al. Degradation of the cancer genomic DNA deaminase APOBEC3B by SIV Vif. Oncotarget. 2015;6:39969-79.

[138] Gaur R, Strebel K. Insights into the Dual Activity of SIVmac239 Vif against Human and African Green Monkey APOBEC3G. Plos One. 2012;7.

[139] Haché G, Shindo K, Albin JS, Harris RS. Evolution of HIV-1 isolates that use a novel Vif-independent mechanism to resist restriction by human APOBEC3G. Curr Biol. 2008;18:819-24.

[140] Doehle BP, Schafer A, Cullen BR. Human APOBEC3B is a potent inhibitor of HIV-1 infectivity and is resistant to HIV-1 Vif. Virology. 2005;339:281-8.

[141] LaRue RS, Lengyel J, Jonsson SR, Andresdottir V, Harris RS. Lentiviral Vif degrades the APOBEC3Z3/APOBEC3H protein of its mammalian host and is capable of cross-species activity. J Virol. 2010;84:8193-201.

[142] Li MM, Wu LI, Emerman M. The range of human APOBEC3H sensitivity to lentiviral Vif proteins. J Virol. 2010;84:88-95.

[143] Compton AA, Emerman M. Convergence and divergence in the evolution of the APOBEC3G-Vif interaction reveal ancient origins of simian immunodeficiency viruses. PLoS Pathog. 2013;9:e1003135.

[144] Dang Y, Wang XJ, Zhou T, York IA, Zheng YH. Identification of a novel WxSLVK motif in the N terminus of human immunodeficiency virus and simian immunodeficiency virus Vif that is critical for APOBEC3G and APOBEC3F neutralization. J Virol. 2009;83:8544-52.

[145] Mehle A, Wilson H, Zhang C, Brazier AJ, McPike M, Pery E, et al. Identification of an APOBEC3G binding site in human immunodeficiency virus type 1 Vif and inhibitors of Vif-APOBEC3G binding. J Virol. 2007;81:13235-41.

[146] Simon V, Zennou V, Murray D, Huang Y, Ho DD, Bieniasz PD. Natural variation in Vif: differential impact on APOBEC3G/3F and a potential role in HIV-1 diversification. PLoS Pathog. 2005;1:e6.

[147] Lavens D, Peelman F, Van der Heyden J, Uyttendaele I, Catteeuw D, Verhee A, et al. Definition of the interacting interfaces of APOBEC3G and HIV-1 Vif using MAPPIT mutagenesis analysis. Nucleic Acids Res. 2010;38:1902-12.

[148] Zhai C, Ma L, Zhang Z, Ding J, Wang J, Zhang Y, et al. Identification and characterization of loop7 motif and its role in regulating biological function of human APOBEC3G through molecular modeling and biological assay. Acta Pharm Sin B. 2017;7:571-82.

[149] Han X, Liang W, Hua D, Zhou X, Du J, Evans SL, et al. Evolutionarily conserved requirement for core binding factor beta in the assembly of the human immunodeficiency virus/simian immunodeficiency virus Vif-cullin 5-RING E3 ubiquitin ligase. J Virol. 2014;88:3320-8.

[150] Hultquist JF, Binka M, LaRue RS, Simon V, Harris RS. Vif proteins of human and simian immunodeficiency viruses require cellular CBFbeta to degrade APOBEC3 restriction factors. J Virol. 2012;86:2874-7.

[151] Stenglein MD, Matsuo H, Harris RS. Two regions within the amino-terminal half of APOBEC3G cooperate to determine cytoplasmic localization. J Virol. 2008;82:9591-9.

[152] Liddament MT, Brown WL, Schumacher AJ, Harris RS. APOBEC3F properties and hypermutation preferences indicate activity against HIV-1 in vivo. Curr Biol. 2004;14:1385-91.

[153] Chesebro B, Wehrly K, Nishio J, Perryman S. Macrophage-tropic human immunodeficiency virus isolates from different patients exhibit unusual V3 envelope sequence homogeneity in comparison with T-cell-tropic isolates: definition of critical amino acids involved in cell tropism. J Virol. 1992;66:6547-54.

[154] Li MM, Emerman M. Polymorphism in human APOBEC3H affects a phenotype dominant for subcellular localization and antiviral activity. J Virol. 2011;85:8197-207.

[155] Kozak SL, Marin M, Rose KM, Bystrom C, Kabat D. The anti-HIV-1 editing enzyme APOBEC3G binds HIV-1 RNA and messenger RNAs that shuttle between polysomes and stress granules. J Biol Chem. 2006;281:29105-19.

[156] Gallois-Montbrun S, Kramer B, Swanson CM, Byers H, Lynham S, Ward M, et al. Antiviral protein APOBEC3G localizes to ribonucleoprotein complexes found in P bodies and stress granules. J Virol. 2007;81:2165-78.

[157] Izumi T, Burdick R, Shigemi M, Plisov S, Hu WS, Pathak VK. Mov10 and APOBEC3G localization to processing bodies is not required for virion incorporation and antiviral activity. J Virol. 2013;87:11047-62.

[158] Phalora PK, Sherer NM, Wolinsky SM, Swanson CM, Malim MH. HIV-1 replication and APOBEC3 antiviral activity are not regulated by P bodies. J Virol. 2012;86:11712-24.

[159] Salamango DJ, Becker JT, McCann JL, Cheng AZ, Demir Ö, Amaro RE, et al. APOBEC3H subcellular localization determinants define zipcode for targeting HIV-1 for restriction. Mol Cell Biol. 2018;38:e00356.

[160] Wichroski MJ, Robb GB, Rana TM. Human retroviral host restriction factors APOBEC3G and APOBEC3F localize to mRNA processing bodies. PLoS Pathog. 2006;2:e41.

[161] Fukuda H, Li S, Sardo L, Smith JL, Yamashita K, Sarca AD, et al. Structural determinants of the APOBEC3G N-terminal domain for HIV-1 RNA association. Front Cell Infect Microbiol. 2019;9:129.

[162] Starrett GJ, Luengas EM, McCann JL, Ebrahimi D, Temiz NA, Love RP, et al. The DNA cytosine deaminase APOBEC3H haplotype I likely contributes to breast and lung cancer mutagenesis. Nat Commun. 2016;7:12918.

[163] Romei MG, Boxer SG. Split green fluorescent proteins: scope, limitations, and outlook. Annu Rev Biophys. 2019;48:19-44.

[164] Foglieni C, Papin S, Salvade A, Afroz T, Pinton S, Pedrioli G, et al. Split GFP technologies to structurally characterize and quantify functional biomolecular interactions of FTD-related proteins. Sci Rep. 2017;7:14013.

[165] Shi K, Demir O, Carpenter MA, Wagner J, Kurahashi K, Harris RS, et al. Conformational switch regulates the DNA cytosine deaminase activity of human APOBEC3B. Sci Rep. 2017;7:17415.

[166] Li J, Chen Y, Li M, Carpenter MA, McDougle RM, Luengas EM, et al. APOBEC3 multimerization correlates with HIV-1 packaging and restriction activity in living cells. J Mol Biol. 2014;426:1296-307.

[167] Zhao K, Du J, Rui Y, Zheng W, Kang J, Hou J, et al. Evolutionarily conserved pressure for the existence of distinct G2/M cell cycle arrest and A3H inactivation functions in HIV-1 Vif. Cell Cycle. 2015;14:838-47.

[168] Mitra M, Singer D, Mano Y, Hritz J, Nam G, Gorelick RJ, et al. Sequence and structural determinants of human APOBEC3H deaminase and anti-HIV-1 activities. Retrovirology. 2015;12:3.

[169] Kamiyama D, Sekine S, Barsi-Rhyne B, Hu J, Chen B, Gilbert LA, et al. Versatile protein tagging in cells with split fluorescent protein. Nat Commun. 2016;7:11046.

[170] Becker JT, Sherer NM. Subcellular localization of HIV-1 gag-pol mRNAs regulates sites of virion assembly. J Virol. 2017;91.

[171] Kabsch W. Xds. Acta Crystallogr D Biol Crystallogr. 2010;66:125-32.

[172] Emsley P, Lohkamp B, Scott WG, Cowtan K. Features and development of Coot. Acta Crystallogr D Biol Crystallogr. 2010;66:486-501.

[173] Adams PD, Afonine PV, Bunkoczi G, Chen VB, Davis IW, Echols N, et al. PHENIX: a comprehensive Python-based system for macromolecular structure solution. Acta Crystallogr D Biol Crystallogr. 2010;66:213-21.

[174] Schindelin J, Arganda-Carreras I, Frise E, Kaynig V, Longair M, Pietzsch T, et al. Fiji: an open-source platform for biological-image analysis. Nat Methods. 2012;9:676-82.

[175] Ooms M, Krikoni A, Kress AK, Simon V, Münk C. APOBEC3A, APOBEC3B, and APOBEC3H haplotype 2 restrict human T-lymphotropic virus type 1. J Virol. 2012;86:6097-108.

[176] Celum C, Wald A, Lingappa JR, Magaret AS, Wang RS, Mugo N, et al. Acyclovir and transmission of HIV-1 from persons infected with HIV-1 and HSV-2. N Engl J Med. 2010;362:427-39.

[177] Lingappa JR, Baeten JM, Wald A, Hughes JP, Thomas KK, Mujugira A, et al. Daily acyclovir for HIV-1 disease progression in people dually infected with HIV-1 and herpes simplex virus type 2: a randomised placebo-controlled trial. Lancet. 2010;375:824-33.

[178] Baeten JM, Donnell D, Ndase P, Mugo NR, Campbell JD, Wangisi J, et al. Antiretroviral prophylaxis for HIV prevention in heterosexual men and women. N Engl J Med. 2012;367:399-410.

[179] Lingappa JR, Kahle E, Mugo N, Mujugira A, Magaret A, Baeten J, et al. Characteristics of HIV-1 discordant couples enrolled in a trial of HSV-2 suppression to reduce HIV-1 transmission: the partners study. PLoS One. 2009;4:e5272.

[180] Mackelprang RD, Baeten JM, Donnell D, Celum C, Farquhar C, de Bruyn G, et al. Quantifying ongoing HIV-1 exposure in HIV-1-serodiscordant couples to identify individuals with potential host resistance to HIV-1. J Infect Dis. 2012;206:1299-308.

[181] Huang Y, Paxton WA, Wolinsky SM, Neumann AU, Zhang L, He T, et al. The role of a mutant CCR5 allele in HIV-1 transmission and disease progression. Nat Med. 1996;2:1240-3.

[182] Liu R, Paxton WA, Choe S, Ceradini D, Martin SR, Horuk R, et al. Homozygous defect in HIV-1 coreceptor accounts for resistance of some multiply-exposed individuals to HIV-1 infection. Cell. 1996;86:367-77.

[183] Dean M, Carrington M, Winkler C, Huttley GA, Smith MW, Allikmets R, et al. Genetic restriction of HIV-1 infection and progression to AIDS by a deletion allele of the CKR5 structural gene. Science. 1996;273:1856-62.

[184] MacDonald KS, Fowke KR, Kimani J, Dunand VA, Nagelkerke NJ, Ball TB, et al. Influence of HLA supertypes on susceptibility and resistance to human immunodeficiency virus type 1 infection. J Infect Dis. 2000;181:1581-9.

[185] Sakurai D, Iwatani Y, Ohtani H, Naruse TK, Terunuma H, Sugiura W, et al. APOBEC3H polymorphisms associated with the susceptibility to HIV-1 infection and AIDS progression in Japanese. Immunogenetics. 2015;67:253-7.

[186] Cassol S, Salas T, Gill MJ, Montpetit M, Rudnik J, Sy CT, et al. Stability of dried blood spot specimens for detection of human immunodeficiency virus DNA by polymerase chain reaction. J Clin Microbiol. 1992;30:3039-42.

[187] He Z, Zhang W, Chen G, Xu R, Yu XF. Characterization of conserved motifs in HIV-1 Vif required for APOBEC3G and APOBEC3F interaction. J Mol Biol. 2008;381:1000-11.

[188] Smith JL, Izumi T, Borbet TC, Hagedorn AN, Pathak VK. HIV-1 and HIV-2 Vif interact with human APOBEC3 proteins using completely different determinants. J Virol. 2014;88:9893-908.

[189] Harris RS, Anderson BD. Evolutionary paradigms from ancient and ongoing conflicts between the lentiviral Vif protein and mammalian APOBEC3 enzymes. Plos Pathog. 2016;12.

[190] Keane SC, Heng X, Lu K, Kharytonchyk S, Ramakrishnan V, Carter G, et al. RNA structure. Structure of the HIV-1 RNA packaging signal. Science. 2015;348:917-21.